Design, Synthesis, and Evaluation of a Cross-Linked Oligonucleotide as the First Nanomolar Inhibitor of APOBEC3A

Harikrishnan M. Kurup[1,2], Maksim V. Kvach[1], Stefan Harjes[1], Fareeda M. Barzak[1], Geoffrey B. Jameson[1,2], Elena Harjes[1,2]*, Vyacheslav V. Filichev[1,2]*

[1]School of Natural Sciences, Massey University, Private Bag 11 222, Palmerston North 4442, New Zealand; [2]Maurice Wilkins Centre for Molecular Biodiscovery, Auckland 1142, New Zealand.

*E-mail: e.harjes@massey.ac.nz, v.filichev@massey.ac.nz

Table of Contents

1. General information

All reactions were performed in oven-dried glassware under an atmosphere of dry argon or nitrogen unless otherwise noted. Moisture-sensitive reactions were carried out using standard syringe septum techniques and under an inert atmosphere of argon or nitrogen. All solvents and reagents were purified by standard techniques unless otherwise noted. Solvents for filtration, transfers, and chromatography were certified ACS grade. Evaporation of solvents was carried out under reduced pressure on a rotary vacuum evaporator below 40 ^{o}C. "Brine" refers to a saturated solution of sodium chloride in water. ^{1}H, ^{13}C, ^{31}P NMR spectra were recorded on Bruker 500- and 700-MHz spectrometers. Chemical shifts are reported in parts per million (ppm) downfield from tetramethylsilane. Spin multiplicities are described as s (singlet), bs (broad singlet), d (doublet), dd (double of doublets), dt (double of triplets), ddd (doublet of doublet of doublets), t (triplet), q (quartet), m (multiplet). Coupling constants are reported in Hertz (Hz). The assignments of signals were done using 2D homonuclear ^{1}H-^{1}H COSY, NOESY and heteronuclear ^{1}H-^{13}C HMQC or HSQC, and HMBC spectra. NMR spectra were processed in TopSpin. High-resolution electrospray mass spectra were recorded on a Thermo Fisher Scientific Q Exactive Focus Hybrid Quadrupole-Orbitrap mass spectrometer. Ions generated by ESI were detected in positive ion mode for small molecules and negative ion mode for oligonucleotides. Total ion count (TIC) was recorded in centroid mode over the *m*/*z* range of 100-3,000 and analyzed using Thermo Fisher Xcalibur Qual Browser. Analytical thin layer chromatography (TLC) was performed on MERCK precoated silica gel 60-F254 (0.5-mm) aluminum plates. Visualization of the spots on TLC plates was achieved either by exposure to UV light or by dipping the plates into aqueous $KMnO_4$ and heating with a heat gun. Silica gel column chromatography was performed using silica gel 60 (40–63 μm). Oligonucleotide syntheses were carried out on a MerMade-4 DNA/RNA synthesizer (BioAutomation) on a 5 μmol scale using standard manufacturer's protocol for unmodified nucleotides.

2. Synthesis of modified azido CPG

2.1. Synthesis of 2-deoxy-3,5-di-*O*-(4-methylbenzoyl)-β-D-*erythro*-pentofuranosyl azide (2)

To a stirring solution of sodium azide (97.5 g, 1.5 mol) and tetrabutylammonium hydrogen sulfate (101.7 g, 0.3 mmol) in saturated sodium bicarbonate solution (1 L), chloroform (1 L) was added, and the mixture was vigorously stirred for about 5 min until a milky emulsion was

formed. Hoffer's chloro-sugar **1** (116.7 g, 0.3 mol) was rapidly added to the emulsion and the mixture was stirred 20 min. After the disappearance of starting material, the organic layer was washed with satd. sodium bicarbonate (1 L), water (2 × 1 L), dried over anhydrous sodium sulfate and was filtered. Solvent was evaporated *in vacuo* and the product was recrystallized from ethanol (450 mL) to yield compound **2** (105 g, 88%, β:α ratio of 19:1).

^{1}H NMR (500 MHz, DMSO-d_6): δ 7.94-7.84 (m, 4H, H-3); 7.36-7.29 (m, 4H, H-4); 5.87 (dd, 1H, J = 6.0 Hz, J = 4.2 Hz, H-1'); 5.56-5.50 (m, 1H, H-3'); 4.59-4.39 (m, 3H, H-4',5'); 2.49-2.42 (m, 1H, H-2'a); 2.375, 2.370 (2s, 6H, H-6); 2.37-2.30 (m, 1H, H-2'b).

^{13}C NMR (125.7 MHz, d_6-DMSO): δ 165.4; 165.3 (2C, C1); 144.0, 143.8 (2C, C5); 129.4, 129.3, 129.2, 129.2 (8C, C3,4); 126.7, 126.4 (2C, C2); 91.6 (C1'); 82.0 (C4'); 74.6 (C3'); 63.9 (C5'); 37.8 (C2'); 21.1, 21.1 (2C, C6).

IR ATR (cm^{-1}): 2943.74, 2126.16, 1715.46, 1611.78, 1509.61, 1443.95, 1407.97, 1378.51, 1271.93, 1238.71, 1176.04, 1114.15, 1101.23, 1083.75, 1059.76, 1035.31, 1019.42, 970.45, 939.79, 885.50, 844.42, 750.80, 691.50.

HRMS (ESI) *m*/*z*: $[M+Na]^+$ Calcd for $C_{21}H_{21}N_3O_5Na$ 418.1379; found 418.1372.

2.2. Synthesis of 2-deoxy-5-*O*-(4,4'-dimethoxytrityl)-β-D-*erythro*-pentofuranosyl azide (3)

Synthesis was performed by a similar procedure described earlier.[1] To a stirring solution of 2-deoxy-3,5-di-*O*-(4-methylbenzoyl)-β-D-*erythro*-pentofuranosyl azide **2** (3.96 g, 10 mmol) in 370 mL methanol was added 37 mL of 30% aq. ammonia solution and kept it stirring for 3 days. After the disappearance of the starting material, volatiles were removed by rotary vacuum evaporator and residue was co-evaporated again with water to remove formed methyl toluate and then freeze dried from water to get the deprotected compound 2-deoxy-β-D-*erythro*-pentofuranosyl azide (1.65 g). This product was used without further purification to protect it with DMT. To a stirring solution of the deprotected azido sugar (1.65 g, 10 mmol) in dry pyridine (40 mL) at 0 °C 4,4'-dimethoxytrityl chloride (3.72 g, 11 mmol) was added and mixture was stirred at r.t. overnight. Pyridine was evaporated *in vacuo*. The residue was dissolved in 50 mL ethyl acetate and washed with brine (2 × 10 mL). The organic layer was dried over anhydrous sodium sulfate, filtered, and evaporated *in vacuo*. The crude product was purified by column chromatography over silica gel treated with 10% Et_3N in DCM and compound **3** was eluted with 5% EtOAc in DCM to afford the desired product **3** as a foam (3.13 g, 68%).

^{1}H NMR (500 MHz, DMSO-d_6): δ 7.47-7.42 (m, 2H, H-2); 7.34-7.26 (m, 6H, H-3, 2''); 7.25-7.19 (m, 1H, H-4); 6.92-6.86 (m, 4H, H-3''); 5.68 (dd, 1H, J = 5.8 Hz, J = 3.1 Hz, H-1'); 5.25 (d, 1H, J = 5.0 Hz, OH); 4.20-4.12 (m, 1H, H-3'); 3.93-3.86 (m, 1H, H-4'); 3.73 (s, 6H, 2×CH_3); 3.15-3.02 (m, 2H, H-5'); 2.04-1.91 (m, 2H, H-2').

^{13}C NMR (125.7 MHz, DMSO-d_6): δ 158.0 (2C, C4''); 144.9 (C1); 135.7, 135.6 (2C, C1''); 129.7 (4C, C2''); 127.8 (2C, C3); 127.7 (2C, C2); 126.6 (C4); 113.2 (4C, C3''); 91.5 (C1'), 85.4 (C4'); 85.3 (CAr$_3$); 69.9 (C3'); 63.9 (C5'); 55.0 (2C, CH$_3$); 40.4 (C2').

IR ATR (cm^{-1}): 2110.79, 1607.41, 1520.20, 1450.36, 1300.72, 1250.46, 1176.80, 1081.96, 1033.97, 829.42.

HRMS (ESI) *m*/*z*: $[M+Na]^+$ Calcd for $C_{26}H_{27}N_3O_5Na$ 484.1848; found 484.1844.

2.3. Synthesis of modified azido-2-deoxyribose CPG (4)

Synthesis of the CPG support **4** was performed following the previously reported procedure.[2] LCAA-CPG (3.0 g) with a pore size of 500 Å and 120-200 mesh size obtained commercially (ChemGenes Corporation) was activated by 3% trifluoroacetic acid in DCM (30 mL) and kept overnight with gentle stirring. The slurry was filtered and washed with 9:1 triethylamine:di*iso*propylethylamine (50 mL), DCM and diethylether, then dried *in vacuo*. Activated LCAA-CPG was then treated with succinic anhydride (6.6 mmol, 0.66 g) and 4-dimethylaminopyridine (DMAP) (0.8 mmol, 0.1 g) in anhydrous pyridine (12 mL) and stirred gently at r.t. overnight. The slurry was filtered off and washed successively with pyridine, DCM, and ether, then dried *in vacuo*. This carboxylic derivatized CPG was then coupled with compound **3** (0.4 mmol, 0.184 g) in presence of 1-ethyl-3-(3-dimethylaminopropyl) carbodiimide (EDC base) (2.7 mmol, 0.48 mL), triethylamine (20 μL) and DMAP (0.8 mmol, 0.1 g) in 1:1 pyridine:DMF (36 mL). After 72 hours pentafluorophenol (1.5 mmol, 0.27 g) was added and mixture was kept overnight. The slurry was filtered and washed with DCM and a mixture of 9:1 pyridine:piperidine (10 mL) during 5 min followed by DCM, acetonitrile, THF and again with DCM, then dried *in vacuo*. The CPG was then treated with the mixture of 2 mL of Cap A (acetic anhydride:2,6-lutidine:THF, 1:1:8, v/v/v) and 2 mL of Cap B (1-methylimidazole:THF, 4:21, v/v) for 2 hours, followed by washing with DCM, methanol, acetonitrile, THF and again with DCM and dried *in vacuo*. The load on the CPG **4** was determined to be 39 μmol/g based on UV absorption of DMT-cation at 504 nm (Ɛ = 76000 L·mol^{-1}·cm^{-1}) that was released from an aliquot of compound by treatment with 3% dichloroacetic acid in DCM.

3. Synthesis of modified 2'-deoxyadenosines

2.4. Synthesis of 2-azidoethyl-4-methylbenzenesulfonate (5)

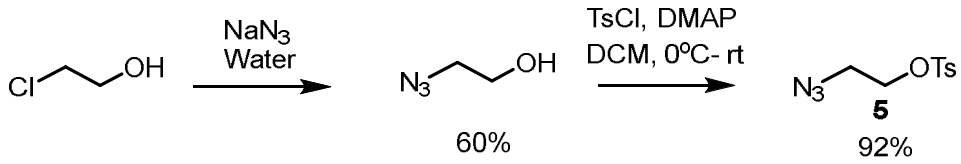

Scheme S1. Synthesis of 2-azidoethyl 4-tosylate (**5**)

2-Azidoethan-1-ol (2.0 g, 23.0 mmol) was prepared according to a reported procedure[3] and was dissolved in DCM (50 ml), cooled to 0 °C, then DMAP (34 mg, 0.27 mmol), tosyl chloride (6.56 g, 34.40 mmol) and Et_3N (6.39 mL, 46.0 mmol) were added. The reaction mixture was stirred for 30 min, diluted with 50 mL more of DCM and washed with brine (2 × 10 mL). The organic layer was dried over anhydrous sodium sulfate, filtered, and concentrated *in vacuo*. The crude product was purified by column chromatography over silica gel, eluting with hexane/EtOAc (7:3) to afford the desired product **5** as an oily liquid (3.12 g, 92%).

^{1}H NMR (500 MHz, DMSO-d_6): δ 7.79 (d, J = 8.3 Hz, 2H); 7.34 (d, J = 8.1 Hz, 2H,); 4.16 (t, 2H, J = 5.2 Hz, $CH_2CH_2N_3$); 3.48 (t, 2H, J = 5.2 Hz, $CH_2CH_2N_3$); 2.45 (s, 3H, Ar-CH_3).

^{13}C NMR (125.7 MHz, $CDCl_3$): δ 145.33 (1C, C1); 132.52 (1C, C4); 130.03 (2C, C3 and C5); 127.95 (2C, C2 and C6); 68.22 (1C, $CH_2CH_2N_3$); 49.58 (1C, $CH_2CH_2N_3$); 21.65 (1C, CH_3).

HRMS (ESI) m/z: $[M+Na]^+$ Calcd for $C_9H_{11}N_3O_3SNa$ 264.0419; found 264.0413.

2.5. N^6,3',5'-Triacetyl-2'-deoxyadenosine (7)

N^6,3',5'-Triacetyl-2'-deoxyadenosine **7** was prepared similar to a reported procedure with some modifications.[4] A mixture of 2'-deoxyadenosine **6** (1.0 g, 3.98 mmol), pyridine (7.5 mL) and Ac_2O (3.5 mL) was stirred at r.t. overnight. The resulting solution was heated to 60 °C for 6 h. After the disappearance of the starting material, monitored by TLC (CH_2Cl_2/MeOH, 95:5, v/v), the reaction was cooled down and quenched with excess of EtOH (20 mL). Volatiles were evaporated *in vacuo*. Traces of pyridine were co-evaporated with successive portions of EtOH and MeOH (20 mL each). The resultant oily liquid was diluted with EtOAc (100 mL) and washed with brine (2 × 20 mL). The organic layer was dried over anhydrous sodium sulfate, filtered, and evaporated *in vacuo*. The crude product was purified by column chromatography on silica gel, eluting with CH_2Cl_2/MeOH (9.5:0.5, v/v) to afford the desired product **7** as a white solid (1.15 g, 76%).

^{1}H NMR (500 MHz, DMSO-d_6): δ 10.70 (s, 1H, N*H*); 8.663, 8.660 (2s, 2H, H-2, H-8); 6.48 (dd, 1H, $J_{1',2'}$ = 6.3, 7.8 Hz, H-1'); 5.44 (dt, 1H, J = 2.8, 6.5 Hz, H-3'); 4.32 (dd, 1H, $J_{4',5'a}$ = 4.2 Hz, $J_{5'a,5'b}$ = 11.0 Hz, H-5'a); 4.28 (ddd, 1H, $J_{3',4'}$ = 2.7 Hz, $J_{4',5'a}$ = 4.2 Hz, $J_{4',5'b}$ = 5.5 Hz, H-4'); 4.22 (dd, 1H, $J_{4',5'b=}$ 5.5 Hz, $J_{5'a,5'b}$ = 11.0 Hz, H-5'b); 3.20 (ddd, 1H, $J_{2'a,3'}$ = 2.8 Hz, $J_{2'a,1'=}$ 6.3 Hz, $J_{2'a,2'b}$ = 14.2 Hz, H-2'a); 2.60 (ddd, 1H, $J_{2'b,3'}$ = 6.6 Hz, $J_{2'b,1'}$ = 7.8 Hz, $J_{2'a,2'b}$ = 14.2 Hz, H-2'b); 2.26 (s, 3H, NHCOC*H*$_3$); 2.10, 2.00 (2s, 6H, OCOC*H*$_3$).

^{13}C NMR (125.7 MHz, DMSO-d_6): δ 170.1 (O<u>CO</u>CH$_3$); 170.0 (O<u>CO</u>CH$_3$); 168.8 (NH<u>CO</u>CH$_3$); 151.7 (C2); 151.5 (C4); 149.7 (C6); 142.9 (C8); 123.8 (C5); 83.7 (C1'); 81.8 (C4'); 74.2 (C3'); 63.5 (C5'); 35.3 (C2'); 24.3 (NHCO<u>CH</u>$_3$); 20.8 (OCO<u>CH</u>$_3$); 20.5 (OCO<u>CH</u>$_3$).

HRMS (ESI) *m*/*z*: $[M+H]^+$ Calcd for $C_{16}H_{20}N_5O_6$ 378.1414; found 378.1397.

2.6. N^6-(2-Azidoethyl)-N^6,3',5'-triacetyl-2'-deoxyadenosine (8)

To a stirring solution of N^6,3',5'-triacetyl-2'-deoxyadenosine **7** (1.0 g, 2.65 mmol) in acetonitrile (15 mL), Cs_2CO_3 (2.50 g, 7.67 mmol) and compound **5** (3.82 g, 15.80 mmol) were added and mixture was heated to 60 ^{o}C. After the disappearance of the starting material on TLC the reaction mixture was diluted with EtOAc (50 mL) and washed with water (2 × 10 mL). Organic layer was dried over anhydrous sodium sulfate, filtered, and concentrated *in vacuo*. The crude product was purified by silica gel column chromatography using CH_2Cl_2/MeOH (9:1,v/v) to get desired compound **8** as a sticky solid.

Yield: 0.94 g, 80%.

^{1}H NMR (500 MHz, DMSO-d_6): δ 8.84 (s, 1H, H-8); 8.82 (s, 1H, H-2); 6.52 (dd, 1H, $J_{1',2a'}$ = 6.7, $J_{1',2'b}$ 7.2 Hz, H-1'); 5.45 (dt, 1H, J = 2.3, 6.4 Hz, H-3'); 4.32 (dd, 1H, $J_{4',5'a}$ = 4.2 Hz, $J_{5'a,5'b}$ = 10.6 Hz, H-5'a); 4.31-4.28 (m, 3H, H5'b and N*CH*$_2$CH$_2$N3); 4.23 (ddd, 1H, $J_{3',4'}$ = 2.3 Hz, $J_{4',5'a}$ = 4.4 Hz, $J_{4',5'b}$ = 5.9 Hz, H-4'); 3.52 (t, J = 7.0 Hz, 2H, NCH$_2$C*H*$_2$N$_3$); 3.20 (ddd, 1H, $J_{2'a,3'}$ = 2.3 Hz, $J_{2'a,1'=}$ 6.7 Hz, $J_{2'a,2'b}$ = 14.3 Hz, H-2'a); 2.63 (ddd, 1H, $J_{2'b,3'}$ = 6.4 Hz, $J_{2'b,1'}$ = 7.2 Hz, $J_{2'a,2'b}$ = 14.3 Hz, H-2'b); 2.17 (s, 3H, NCOC*H*$_3$); 2.10 (s, 3H, OCOC*H*$_3$); 1.99 (s, 3H, OCOC*H*$_3$).

^{13}C NMR (125.7 MHz, DMSO-d_6): δ 170.8 (O<u>CO</u>CH$_3$); 170.1 (O<u>CO</u>CH$_3$); 170.0 (N<u>CO</u>CH$_3$); 152.6 (C6); 152.3 (C4); 151.6 (C8); 144.5 (C2); 126.7 (C5); 83.9 (C1'); 81.8 (C4'); 74.1 (C3'); 63.4 (C5'); 49.4 (NCH$_2$<u>CH</u>$_2$N$_3$); 45.6 (N<u>C</u>H$_2$CH$_2$N$_3$); 35.4 (C2'); 23.8 (NCO<u>CH</u>$_3$); 20.8 (OCO<u>CH3</u>); 20.5 (OCO<u>CH</u>$_3$).

IR ATR (cm^{-1}): 3440.67, 2306.61, 2339.80, 2251.73, 2124.62, 1667.50, 1058.50, 1037.65, 1008.07, 823.02, 760.59, 667.93, 624.85.

HRMS (ESI) *m*/*z*: $[M+H]^+$ Calcd for $C_{18}H_{23}N_8O_6$ 447.1741; found 447.1737.

2.7. N^6-(2-Azidoethyl)-N^6-acetyl-2'-deoxyadenosine (9)

To a stirring solution of compound **8** (0.9 g, 2.0 mmol) in MeOH:water (10:10 mL) Et_3N (1.5 mL) was added at r.t. The reaction was monitored by TLC. After 15 min volatiles were evaporated *in vacuo*. The crude product was purified by silica gel column chromatography using CH_2Cl_2/MeOH (7:3) to get desired compound **9** as a semisolid (0.65 g, 89%).

^{1}H NMR (500 MHz, DMSO-d_6): δ 8.83 (s, 1H, H-8); 8.82 (s, 1H, H-2); 6.49 (app t, J = 6.7 Hz, 1H, H-1'); 5.43 (s, 1H, 3'-OH), 5.05 (s, 1H, 5'-OH), 4.45 (dt, 1H, J = 3.2, 5.6 Hz, H-3'); 4.29 (t, J = 6.1 Hz, 2H, NC$H_2$$CH_2N_3$); 3.90 (ddd, 1H, $J_{3',4'}$ = 2.3 Hz, $J_{4',5'b}$ = 4.6 Hz, $J_{4',5'a}$ = 5.9 Hz, H-4'); 3.63 (dd, 1H, $J_{4',5'a}$ = 5.9 Hz, $J_{5'a,5'b}$ = 11.7 Hz, H-5'a); 3.54 (dd, 1H, $J_{4',5'b}$= 4.6 Hz, $J_{5'a,5'b}$ = 11.7 Hz, H-5'b); 3.52 (t, 2H, J = 6.1 Hz, 2H, $NCH_2$$CH_2N_3$); 2.77 (ddd, 1H, $J_{2'a,3'}$ = 2.8 Hz, $J_{2'a,1'}$= 6.3 Hz, $J_{2'a,2'b}$ = 13.2 Hz, H-2'a); 2.37 (ddd, 1H, $J_{2'b,3'}$ = 6.2 Hz, $J_{2'b,1'}$ = 9.8 Hz, $J_{2'a,2'b}$ = 13.2 Hz, H-2'b); 2.16 (s, 3H, NCOCH_3).

^{13}C NMR (125.7 MHz, DMSO-d_6): δ 170.8 (N<u>CO</u>CH_3); 152.5 (C2); 152.1 (C6); 151.5 (C4); 144.3 (C8); 126.6 (C5); 88.0 (C4'); 83.8 (C1'); 70.5 (C3'); 61.4 (C5'); 49.3 (NCH_2<u>CH_2</u>N_3): 45.6(N<u>C</u>$H_2CH_2N_3$), 39.8 (C2'); 23.8 (NCO<u>C</u>H_3).

HRMS (ESI) *m*/*z*: $[M + Na]^+$ Calcd for $C_{14}H_{18}N_8O_4Na$ 385.1349; found 385.1342.

2.8. 5'-*O*-(4,4'-Dimethoxytrityl)-N^6-(2-azidoethyl)-N^6-acetyl-2'-deoxyadenosine (10)

To a stirring solution of compound **9** (0.6 g, 1.66 mmol) in dry pyridine (5 mL) 4,4'-dimethoxytrityl chloride (0.67 g, 2.0 mmol) was added at 0 ^{o}C and the mixture was stirred at r.t. overnight under argon. Pyridine was evaporated *in vacuo* and the residue was dissolved in 50 mL DCM, washed with brine (2 × 10 mL), organic layer was dried over anhydrous sodium sulfate, filtered, and concentrated *in vacuo*. The crude product was purified by column chromatography over silica gel treated with 10% Et_3N in DCM and eluted with 5% EtOAc in CH_2Cl_2 to afford the desired product **10** as a foam (0.81 g, 74%).

Yield: 0.81 g, 74%.

^{1}H NMR (500 MHz, DMSO-d_6): δ 8.75 (s, 1H, H-8); 8.72 (s, 1H, H-2); 7.32-7.30 (m, 2H,H-2"); 7.21-7.16 (m,7H, H-3", 4"and 2'"); 6.81-6.77 (m, 4H, H-3'"); 6.51 (dd, 1H, $J_{1',2'}$ = 5.9, 6.7 Hz, H-1'); 5.43 (d, 1H, $J_{3'OH}$ = 4.65 Hz, 3'-OH); 4.54-4.50 (m, 1H, H-3'); 4.27 (t, J = 6.17 Hz, 2H, NC$H_2$$CH_2N_3$); 4.09-4.02 (m, 1H, H-4'); 3.714 (s, 3H,OCH_3); 3.710 (s, 3H, OCH_3); 3.49 (t,

J = 6.10 Hz, 1H, $NCH_2CH_2N_3$); 3.23-3.16 (m, 2H, H-5'); 2.95-2.90 (m, 1H, 1H, H-2'a); 2.43-2.38 (m, 1H, H-2'b); 2.11 (s, 3H, $NCOCH_3$).

^{13}C NMR (125.7 MHz, DMSO-d_6): δ 171.2 ($NCOCH_3$); 158.4, 158.4 (2C, C4'''); 152.9 (C6) 152.6 (C4); 151.9 (C2); 145.3 (C1''); 145.0 (C8); 136.0, 135.9 (2C, C1'''); 130.1 (4C, C2'''); 128.1 (2C, C3''); 128.1 (2C, C2''); 127.1 (C5); 127.0 (C4''); 113.5, 113.5 (4C, C3'''); 86.5 (C4'); 85.8 (C-Ar_3); 84.3 (C1'); 70.9 (C3'); 64.5 (C5'); 55.4 ($OCH3$); 55.4 ($OCH3$); 49.8 ($NCH_2CH_2N_3$); 46.0 ($NCH_2CH_2N_3$); 38.9 (C2'); 24.2 ($NCOCH_3$).

IR ATR (cm^{-1}): 3440.50, 2951.36, 2098.43, 1682.24, 1574.42, 1505.16, 1446.01, 1364.68, 1295.85, 1248.04, 1211.82, 1175.50, 1032.04, 826.80, 700.85, 579.51.

HRMS (ESI) *m*/*z*: $[M+H]^+$ Calcd for $C_{35}H_{37}N_8O_6$ 665.2836; found 665.2831.

2.9. 5'-*O*-(4,4'-Dimethoxytrityl)-N^6-(2-azidoethyl)-N^6-acetyl-3'-*O*-(*N*,*N*-di*iso*propylamino-2-cyanoethoxyphosphanyl)-2'-deoxyadenosine (11)

To a stirring solution of compound **10** (0.6 g, 0.90 mmol) in dry $CDCl_3$ (5 mL), Et_3N (0.16 mL, 1 mmol) followed by 2-cyanoethyl-*N*,*N*-di*iso*propyl chlorophosphoramidite (0.27 mL, 1.08 mmol) were added under argon at 0 °C. After the consumption of the starting material, reaction mixture was washed with saturated $NaHCO_3$ solution (2 × 5 mL) followed by brine (5 mL). The organic layer was dried by passing through a column (12 × 1.5 cm) of anhydrous sodium sulfate. The solution of compound **11** in $CDCl_3$ contains excess of phosphitylation reagent as shown by NMR (**Figure S61**). For automated DNA synthesis, the reaction was performed under the same conditions using dry DCM as a solvent. The concentration of azide phosphoramidite in DCM solution was calculated as 0.2 M based on UV absorption of DMT-cation at 504 nm (ε = 76,000 $L \cdot mol^{-1} \cdot cm^{-1}$) that was released from an aliquot of compound **11** by treatment with 3% dichloroacetic acid in DCM.

^{1}H NMR (500 MHz, $CDCl_3$): δ 8.72 (s, 1H, H-8); 8.27, 8.24 (2s, 1H, H-2); 7.39-7.37 (m, 2H, H-2''); 7.29-7.19 (m, 7H, H-3'', H-4'' and H-2'''); 6.80-6.77 (m, 4H, H-3'''); 6.54-6.51 (m, 1H, H-1'); 4.84-4.77 (m, 1H, H-3'); 4.40-4.37 (m, 2H, $NCH_2CH_2N_3$); 4.22-4.16 (m, 1H, H-4'); 4.15-4.09 (m, 2H, CH_2CH_2CN); 3.77 (2s, 6H, OCH_3); 3.63-3.55 (m, 2H, NCH_2CH_2CN); 3.60-3.50 (m, 2H, $NCHCH_3$); 3.50-3.46 (m, 2H, H-5'); 2.93 (ddd,1H, *J*= 6.6, 9.8, 13.4 Hz, H-2'b); 2.76-2.73 (m, 2H, CH_2CH_2CN); 2.64-2.61 (m, 1H, H-2'a); 2.58-2.54 (m, 2H, $NCH_2CH_2N_3$); 2.25, 2.24 (2s, 3H, $NCOCH_3$); 1.20-1.18 (m, 10H, $NCHCH_3$); 1.13 (d, 2H, $NCHCH_3$, *J* = 6.5 Hz).

^{13}C NMR (125.7 MHz, $CDCl_3$): δ 171.6 ($NCOCH_3$); 158.5 (2C, C4'''); 153.0 (C6); 152.8 (C4); 152.7 (C6); 151.8 (1C, C2); 144.4 (C8); 142.5 (C1''); 135.56, 135.52, (2C, C1'''); 130.09,

130.06, 130.04, 130.02 (4C, C2'''); 128.1, 128.0, (4C, C2'', 3''); 127.8, 127.0, 126.99, 126.94, 126.91 (C4''); 117.58, 117.46 (CN); 116.9 (C5); 113.1 (4C, C3'''); 86.5 (C-Ar_3); 86.0, 85.8 (1C, C1'); 84.8, 84.7 (1C, C4'); 74.0, 73.9; 73.4, 73.3 (1C, C3'); 63.2, 63.1 (C5'); 58.3, 58.2, 58.16, 58.11 (1C, N$\underline{CH_2}CH_2CN$); 55.2, 55.1 (2C, OCH_3); 49.98, 49.95 (1C, NH$\underline{CH_2}CH_2N_3$); 46.1 (1C, 2'); 45.3, 45.2 (1C, $NHCH_2\underline{CH_2}N_3$); 24.65, 24.61, 24.57, 24.51 (1C, NCO$\underline{CH_3}$); 22.97, 22.95, 22.89, 22.87 (NCH$\underline{CH_3}$); 20.46, 20.40, 20.2, 20.1, 20.05 ($CH_2\underline{CH_2}CN$).

^{31}P NMR (202.5 MHz, DMSO-d_6, ref. 85% H_3PO_4) δ 148.8.

IR ATR (cm^{-1}): 3673.51, 2969.69, 2361.85, 2251.42, 2097.34, 1673.86, 1574.37, 1508.81, 1462.87, 1367.94, 1330.70, 1298.57, 1250.22, 1179.36, 1036.65, 911.31, 829.03, 732.85, 646.64, 558.98, 421.81.

4. Oligonucleotide synthesis and purification

Oligonucleotides were prepared on a MerMade-4 DNA/RNA synthesizer (BioAutomation) on a 5 μmol scale using standard manufacturer's protocol. Coupling times of 2'-deoxyzebularine (**dZ**) and other modified phosphoramidites were increased from 2 to 10 min. The final detritylated oligonucleotides were cleaved from the solid support and deprotected with 30% aq. ammonia solution (1.0 mL) at room temperature for 24 h. After filtering, an aq. solution of 0.3 M $LiClO_4$ (0.5 mL) was added and oligonucleotides were precipitated with acetone (14 mL). The pellets were washed with acetone and dried. Dry pellets were dissolved in milli-Q water (1 mL), oligonucleotides were purified and isolated by reverse phase HPLC on 250/4.6 mm, 5 μm, 300 Å C18 column (Thermo Fisher Scientific) in a gradient of CH_3CN (0→20% for 20 min, 1.3 mL/min) in 0.1 M TEAA buffer (pH 7.0) with a detection at 260 nm. Oligonucleotides were freeze-dried, pellets were dissolved in milli-Q water (1.5 mL) and desalted by reverse-phase HPLC on 100/10 mm, 5μm, 300 Å C18 column (Phenomenex) in a gradient of CH_3CN (0→80% for 15 min, 5 mL/min) in milli-Q water with detection at 260 nm. Pure products were quantified by measuring absorbance at 260 nm, analyzed by ESI-MS and concentrated by freeze-drying.

5. Cross-linking of linear oligonucleotides by CuAAC

The purified linear oligonucleotides were cross-linked by copper(I)-catalyzed azide-alkyne cycloaddition (CuAAC) using the following protocol implemented in our laboratory (**Table S1**).

Table S1. Protocol employed for the CuAAC reaction.

OD_{260} units	5<	5-10	10-15	15-20	20-25	25-30	30-35	35-40
Oligonucleotide, µL	30	60	90	120	150	180	210	240
2M TEAA (pH 7.0), µL	10	20	30	40	50	60	70	80
DMSO, µL	40	80	120	160	200	240	280	320
'Click catalyst', µL*	10	20	30	40	50	60	70	80
Sodium ascorbate (10 mM), µL	5	10	15	20	25	30	35	40

*The 'click catalyst' is prepared fresh by mixing 10 mM of tris[(1-benzyl-1*H*-1,2,3-triazol-4-yl)methyl]amine (TBTA) dissolved in DMSO and 10 mM of Cu(II) sulfate in water (1:1, v/v).

The oligonucleotides were dissolved in the required quantity of 2 M TEAA (pH 7.0) followed by addition of DMSO. The bright blue colored 'click catalyst' was then added to the above contents in a tube that was purged with argon, followed by addition of freshly prepared sodium ascorbate solution in water. Reaction mixture was kept overnight at room temperature. A 10 µL aliquot of the reaction mixture was taken and the oligonucleotide was precipitated by adding 25 µL of 2 M $LiClO_4$ and five-fold volume of acetone. The contents were centrifuged using an Eppendorf MiniSpin Plus at 14500 rpm, 14100 x*g*, for 2 min. The supernatant was discarded, and the pellet was washed carefully with acetone and dried. The dry pellet was dissolved in 10 µL milli-Q water and analyzed by reverse-phase HPLC for the product formation. After the completion of the reaction as shown by reverse phase HPLC, the oligos were precipitated by adding 1 mL of 2 M $LiClO_4$, ten-fold volume of acetone and mixed well. The contents were centrifuged using a Thermo Fisher Heraeus Multifuge X1R centrifuge with swing bucket rotor at 5000 rpm, 4700 x*g* for 30 min. The supernatant was discarded, and the pellet was washed carefully with acetone and dried. The dry pellet was dissolved in 10 mL milli-Q water, purified and isolated by reverse-phase HPLC on 250/4.6 mm, 5 µm, 300 Å C18 column (Thermo Fisher Scientific) in a gradient of CH_3CN (0→20% for 20 min, 1.3 mL/min) in 0.1 M TEAA buffer

(pH 7.0) with a detection at 260 nm. Purified oligos were freeze-dried, pellets were dissolved in milli-Q water (1.5 mL) and desalted by reverse-phase HPLC on 100/10 mm, 5 μm, 300 Å C18 column (Phenomenex) in a gradient of CH_3CN (0→80% for 15 min, 5 mL/min) in milli-Q water with detection at 260 nm. Cross-linked oligos were quantified by measuring absorbance at 260 nm, analyzed by ESI-MS and concentrated by freeze-drying.

2.10. Proof of cross-linking by RP-HPLC, HRMS and NMR experiments using an oligo synthesized for pilot studies

As the internal cross-linking strategy of oligos has been done rarely in the past, we decided to perform a pilot study of an oligo containing an alkyne attached to 2'-deoxyadenosine (**dA^{Y2}**) at +1 position and our azido sugar (**dR^{N3}**) at -2 position creating cross-link 1 (**Figure S1**). We performed a trial cross-linking of the sequence using CuAAC and monitored the reaction using reverse phase HPLC, isolated the product peak, which gave us the same mass as that of the starting material as the product and starting material have the same atomic composition (**Figures S2** and **S3**). While this was one of the proofs of cross-linking, we decided to use NMR experiments to provide further evidence of the successful cross-linking.

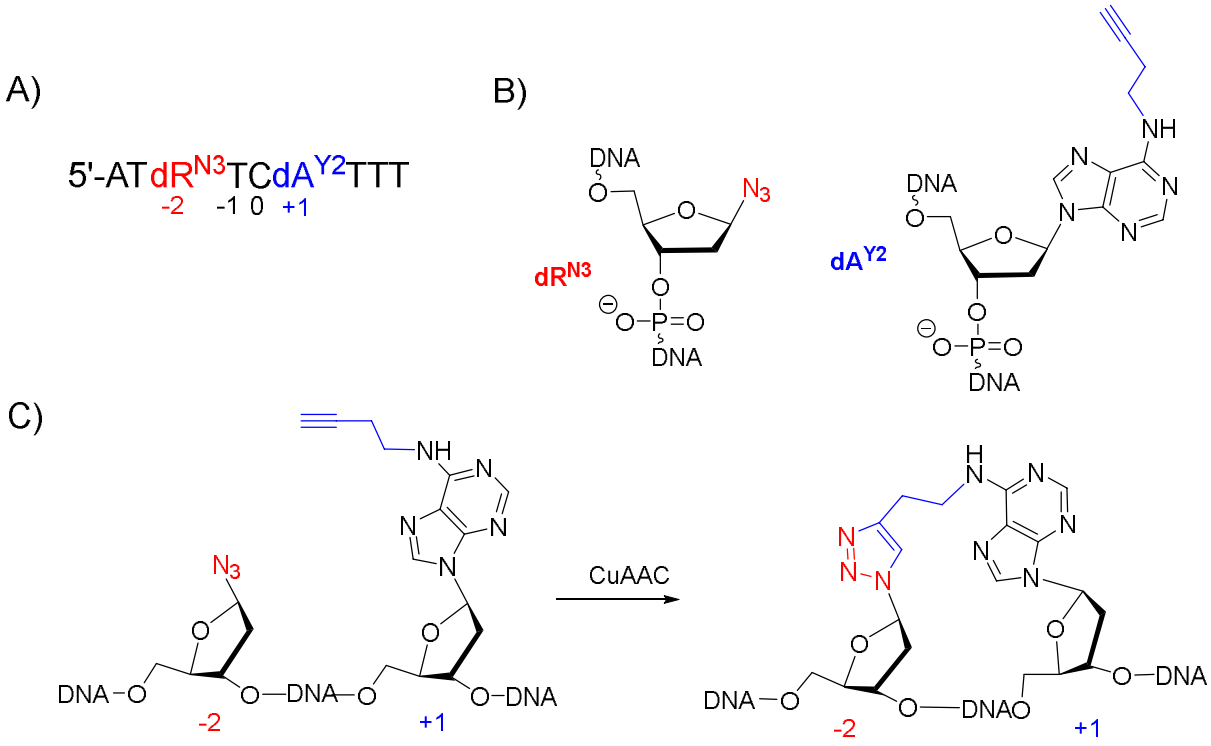

Figure S1. (A) Sequence of a linear oligo dC[R^{N3}(–2), A^{Y2}(+1)] used for internal cross-linking pilot study. (**B**) Chemical structure of modifications used in the sequence. (**C**) A representation of the cross-linking reaction using CuAAC.

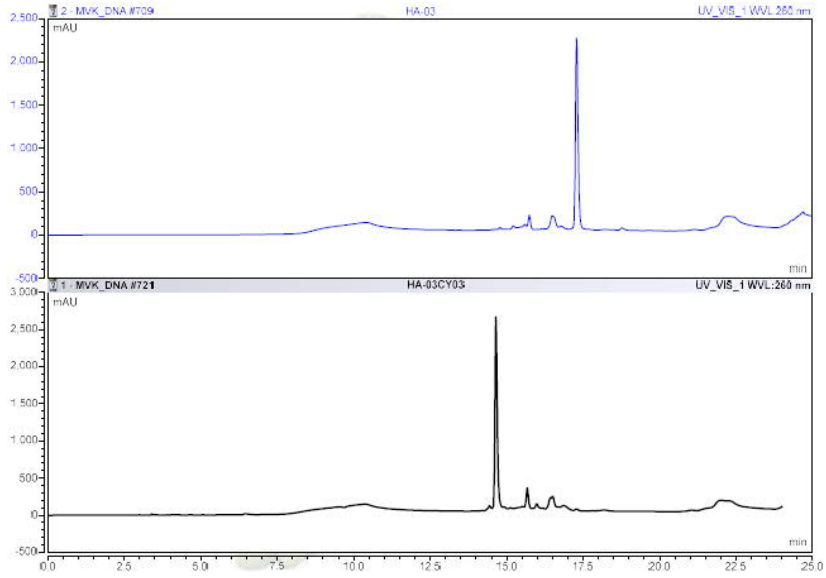

Figure S2. RP-HPLC profiles (on 250/4.6 mm, C18 column) of oligo used in pilot study before (top) and after (bottom) CuAAC reaction showing the difference in retention times of the starting material and the cross-linked product.

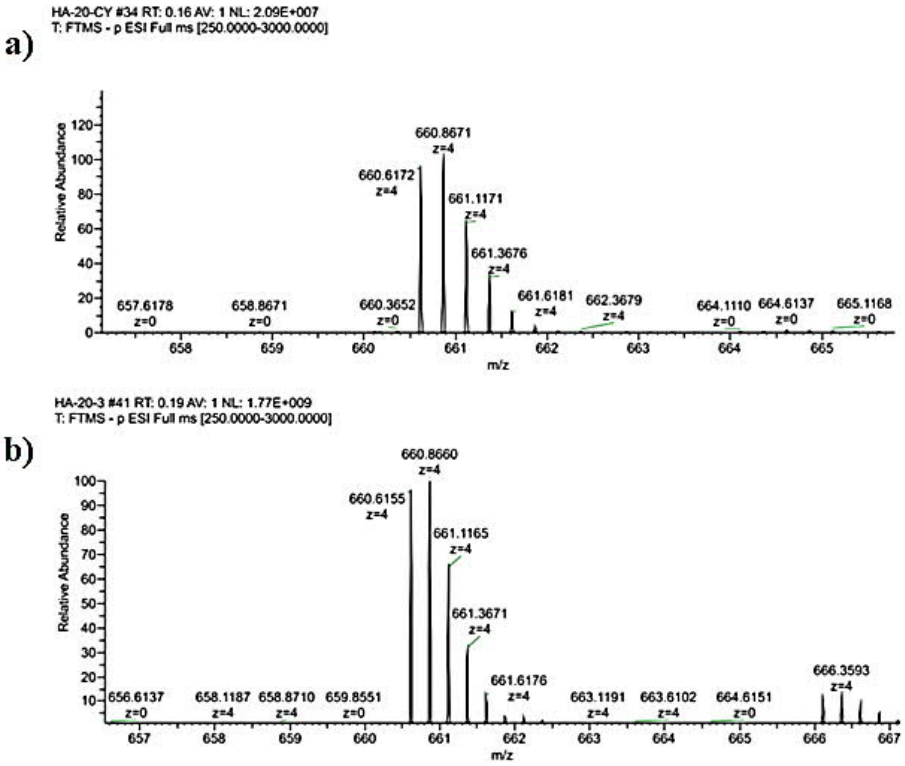

Figure S3. HRMS spectra showing the m/z of linear oligo (**a**) and cross-linked oligo (**b**) done as a part of the pilot study.

^{1}H NMR of linear oligo and cross-linked oligo showed an obvious difference in the overall chemical shifts (**Figures S4** and **S5**) All the methyl peaks arising from the thymidines were shifted (between 1.6 to 2.0 ppm) in cross-linked oligo compared to the linear oligo (**Figure S13**), suggesting the formation of a new product (cross-linked oligo) as the result of CuAAC

reaction. The anomeric proton of the azide 2'-deoxyribose in the linear oligo (triplet at 5.64 ppm, J = 5.60 Hz) and anomeric proton of the triazole nucleoside on the cross-linked oligo (6.16-6.18 ppm as a part of a multiplet) had different chemical shifts. Assignment of these peaks was done by 2D NMR experiments. In the linear oligonucleotide only one of the anomeric protons at 5.64 ppm has no cross peaks with the aromatic region as there is no aromatic nucleobase in the azide nucleotide as shown by the HMBC and NOESY NMR experiments (**Figures S6-S8**). When it was cross-linked, there was an additional proton (8.13 ppm) in the aromatic region together with four aromatic protons of 2'-deoxyadenosines (**Figure S9**). This proton has a cross peak with the proton at 6.18 ppm in the NOESY NMR spectrum, which is the anomeric proton of the triazole nucleotide (**Figure S10**). In addition, acetylenic proton (2.44 ppm) in the linear oligo was also assigned by HMBC NMR cross peak with the $\underline{C}H_2$ (18.30 ppm) immediately next to it (**Figures S11 and S12**). This characteristic peak was absent in the cross-linked oligo and provided additional evidence of the successful cross-linking by CuAAC.

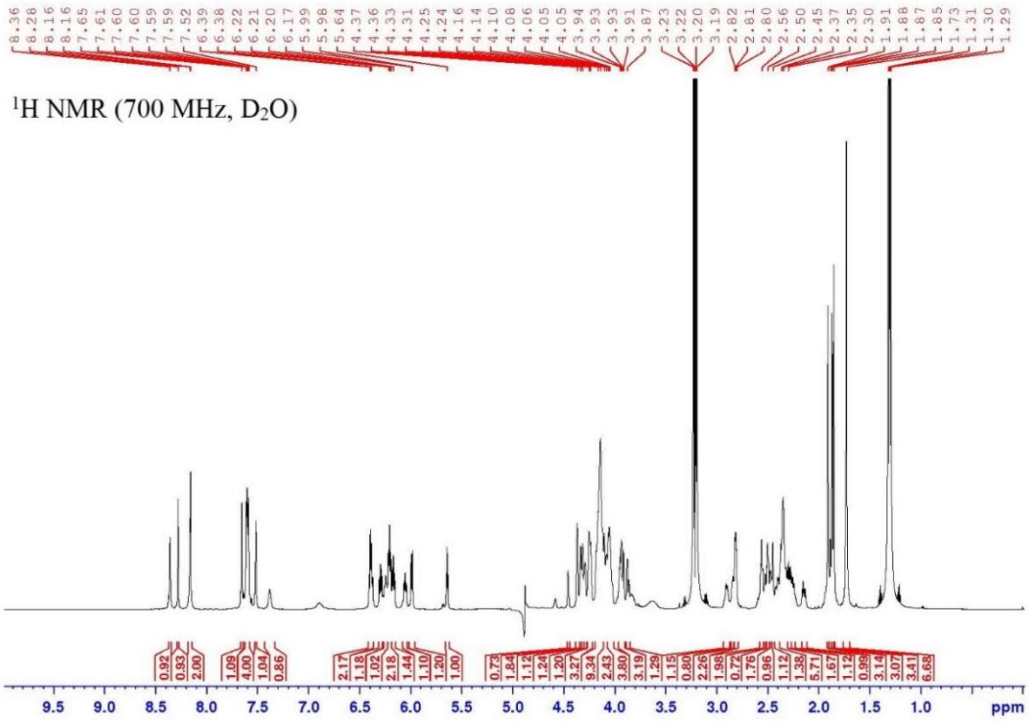

Figure S4. ^{1}H NMR spectrum of the linear oligonucleotide dC[R^{N3}(–2), A^{Y2}(+1)] used in internal cross-linking pilot study.

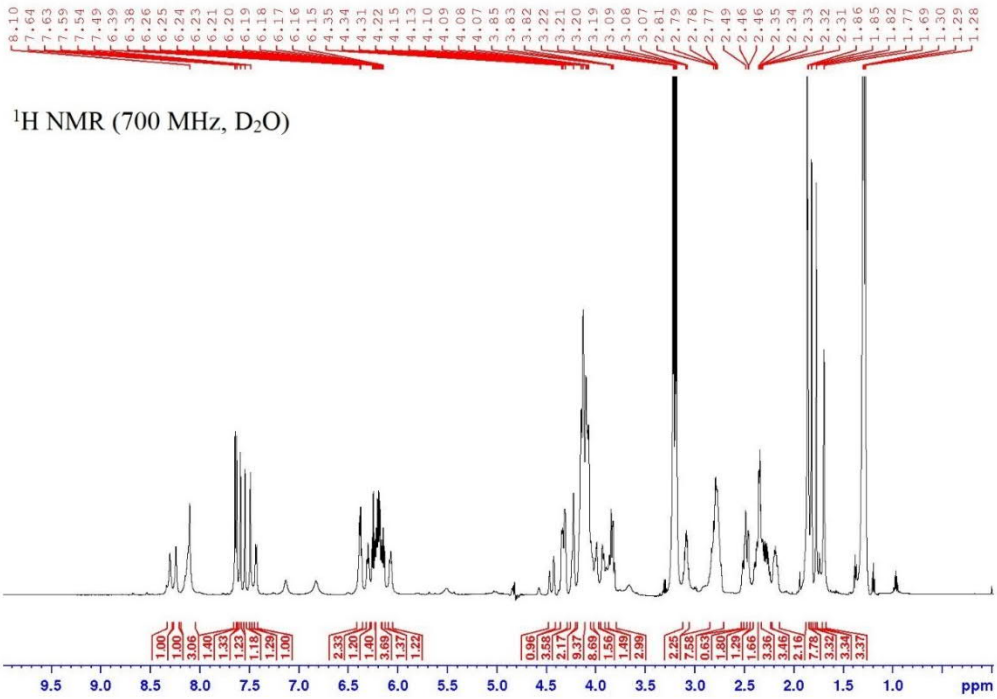

Figure S5. ^{1}H NMR spectrum of the cross-linked oligonucleotide dC[R^{N3}(–2), A^{Y2}(+1)]X used in internal cross-linking pilot study.

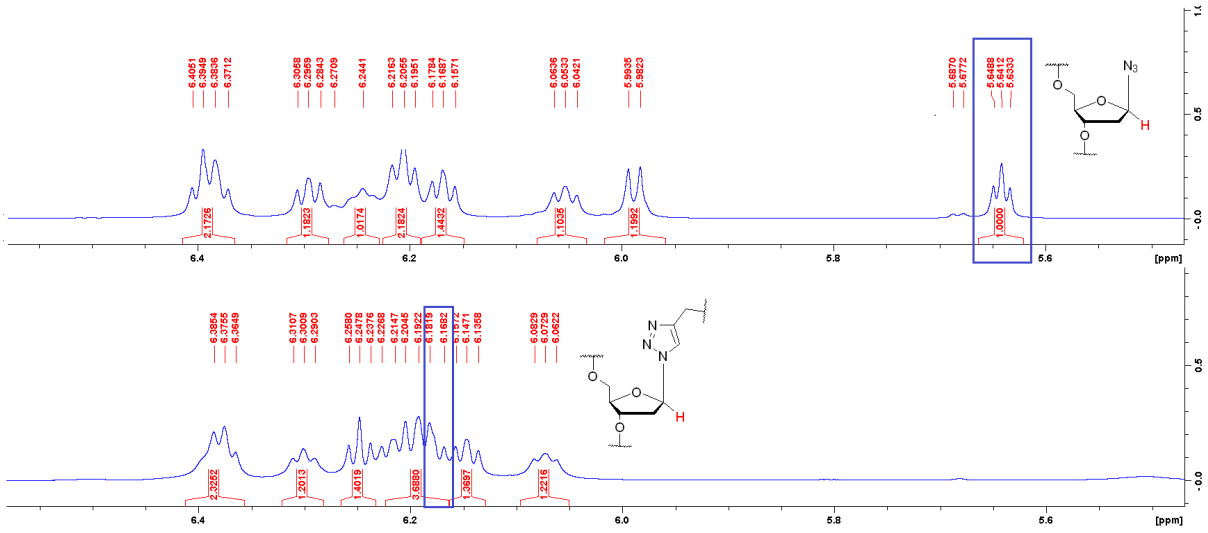

Figure S6. ^{1}H NMR spectra showing characteristic chemical shifts of anomeric protons of azido nucleotide (bottom) and triazole nucleotide after CuAAC (top).

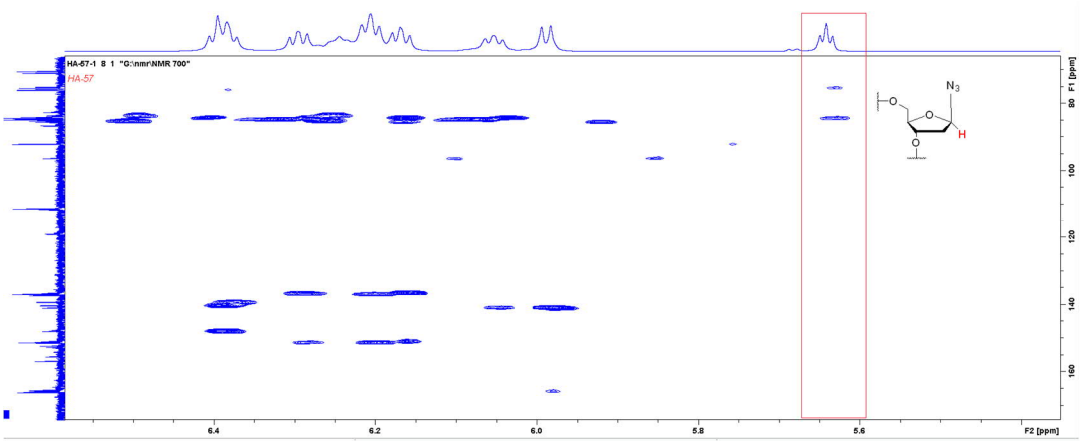

Figure S7. HMBC NMR spectrum showing no cross-peaks between the anomeric proton of azido nucleoside and aromatic carbons.

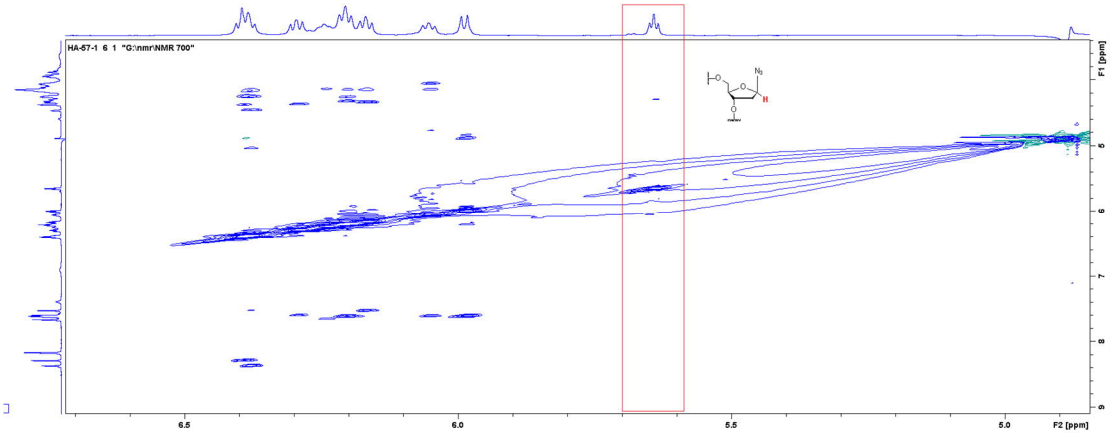

Figure S8. NOESY NMR spectrum showing no cross-peaks between anomeric proton of azido nucleotide and aromatic protons (see area in the box).

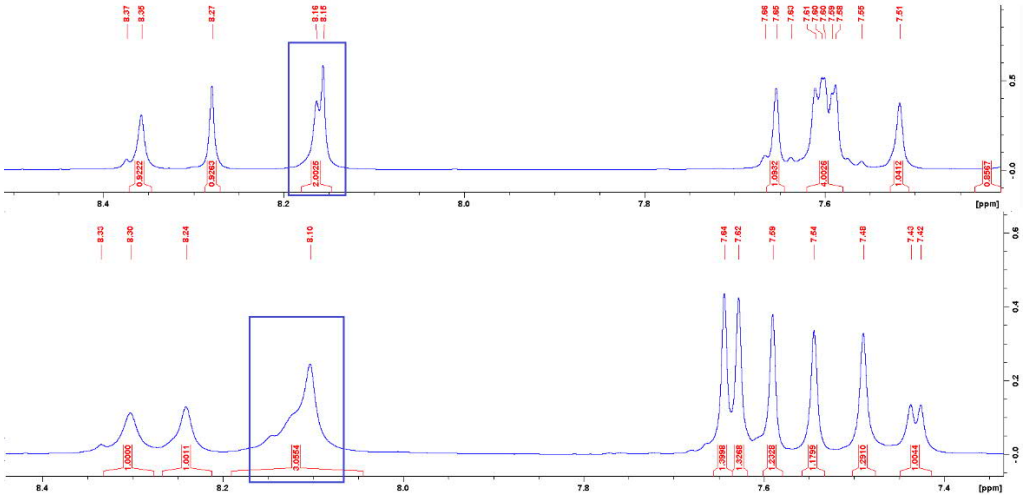

Figure S9. ^{1}H NMR spectra showing the aromatic protons without the triazole proton in the linear oligonucleotide (top) and with the triazole proton (bottom) in the cross-linked oligonucleotide. Area in the box shows appearance of an extra proton that belongs to a triazole in the cross-linked oligo, in comparison with the linear oligo (top).

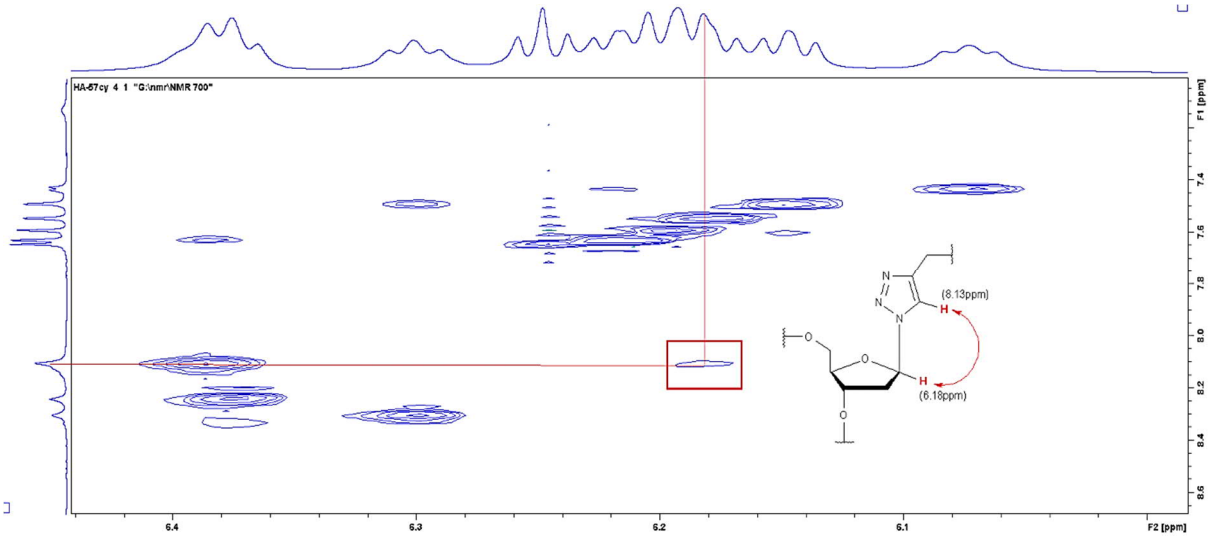

Figure S10. NOESY NMR spectrum showing cross-peaks of a triazole proton and an anomeric proton of the triazole nucleotide.

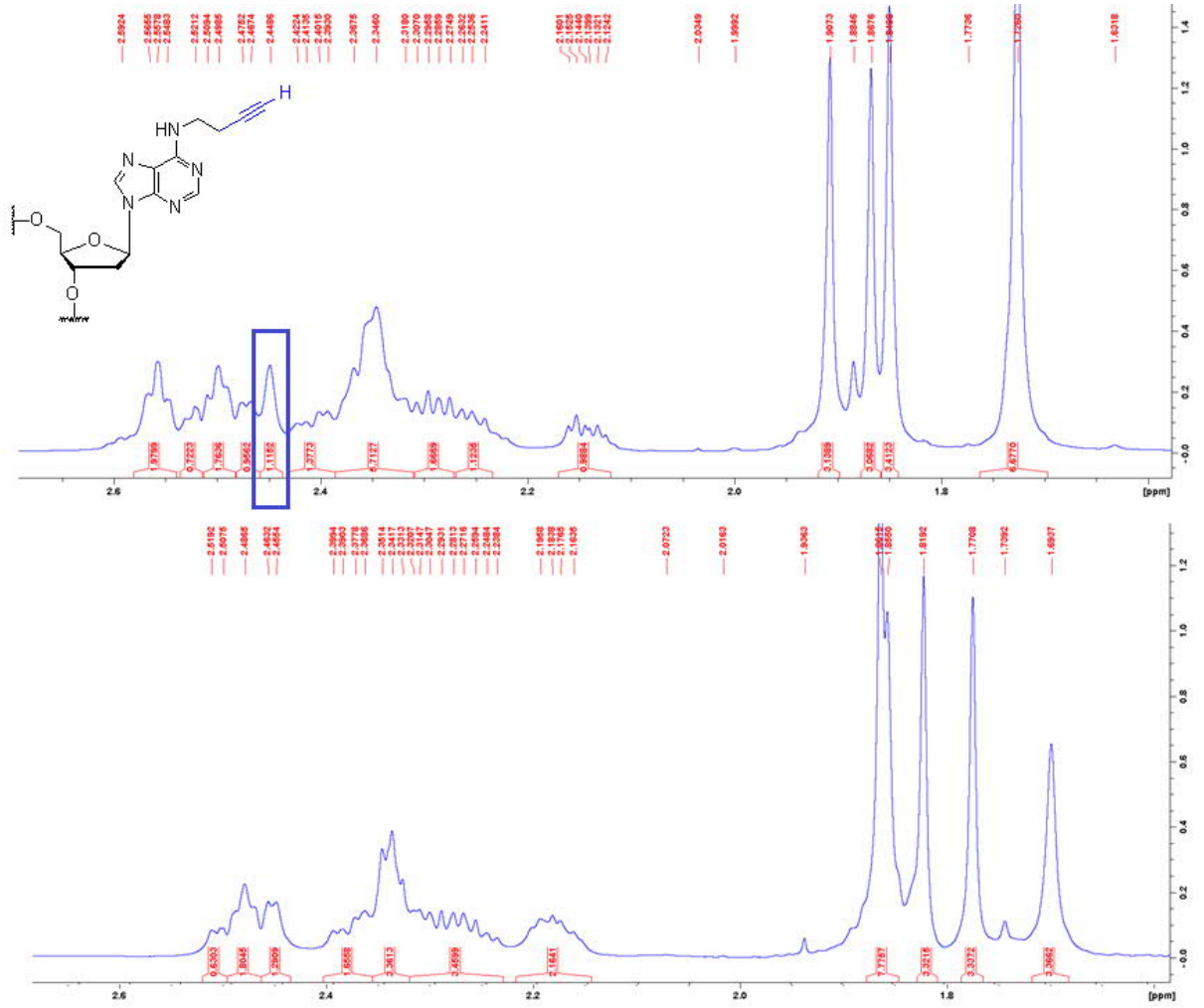

Figure S11. ^{1}H NMR showing acetylenic proton attached to 2'-deoxyadenosine nucleotide in the linear oligonucleotide (top) and the absence of it in the cross-linked oligo (bottom).

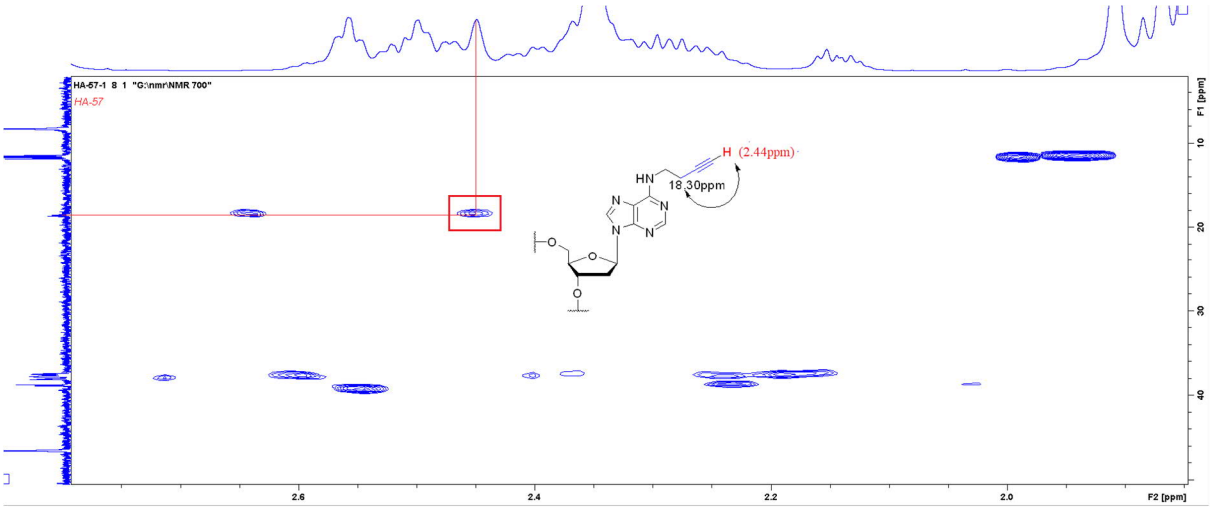

Figure S12. HMBC NMR spectrum showing two cross-peaks of acetylenic proton attached to 2'-deoxyadenosine with the $\underline{C}H_2$ in the linear oligo.

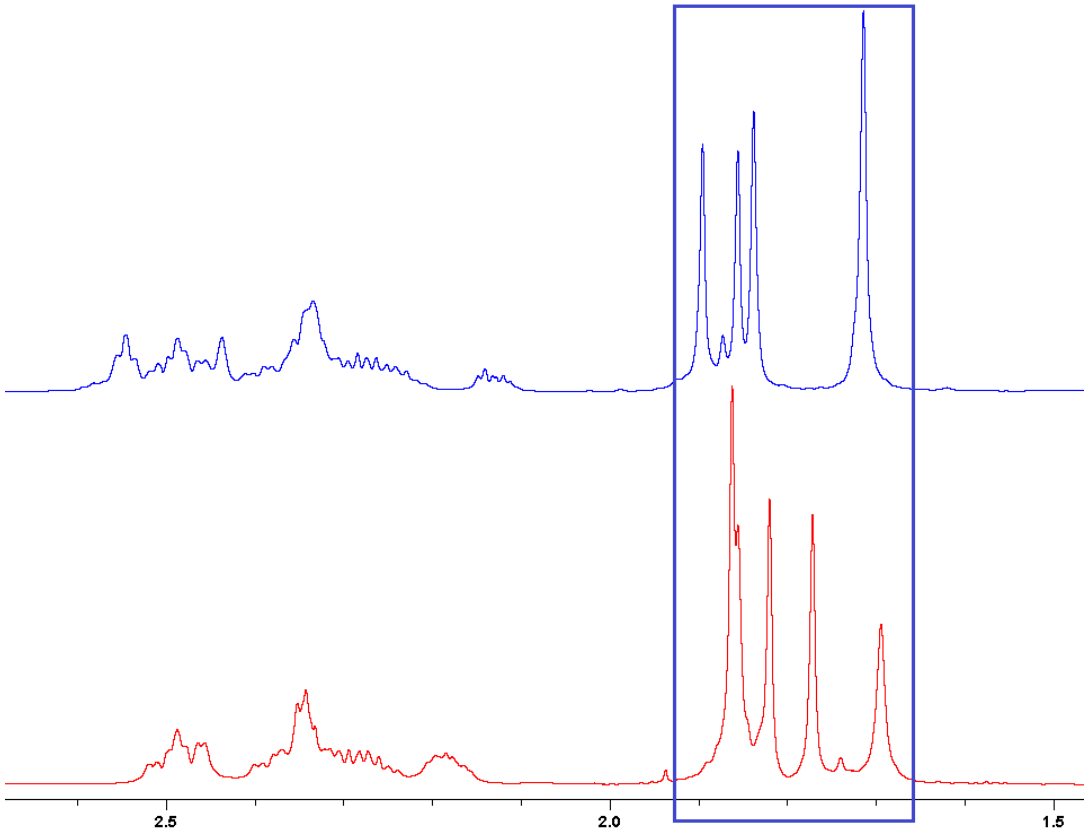

Figure S13. ^{1}H NMR chemical shifts of methyl peaks arising from five thymidines in linear (top) and cross-linked (bottom) oligos.

The above NMR experiments together with reverse-phase HPLC retention time differences and HRMS suggest the formation of the monomeric cross-linked oligo as a product of CuAAC reaction.

6. Enzymes used in the current study

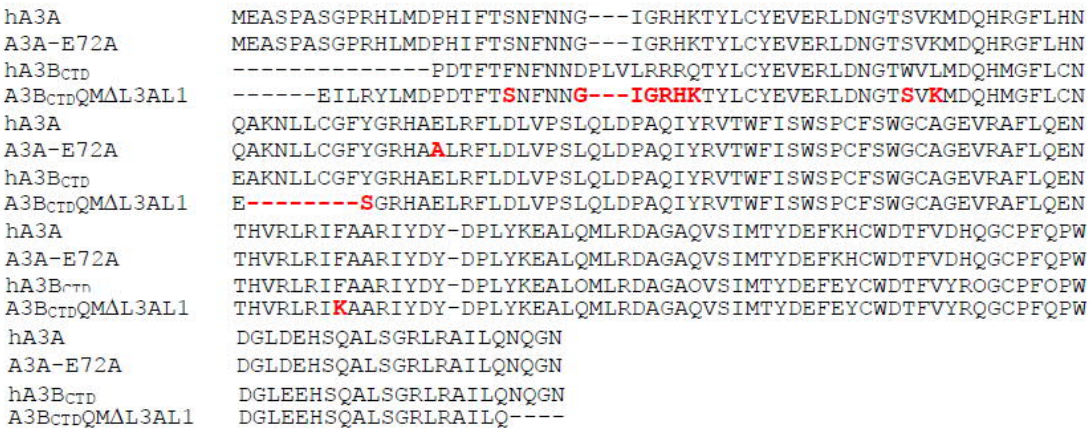

Figure S14. Amino acid sequences of human A3A (hA3A, hA3B$_{CTD}$ in comparison with the enzymes used in this work. A3B$_{CTD}$ is the C-terminal domain of A3B. A3B$_{CTD}$-QM-ΔL3-AL1swap (loop 1 swapped with A3A); A3A-E72A-active site glutamate mutated to alanine.

7. Kinetic characterization of 5'-T_4CAT as a substrate of A3B$_{CTD}$-QM-ΔL3-AL1swap

For the purpose of inhibition assays, we decided to use a 7-mer DNA oligo 5'-T_4CAT as substrate instead of our previously reported procedure with 9-mer oligo 5'-AT_3CAT_3. This was due to the complex ^{1}H NMR spectrum arising from the broad singlets of 2'-deoxyadenosines' amines seen for the 9-mer oligo substrate (**Figure S15A**). In contrast, 5'-T_4CAT produced a much cleaner spectrum (**Figure S15B**), making it easier for evaluation and quantification of deamination reaction. A3-catalyzed deamination was evaluated using the NMR-based assay described previously.[5-7] Data acquisitions were done on a 700-MHz Bruker NMR spectrometer equipped with a 1.7 mm cryoprobe at 298 K. A series of ^{1}H NMR spectra was recorded of the substrate at various concentrations from 200 to 800 µM with 300 nM of A3B$_{CTD}$-QM-ΔL3-AL1swap[8] in buffer (pH 6.0) containing 50 mM sodium phosphate, 100 mM NaCl, 2.5 mM β-mercaptoethanol, 0.1 M EDTA, 50 µM 3-(trimethylsilyl)-2,2,3,3-tetradeuteropropionic acid (TSP). The H-5 proton doublet signal of the cytosine, which appears at 5.88 ppm (J = 7.7 Hz), was baselined and integrated (**Figure S15B**). The signal of TSP at 0 ppm was used as an internal standard to determine the concentration of the substrate and its conversion during the reaction to the product, for which the signal appears at 5.71 ppm (J = 8.3 Hz).

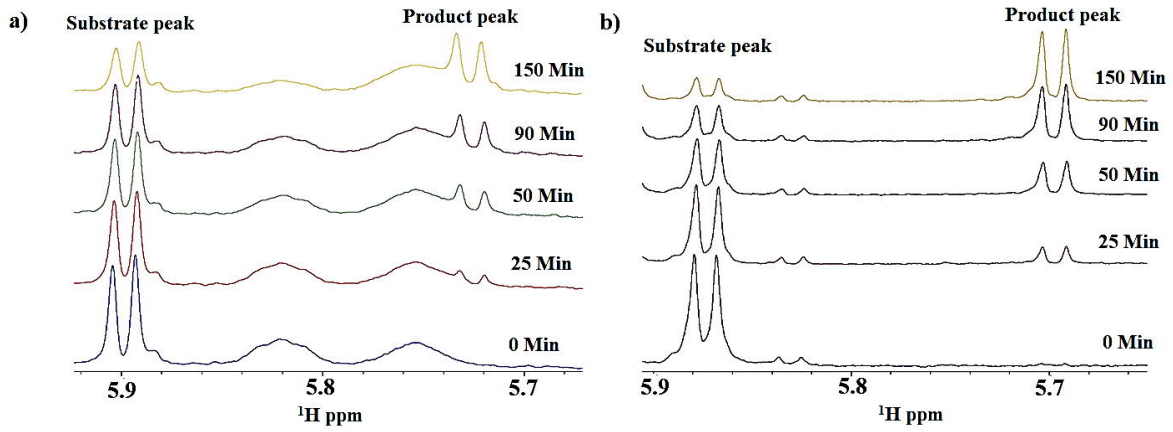

Figure S15. (**a**) ^{1}H-NMR spectra for the substrate (5'-AT_3CAT_3) and its conversion to the product (5'-AT_3**dU**AT_3, **dU** is 2'-deoxyuridine) over time in the presence of A3B$_{CTD}$-QM-ΔL3-AL1swap (50 nM) at 298 K in activity assay buffer (pH 5.5) containing 10 % deuterium oxide; 50 mM citrate-phosphate, 200 mM NaCl, 2 mM β-mercaptoethanol, 200 µM 4,4-dimethyl-4-silapentane-1-sulfonic acid (DSS). (**b**) ^{1}H-NMR spectra for the substrate (5'-T_4CAT) and its conversion to the product (5'-T_4**dU**AT) over time in the presence of A3B$_{CTD}$-QM-ΔL3-AL1swap (300 nM) at 298 K in activity assay buffer (pH 6.0) containing 50 mM sodium phosphate, 100 mM NaCl, 2.5 mM β-mercaptoethanol, 0.1 M EDTA, 50 µM 3-(trimethylsilyl)-2,2,3,3-tetradeuteropropionic acid (TSP).

The area of the integrated signal was converted to substrate concentration and plotted versus reaction time. Linear regression was used to fit the data to determine the initial speed of the reaction. **Figure S16** shows the relationship between speed of the deamination reaction and substrate concentration for $A3B_{CTD}$-QM-ΔL3-AL1swap. The double reciprocal plot which shows the linear dependence of substrate concentration on the speed of deamination **(Figure S17)** were then fitted with linear regression to determine K_m and k_{cat} for $A3B_{CTD}$-QM-ΔL3-AL1swap using the following formula with enzyme concentration [E] = 300 nM:

$$y = V_0 = k_{cat}[\mathrm{E}]\frac{[\mathrm{S}]}{K_m + [\mathrm{S}]}$$

$$\frac{1}{V_0} = \frac{K_m + [\mathrm{S}]}{k_{cat}[\mathrm{E}][\mathrm{S}]}$$

$$\frac{1}{V_0} = \frac{K_m}{k_{cat}[\mathrm{E}]}\frac{1}{[\mathrm{S}]} + \frac{1}{k_{cat}[\mathrm{E}]}$$

$$y = ax + b$$

where a and b are, respectively, the slope and intercept obtained from the plot shown in **Figure S17**.

$$b = \frac{1}{k_{cat}[\mathrm{E}]} = 17.95\ \mathrm{s\ \mu M^{-1}}$$

$$k_{cat} = 0.19 \pm 0.03\ \mathrm{s^{-1}}$$

$$a = \frac{K_m}{k_{cat}[\mathrm{E}]} = 6335.4\ \mathrm{s}$$

$$K_m = {}^{a}/_{b} = 352 \pm 65\ \mu\mathrm{M}$$

Uncertainties in a and b were calculated from regression fit (**Figure S17**) using LINEST function of Excel and uncertainties in K_m and k_{cat} were calculated by standard error propagation, as detailed by us.[6]

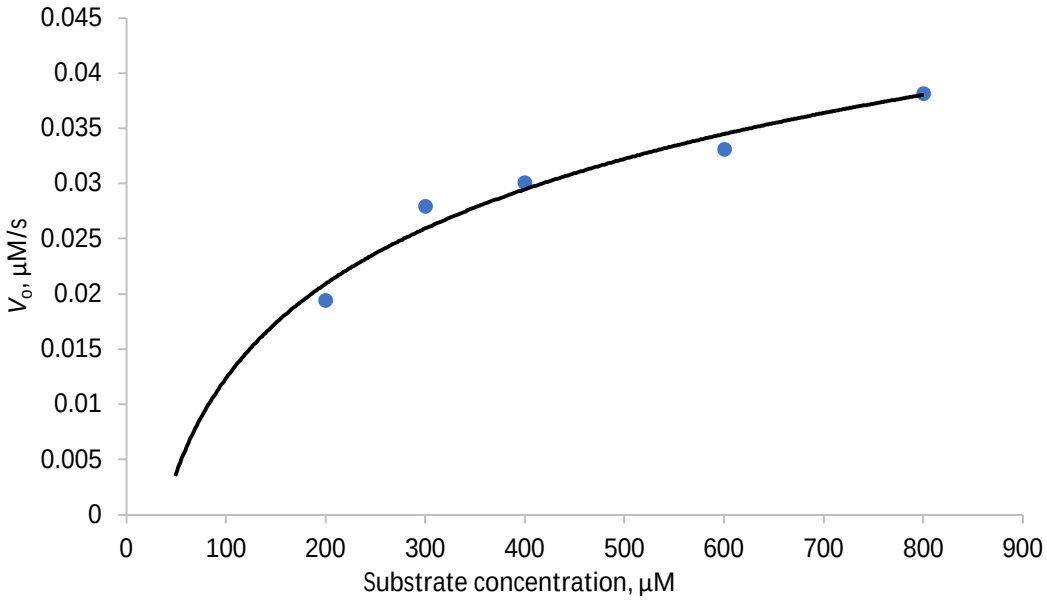

Figure S16. Initial rate of deamination 5'-T_4CAT catalyzed by $A3B_{CTD}$-QM-ΔL3-AL1swap (300 nM) as a function of substrate concentration. The curve is for visual reference only.

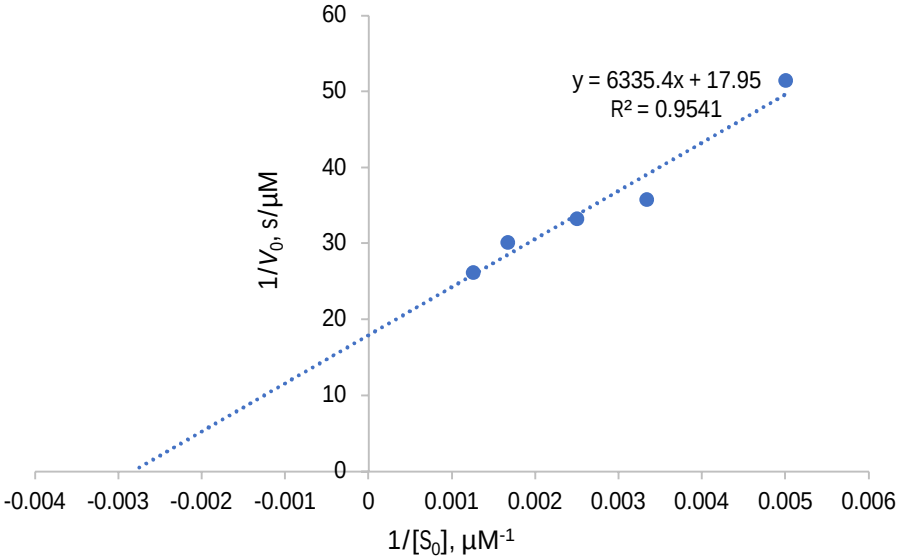

Figure S17. Double reciprocal plot of inversed speed of deamination catalyzed by $A3B_{CTD}$-QM-ΔL3-AL1swap (300 nM) as a function of the inversed substrate concentration (5'-T_4CAT), showing the linear dependence of speed of deamination with the concentration of the substrate.

The non-linear regression analysis of the data is presented in **Figure S18** and was performed by XLSTAT add-on in Excel (Microsoft) using the Michaelis-Menten enzyme kinetic equation providing the following parameters of the system:

Table S2. Model parameters of A3B$_{CTD}$-QM-ΔL3-AL1swap catalyzed deamination of 5'-T$_4$CAT obtained using non-linear regression analysis.

Parameters	Value	Standard error
V_{max}, μM/s	0.051	0.005
K_m, μM	291.966	67.145

A) B) C)

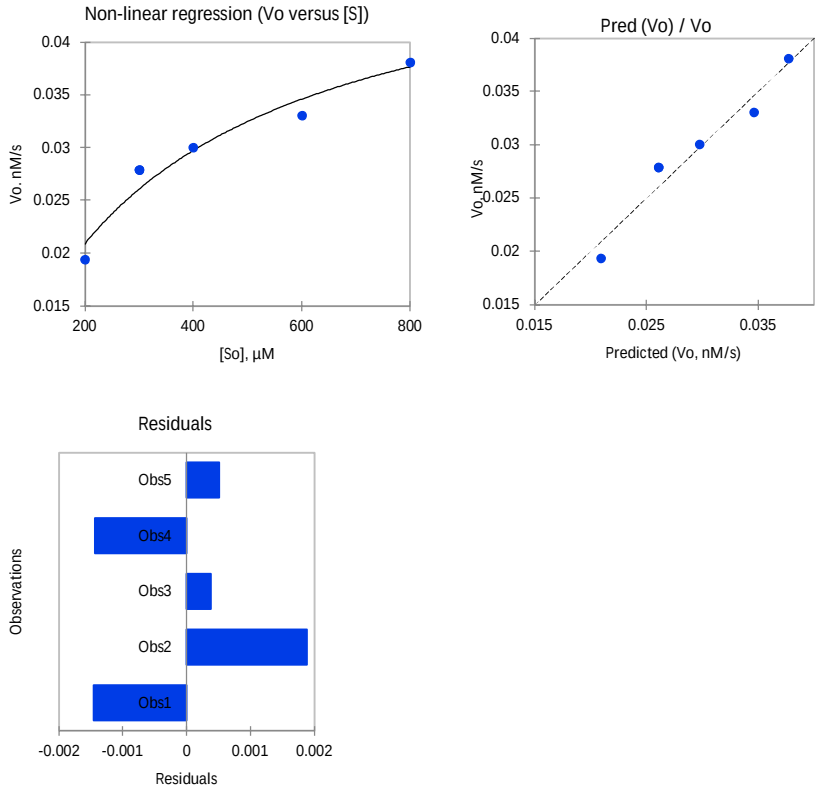

Figure S18. Non-linear regression analysis of A3B$_{CTD}$-QM-ΔL3-AL1swap-catalyzed cytosine deamination of 5'-T$_4$CAT. A) Plot of initial rate of deamination V_0 as a function of substrate concentration [S_0] fitted with a non-linear regression model to derive K_m and V_{max} reported in Table 2 (main text); B) observed versus predicted values of initial rate of deamination; C) Residuals calculated from the model for each observation, showing random distribution of residuals.

8. Evaluation of substrate activity of cross-linked oligonucleotides using ^{1}H NMR assay

Substrate preference and deamination activity by A3B$_{CTD}$-QM-ΔL3-AL1swap on the synthesized cross-linked oligonucleotides with dC were evaluated using the NMR-based assay as described above using substrates and A3B$_{CTD}$-QM-ΔL3-AL1swap at concentrations shown in **Figure 4** (main text) in a buffer (pH 6.0) containing 10 % deuterium oxide, 50 mM citrate-phosphate, 200 mM NaCl, 2 mM β-mercaptoethanol, 200 µM 4,4-dimethyl-4-silapentane-1-sulfonic acid (DSS). The H-5 proton doublet signals of the cytosine from different oligonucleotides were baselined and integrated. A doublet of doublets at 2.63 ppm originating from the citrate buffer or peaks of TSP or DSS were used as an internal standard to determine the concentration of the substrate which appears at 5.88 ppm (J = 7.7 Hz) and converted to 5.71 ppm (J = 8.3 Hz) during the reaction over a period of time (**Figure S15B**). The integrated signal area was converted to substrate concentration and plotted versus time of the reaction. The data were then fitted with linear regression to determine the initial speed of the reaction.

9. Qualitative evaluation of inhibitors of A3B$_{CTD}$-catalyzed deamination using ^{1}H NMR assay

Competitive inhibition of the synthesized oligonucleotides was performed by a similar procedure reported by us previously.[6, 7] A series of spectra was recorded in a similar fashion as that of substrate analysis. Here, we used 400 μM of a standard 7-mer oligonucleotide substrate 5'-T$_4$CAT, 8 μM of **dZ**-containing cross-linked oligos, 300 nM of A3B$_{CTD}$-QM-ΔL3-AL1swap in a buffer containing 50 mM sodium phosphate (pH 6.0), 100 mM NaCl, 2.5 mM β-mercaptoethanol, 0.1 M EDTA, 50 μM TSP. Deamination activity was monitored by the same method as for DNA substrates.

10. Quantitative evaluation of inhibitors of A3B$_{CTD}$-catalyzed deamination using ^{1}H NMR assay

The best inhibitors were characterized further by varying the concentration of the inhibitor ranging from 1 μM to 8 μM in the presence of 300 nM of A3B$_{CTD}$-QM-ΔL3-AL1swap in activity assay buffer. After the rate of the reaction was determined at various inhibitor concentrations, the data were analyzed by different methods.

2.11. Analysis of inhibitors of A3B$_{CTD}$-catalyzed deamination using Dixon plot

In the first instance, the data were analyzed using a plot of inverse speed versus inhibitor concentration, the so-called Dixon plot (**Figure S19**), which was then fitted with linear regression to derive the inhibition constant (K_i).

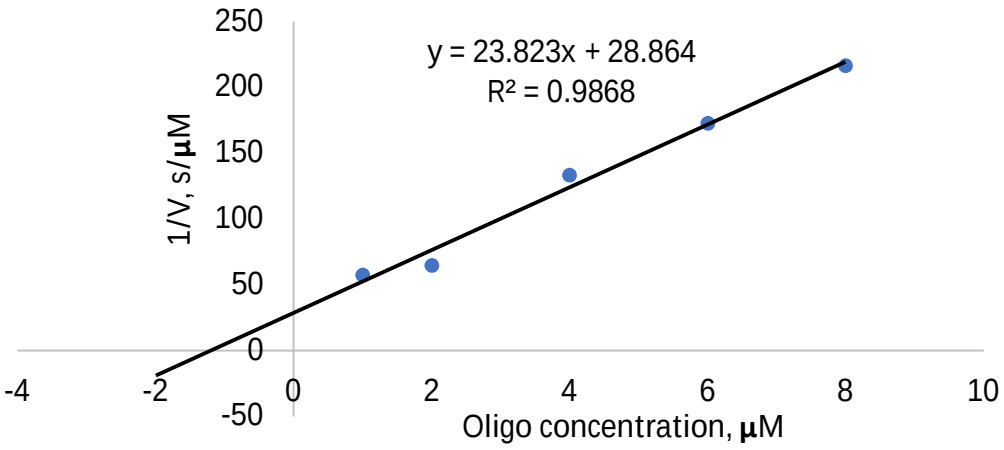

Figure S19. Dixon plot of inversed rates of A3B$_{CTD}$-QM-ΔL3-AL1swap-catalyzed deamination of 5'-T$_4$CAT (400 μM) at various concentrations of cross-linked oligo at 298 K. Enzyme concentration is 300 nM.

Here, we assumed the competitive character of inhibition and, therefore, Michaelis-Menten expression for deamination velocity *v* becomes:

$$v = \frac{v_{\max}[\mathrm{S}]}{K_{\mathrm{m}}\left[1 + \frac{[\mathrm{I}]}{K_{\mathrm{i}}}\right] + [\mathrm{S}]}$$

$$\frac{1}{v} = \left[\frac{K_{\mathrm{m}}}{K_{\mathrm{i}} v_{\max}[\mathrm{S}]}\right][\mathrm{I}] + \frac{K_{\mathrm{m}} + [\mathrm{S}]}{v_{\max}[\mathrm{S}]}$$

By using K_{m} derived from the Lineweaver-Burk plot (**Figure S17**) and using the trend line for dZ[U^{E}(-2), A^{N3}(+1)]X:

$$y = ax + b$$

$$b = 35.692\ \mu\mathrm{M}^{-1}, a = 24.061\ \mathrm{s}\ \mu\mathrm{M}^{-1}$$

$$K_{\mathrm{m}} = 353\ \mu\mathrm{M}, [\mathrm{S}] = 400\ \mu\mathrm{M}$$

$$K_{\mathrm{i}} = \frac{K_{\mathrm{m}} b k_{\mathrm{cat}}[\mathrm{S}]}{a k_{\mathrm{cat}}[\mathrm{S}](K_{\mathrm{m}} + [\mathrm{S}])} = \frac{b K_{\mathrm{m}}}{a(K_{\mathrm{m}} + [\mathrm{S}])} = 0.66 \pm 0.14\ \mu\mathrm{M}$$

Uncertainties in *a* and b were calculated from regression fit (**Figure S19**) using LINEST function of Excel; uncertainty of K_{i} was calculated by standard error propagation, as detailed by us.[6]

2.12. Analysis of inhibitors of A3B$_{CTD}$-catalyzed deamination using non-linear regression

The second method used the non-linear regression analysis using XLSTAT add-on in Excel (Microsoft) and performing a three-parameter fit ($V_{\max}$, K_{m} and K_{i}) in the Michaelis-Menten enzyme kinetic equation for the competitive inhibitor. Statistical parameters and details of non-linear regression analysis are provided below.

Table S3. Correlation matrices for non-linear regression analysis of $A3B_{CTD}$-QM-ΔL3-AL1swap-catalyzed deamination of 5'-AT_3CAT_3 in the presence of varying concentrations of **dZ**-linear.

Variable	[S]	[I]	Rate
[S]	**1.000**	0.181	0.547
[I]	0.181	**1.000**	-0.604
Rate	0.547	-0.604	**1.000**

Table S4. Correlation matrices for non-linear regression analysis of $A3B_{CTD}$-QM-ΔL3-AL1swap-catalyzed deamination of 5'-T_4CAT in the presence of varying concentrations of cross-linked inhibitor.

dZ[U^E(-2),A^{N3}(+1)]X

Variable	[S]	[I]	Rate
[S]	**1.000**	-0.120	0.408
[I]	-0.120	**1.000**	-0.856
Rate	0.408	-0.856	**1.000**

Table S5. Statistics of fit for non-linear regression analysis $A3B_{CTD}$-QM-ΔL3-AL1swap-catalyzed deamination of 5'-AT_3CAT_3 in the presence of varying concentrations of **dZ**-linear.

Statistic	dZ-linear
Observations	12
DF	9.000
R^2	0.975
SSE	0.000
MSE	0.000
RMSE	0.001
AIC	-177.018
AICC	-171.304
Iterations	8.000

Table S6. Statistics of fit for non-linear regression analysis $A3B_{CTD}$-QM-ΔL3-AL1swap-catalyzed deamination of 5'-T_4CAT in the presence of varying concentrations of inhibitor.

Statistic	dZ[U^E(-2),A^{N3}(+1)]X
Observations	23
DF	20
R^2	0.964
SSE	0.000
MSE	0.000
RMSE	0.002
AIC	-277.790
AICC	-275.567
Iterations	5.000

Table S7. Parameters of $A3B_{CTD}$-QM-ΔL3-AL1swap-catalyzed deamination of 5'-AT_3CAT_3 in the presence of varying concentrations of **dZ**-linear using non-linear regression analysis.

Parameters	**dZ**-linear	
	Value	Standard error
V_{max}, μM/s	0.0126	0.0008
K_m, μM	146.	28
K_i, μM	7.0	1.3

Table S8. Parameters of $A3B_{CTD}$-QM-ΔL3-AL1swap-catalyzed deamination of 5'-T_4CAT in the presence of varying concentrations of cross-linked inhibitor using non-linear regression analysis.

Parameters	dZ[U^E(-2), A^{N3}(+1)]X	
	Value	Standard error
V_{max}, μM/s	0.052	0.006
K_m, μM	320	90
K_i, μM	0.69	0.14

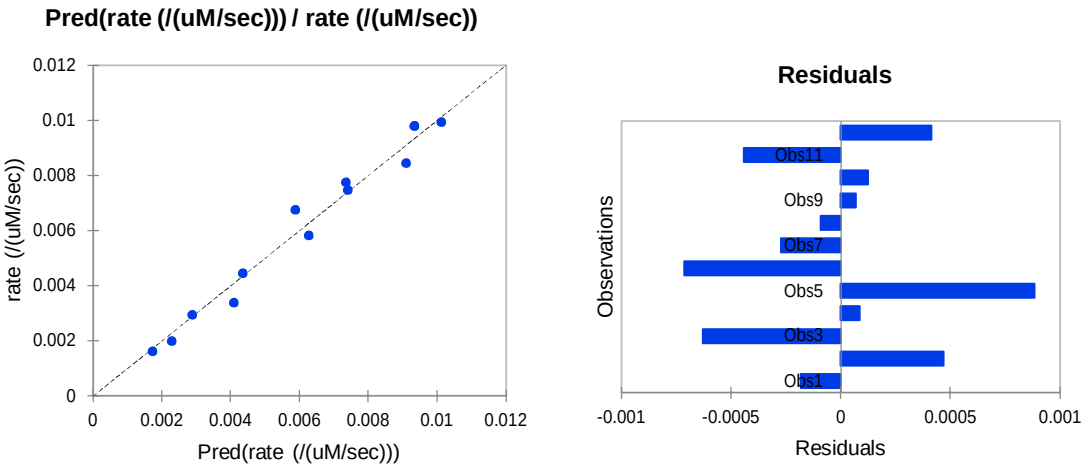

Figure S20. Non-linear regression analysis of $A3B_{CTD}$-QM-ΔL3-AL1swap-catalyzed cytosine deamination of AT_3CAT_3 in the presence of varying concentrations of **dZ**-linear inhibitor. Left column: observed versus predicted values of initial rate of deamination; Right column: residuals calculated from the model for each observation.

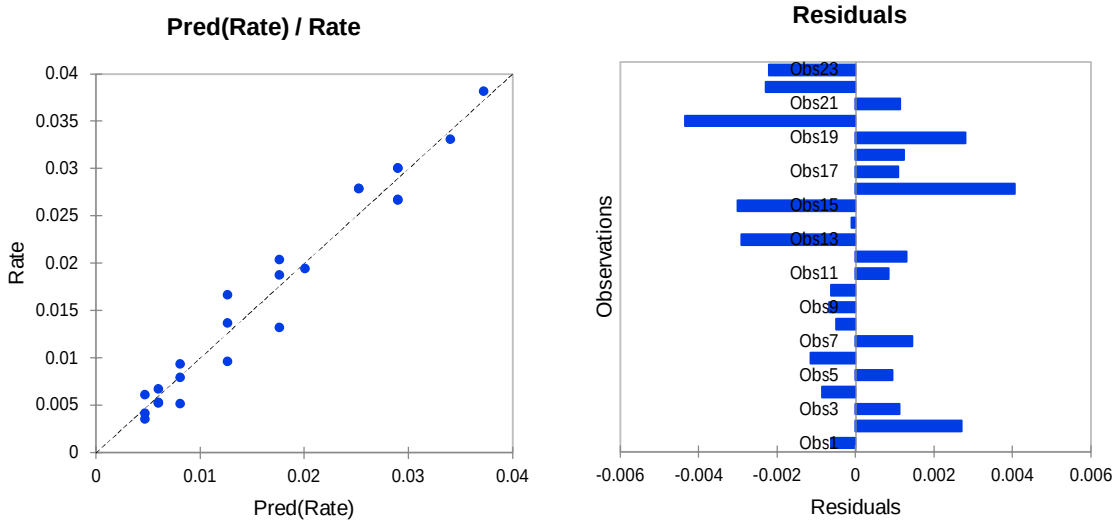

Figure S21. Non-linear regression analysis of $A3B_{CTD}$-QM-ΔL3-AL1swap-catalyzed cytosine deamination of 5'-T_4CAT in the presence of varying concentrations of cross-linked inhibitor dZ[U^E(-2), A^{N3}(+1)]X. Left column: observed versus predicted values of initial rate of deamination; Right column: residuals calculated from the model for each observation.

2.13. Evaluation of dZ[U^{E}(–2), A^{N3}(+1)]X as inhibitor of A3A

2.13.1. Expression of wild-type A3A

A3Awt with a His_6 fusion tag at the C-terminus was cloned into pET27-b(+) (via NdeI/BamHI). The plasmid was transformed into *E. coli* AI (T7 polymerase under control of the arabinose promotor) together with the helper plasmid pLysS. The cells were selected for kanamycin, tetracycline and chloramphenicol resistance on plates of non-inducing medium MDAG-135.[9] For expression, the cells were grown to 5 mL high density in MDAG-135 and then to 1 L volumes in ZYM-5052 supplemented with 100 µM $ZnCl_2$ and 0.05% (w/v) arabinose. After reaching 0.4 OD the cells, which were previously grown at 37 °C exclusively, were now cooled to 20 °C and incubated overnight. Next morning, all subsequent steps were performed at 4 °C. The cells were harvested by centrifugation at 10,000*g* for 10 min and resuspended in buffer (50 mM Na^+/K^+ phosphate pH 6.5, 300 mM sodium acetate, 300 mM (2-hydroxyethyl)trimethylammonium chloride (choline chloride), 200 mM NaCl, 1 mM TCEP with 1 tablet of complete ultra EDTA-free protease inhibitor). The cells were lysed on a French press at 4,000 – 5,000 psi and then sonicated at 35 W for 1 min. The cell lysate was centrifuged at 30,000*g* for 30 min and the supernatant applied to a Ni^{2+}-NTA affinity column (BioRad). After washing three times with the buffer the protein was eluted in the above buffer with 800 mM imidazole. The eluted liquid was saturated with $(NH_4)_2SO_4$ (ca 8 g in 25 mL) and all fractions containing proteins were precipitated. Aliquots were pelleted and then resuspended in the above buffer and used as needed.

2.13.2. Evaluation of dZ[U^{E}(–2), A^{N3}(+1)]X as inhibitor of His_6-A3A-catalyzed deamination of dC-hairpin using Lambert's W function

Time-resolved ^{1}H NMR kinetics were measured in 50 mM K^+/Na^+ phosphate buffer (pH 7.4) supplemented with 100 mM NaCl, 1 mM TCEP, 100 µM sodium trimethylsilylpropanesulfonate (DSS) and 10% D_2O. Substrate (dC-hairpin, TGCGCTTCGCGCT, underlined C is deaminated) was at 500 µM concentration. Reaction was performed in the presence of 140 nM of His_6-A3A at 298 K. The course of the reaction was followed by ^{1}H NMR until the substrate was consumed (28 hours). Subsequently the amount of substrate or product at each time point was calculated by integrating the decreasing substrate peak at 7.752 ppm (singlet) or the increasing product peak at 5.726 ppm (doublet) and calibrated by the area of DSS standard peak at 0.0 ppm. Using the known concentration of the standard, the peak was converted to a corresponding substrate concentration. The time at which each spectrum was recorded as a difference to the first spectrum was used as the time

passed. The product or substrate concentration *versus* the time of reaction was plotted and fitted using the integrated form of the Michaelis-Menten equation (**Figure S22A**):

$$[S]_t = K_m\, W\left(\frac{[S]_0}{K_m} \cdot e^{\frac{[S]_0 - V_{max}\, t}{K_m}}\right)$$

where W is Lambert's W function, $[S]_t$ is the substrate concentration at specific time, $[S]_0$ is the initial substrate concentration, V_{max} and K_m are the Michaelis-Menten constants and t is the time. The two Michaelis Menten constants, the initial substrate concentration and an offset which corrects for the integration baseline in the NMR spectra were fitted using Lambert's W function in Gnuplot.

By varying the concentration of an inhibitor, the plots of observed K_m versus inhibitor concentration were obtained (**Figures S22B** and **C**) and K_i values were calculated. This allowed determination of K_m of the substrate (21 ± 7 µM in **Figure S22B** and 17 ± 7 µM in **Figure S22C**) and K_i of inhibitors (360 ± 120 nM for dZ[U^E(–2), A^{N3}(+1)]X and 2.4 ± 0.9 µM for **FdZ**-linear).

A)

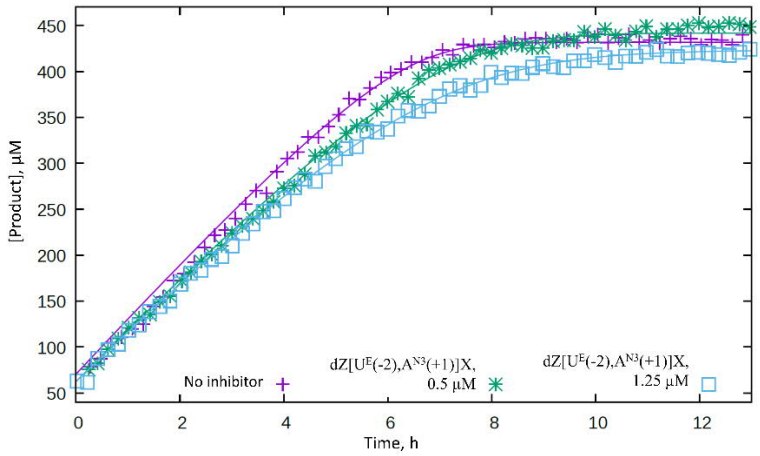

B)

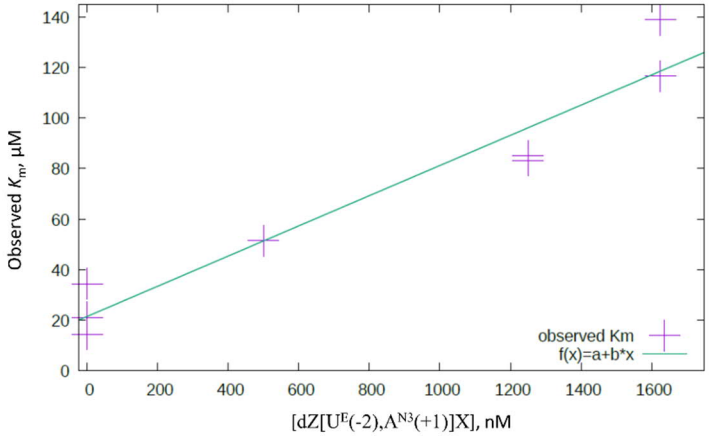

C)

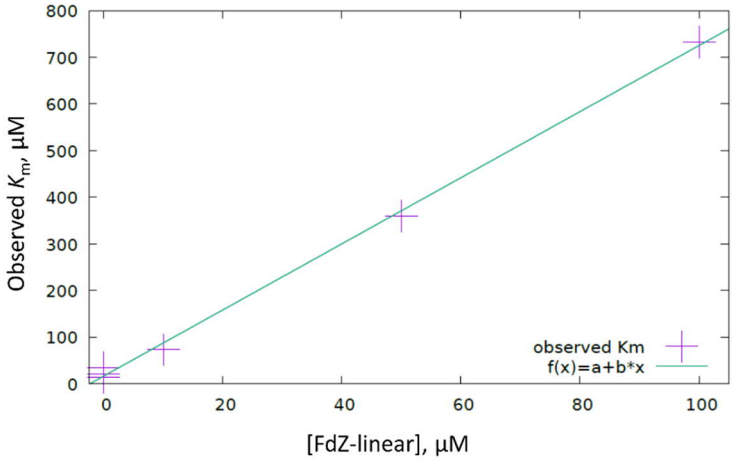

Figure S22. A) His_6-A3A catalyzed formation of dU-hairpin (TGCGCTT**dU**GCGCT, dU is 2'-deoxyuridine) as a result of deamination of dC-hairpin in the absence and presence of varying concentrations of dZ[U^E(–2), A^{N3}(+1)]X showing the fit of experimental data using the integrated form of the Michaelis-Menten equation (solid lines). B) Observed K_m values of His_6-A3A catalyzed deamination of dC-hairpin versus concentrations of dZ[U^E(–2), A^{N3}(+1)]X and the linear fit of the data (solid line). C) Observed K_m values of His_6-A3A catalyzed deamination of dC-hairpin versus concentrations of **FdZ**-linear and the linear fit of the data (solid line).

11. Isothermal titration calorimetry

We tested the thermodynamics of binding of our cross-linked oligos with A3 enzymes in comparison to the linear oligos using A3A-E72A and the catalytically competent $A3B_{CTD}$-QM-ΔL3-AL1swap. Desalted unmodified DNA oligonucleotides were purchased (Integrated DNA Technologies) at 1 or 5 μmol synthesis scale and dissolved in one of the buffers described below to give 10 mM solutions. ITC experiments were conducted at 25 °C using a MicroCal ITC200 (now Malvern Instruments) isothermal titration calorimeter. Protein A3A-E72A, which is an inactive protein, was diluted in ITC buffer to concentrations of 10-100 μM and titrated with dC oligonucleotides [5'-AT_3CAT_3, 5'-T_4CAT, cross-linked oligos] in ITC buffer. The ratio of protein to oligonucleotide concentration is usually 1:10. Titrations are made up of 30 individual additions. To prevent protein precipitation during the long time-scale of the experiment it was necessary to use improved ITC buffers. ITC buffer 1: 50 mM MES, pH 6.0, 100 mM NaCl, 200 μM EDTA, 1 mM β-mercaptoethanol and ITC buffer 2 (freshly prepared): 50 mM Na^+/K^+ phosphate, pH 6.0, 50 mM NaCl, 50 mM choline acetate, 2.5 mM TCEP, 200 μM EDTA with 30 mg/mL BSA.

Protein $A3B_{CTD}$-QM-ΔL3-AL1swap, which is an active protein, was used for establishing the binding affinity of **dZ**-containing oligos [**dZ**-linear and dZ[U^E(-2), A^{N3}(+1)]X]. For $A3B_{CTD}$-QM-ΔL3-AL1swap we used ITC buffer 3: 50 mM Na^+/K^+ phosphate, pH 6.0, 200 mM trimethylamine *N*-oxide dihydrate, 2.5 mM TCEP, 200 μM EDTA. Data evaluation was performed with the software provided by the supplier of MicroCal ITC200.

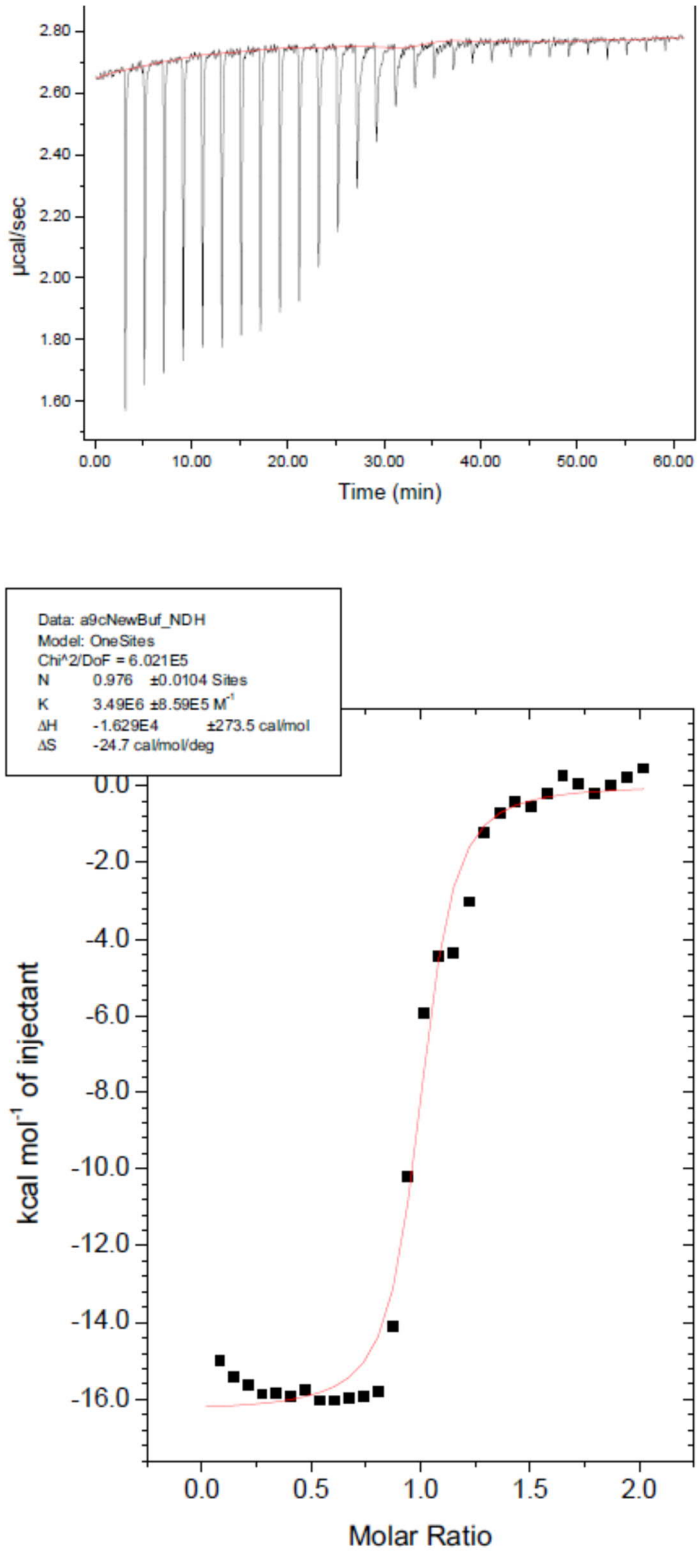

Figure S23. Representative titration of 5'-AT_3CAT_3 into A3A-E72A in the ITC buffer-1. The upper panel shows raw injection data and the lower panel shows integrated injection enthalpies after background correction. The solid line in the middle panel represents a fit of the data to a one-site binding model.

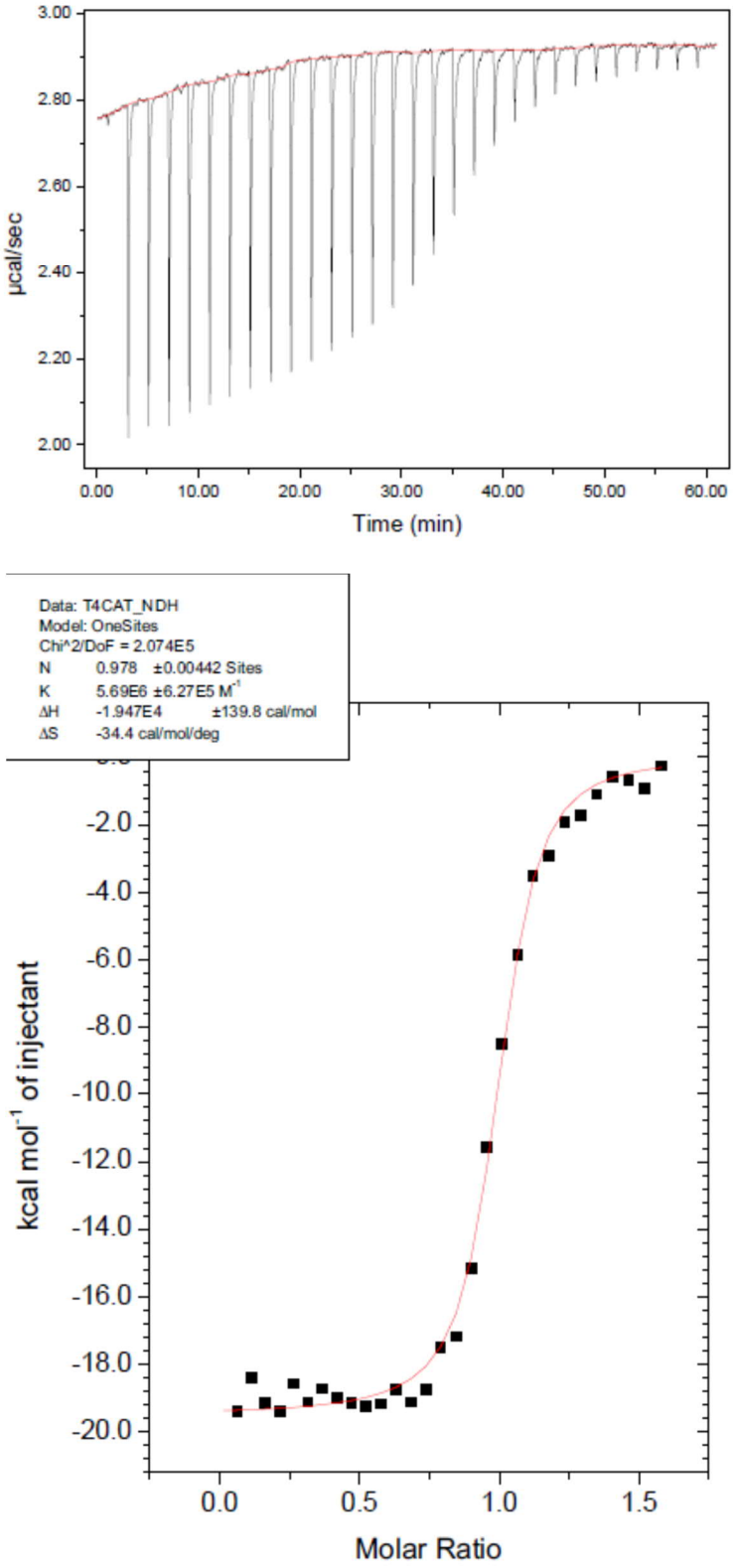

Figure S24. Representative titration of 5'-T_4CAT into A3A-E72A in the ITC buffer-1. The upper panel shows raw injection data and the lower panel shows integrated injection enthalpies after background correction. The solid line in the middle panel represents a fit of the data to a one-site binding model.

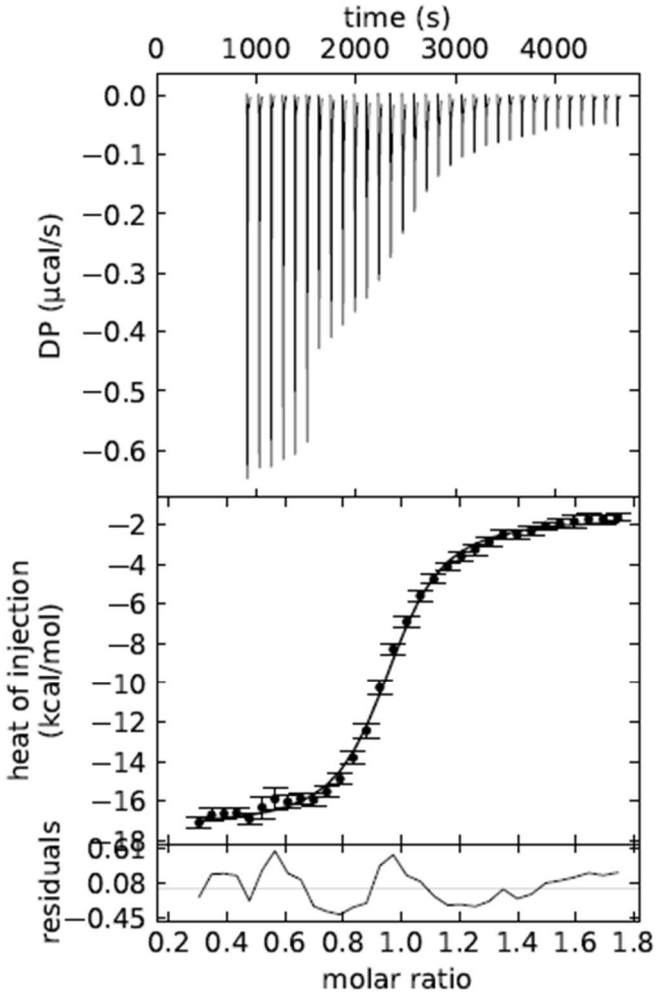

Figure S25. Titration of dC-9-mer-X into A3A-E72A in the ITC buffer-1. The upper panel shows raw injection data and the middle panel shows integrated injection enthalpies after background correction. The solid line in the middle panel represents a fit of the data to a one-site binding model. The bottom panel shows residuals between observed and calculated data points.

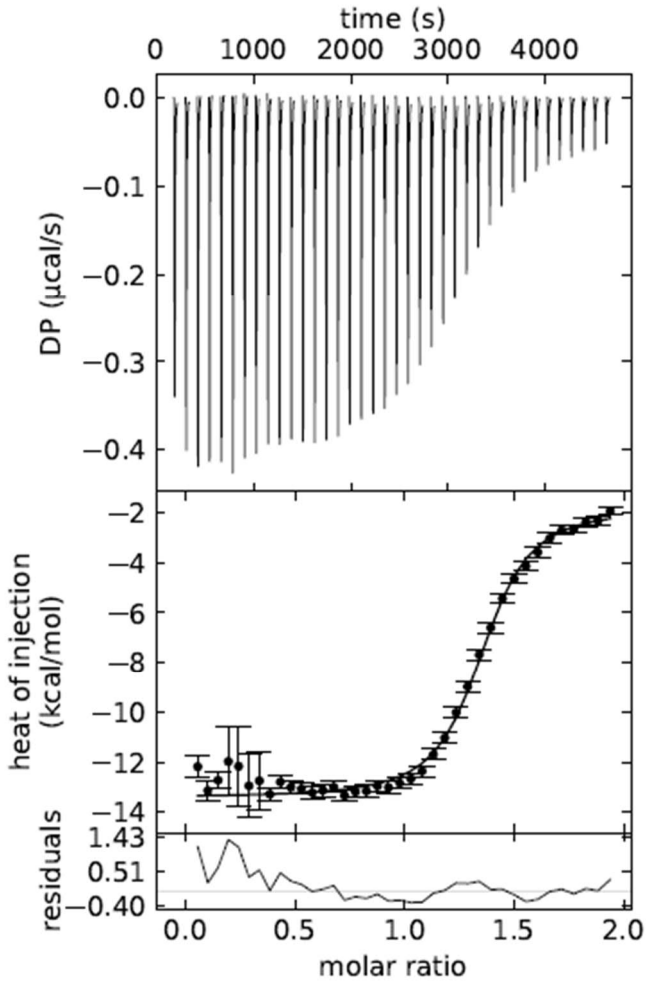

Figure S26. Titration of dC-7-mer-X into A3A-E72A in the ITC buffer-1. The upper panel shows raw injection data and the middle panel shows integrated injection enthalpies after background correction. The solid line in the middle panel represents a fit of the data to a one-site binding model. The bottom panel shows residuals between observed and calculated data points.

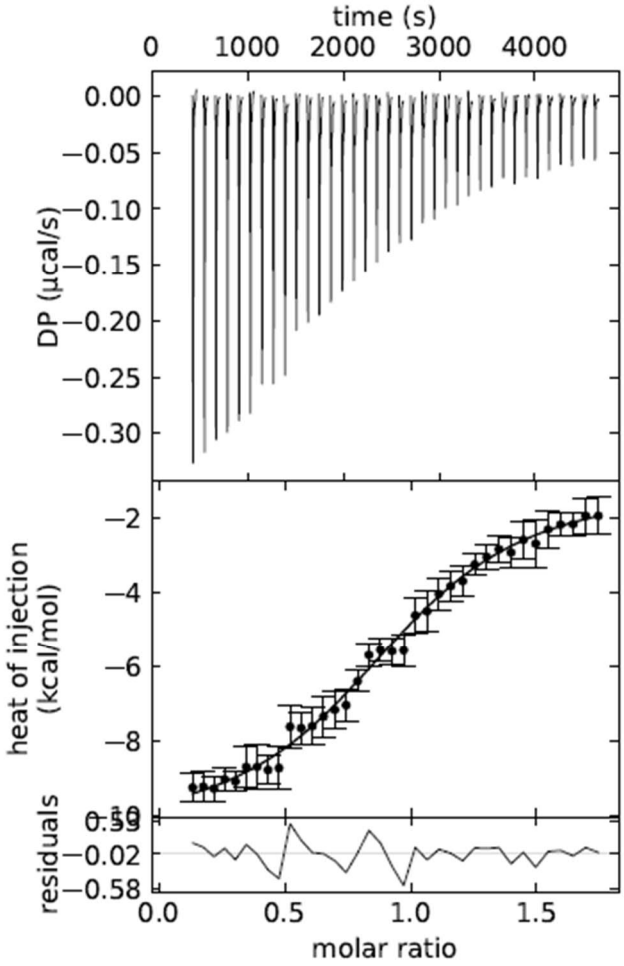

Figure S27. Titration of dC-5-mer-X into A3A-E72A in the ITC buffer 1. The upper panel shows raw injection data, and the middle panel shows integrated injection enthalpies after background correction. The solid line in the middle panel represents a fit of the data to a one-site binding model. The bottom panel shows residuals between observed and calculated data points.

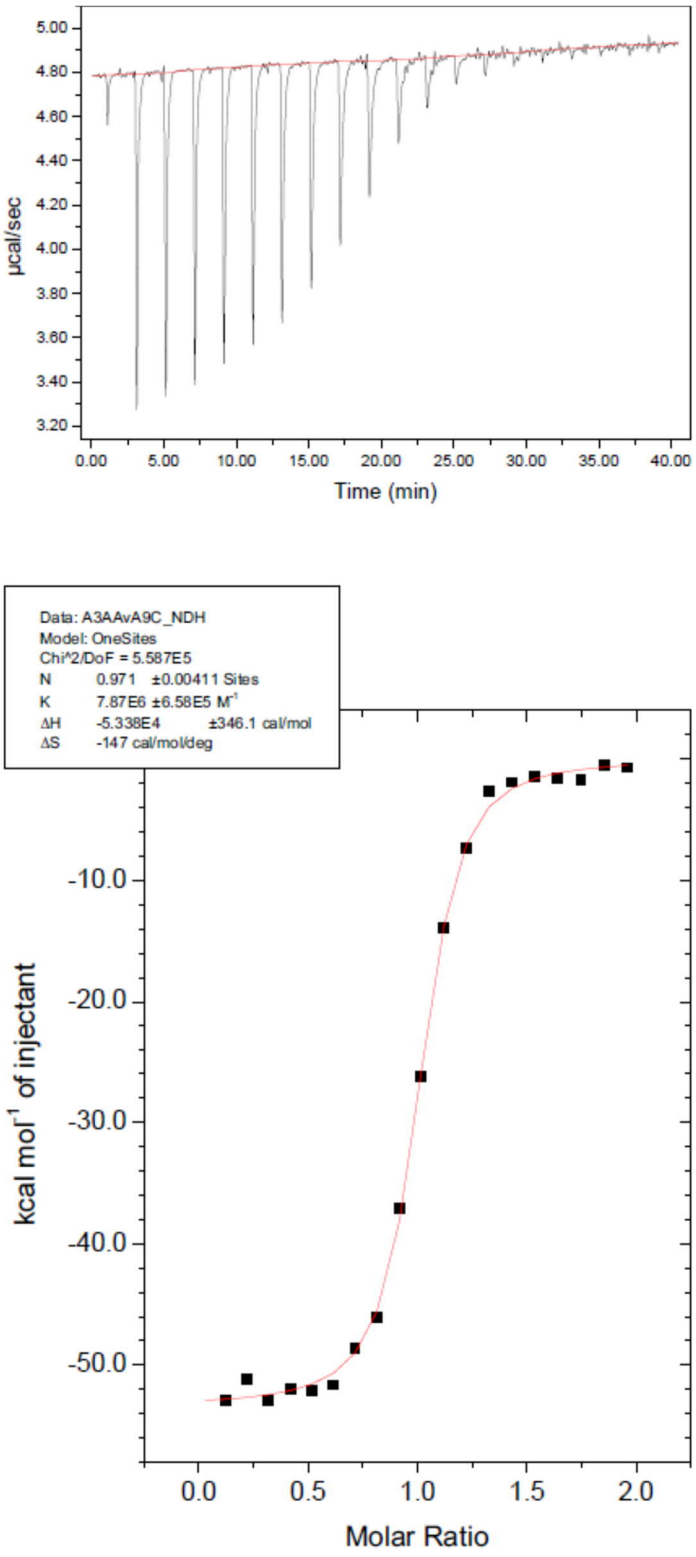

Figure S28. Titration of 5'-AT_3CAT_3 into A3A-E72A in the ITC buffer-2. The upper panel shows raw injection data, and the lower panel shows integrated injection enthalpies after background correction. The solid line in the lower panel represents a fit of the data to a one-site binding model.

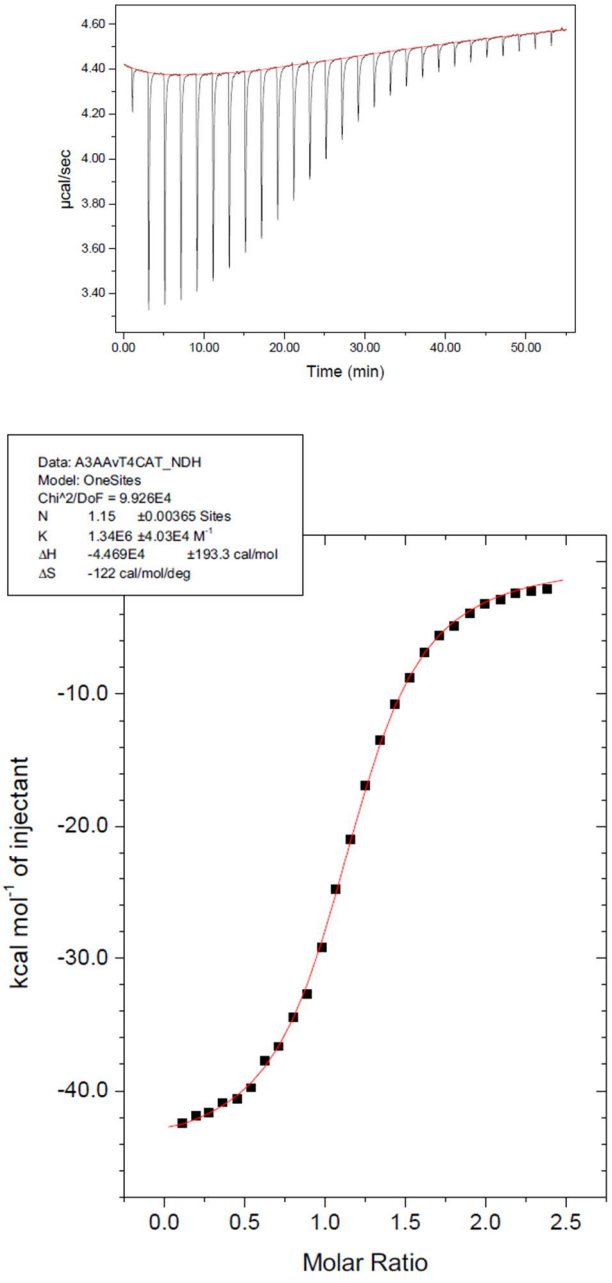

Figure S29. Titration of 5'-T_4CAT into A3A-E72A in the ITC buffer-2. The upper panel shows raw injection data, and the middle panel shows integrated injection enthalpies after background correction. The solid line in the middle panel represents a fit of the data to a one-site binding model.

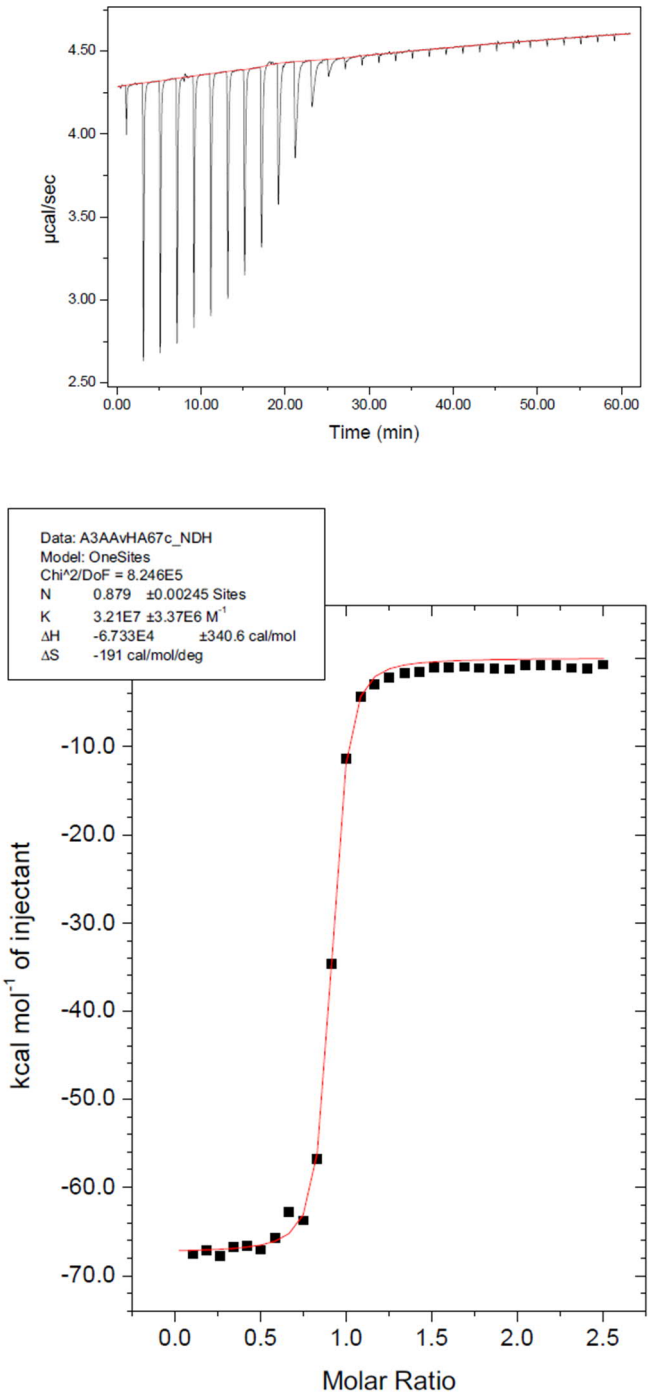

Figure S30. Titration of dC[U^{E}(–2), A^{N3}(+1)]X into A3A-E72A in the ITC buffer-2. The upper panel shows raw injection data, and the lower panel shows integrated injection enthalpies after background correction. The solid line in the lower panel represents a fit of the data to a one-site binding model.

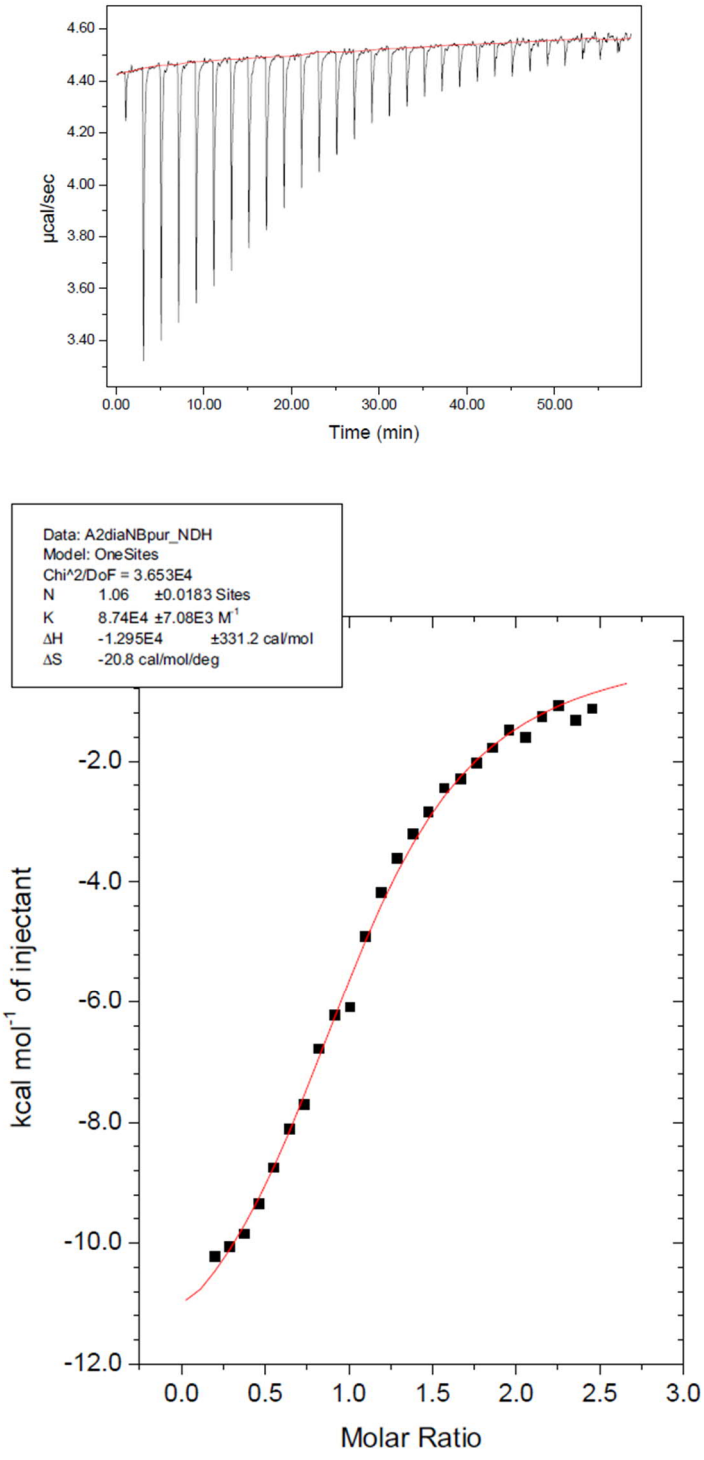

Figure S31. Titration of **dZ**-linear into A3B$_{CTD}$-QM-ΔL3-AL1swap in the ITC buffer-3. The upper panel shows raw injection data, and the lower panel shows integrated injection enthalpies after background correction. The solid line in the lower panel represents a fit of the data to a one-site binding model.

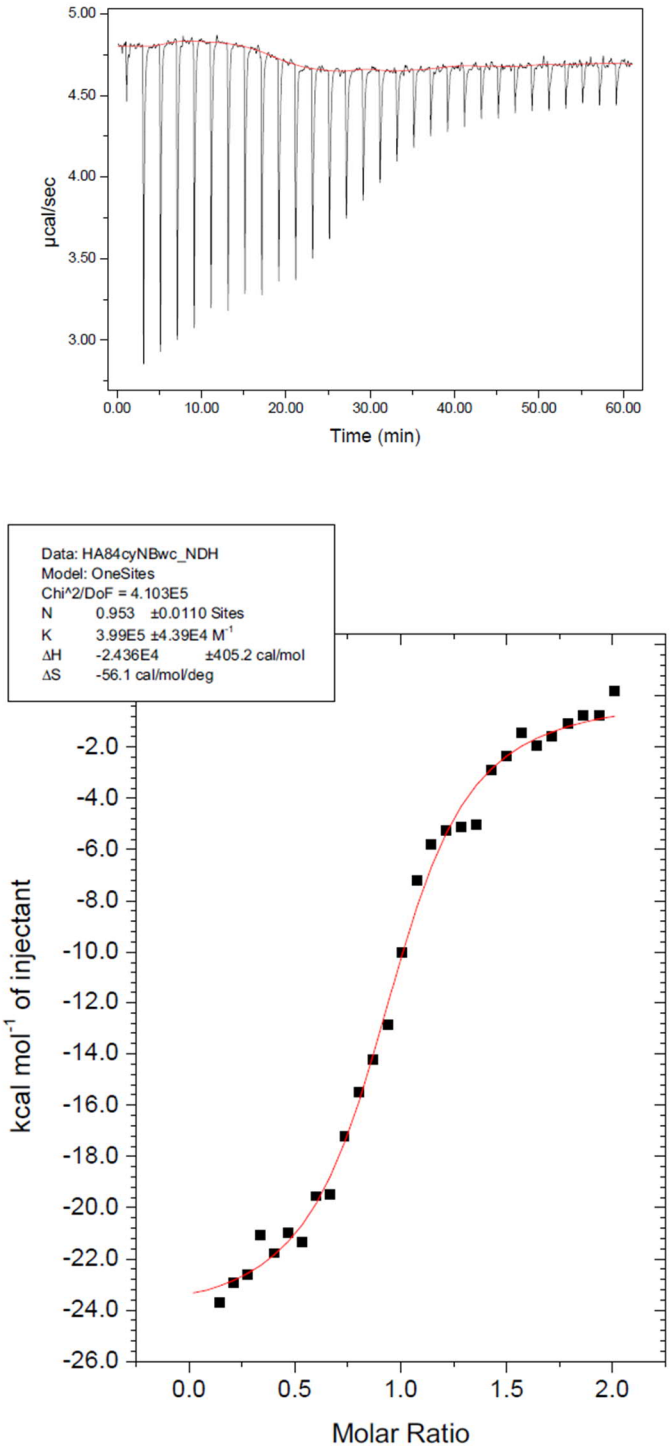

Figure S32. Titration of dZ[U^{E}(−2), A^{N3}(+1)]X into $A3B_{CTD}$ -QM-ΔL3-AL1swap in the ITC buffer-3. The upper panel shows raw injection data, and the lower panel shows integrated injection enthalpies after background correction. The solid line in the lower panel represents a fit of the data to a one-site binding model.

12. References

(1) Vives, M.; Eritja, R.; Tauler, R.; Marquez, V.; Gargallo, R. Synthesis, stability, and protonation studies of a self-complementary dodecamer containing the modified nucleoside 2′-deoxyzebularine. *Biopolymers: Original Research on Biomolecules* **2004**, *73* (1), 27-43.
(2) Damha, M. J.; Giannaris, P. A.; Zabarylo, S. V. An improved procedure for derivatization of controlled-pore glass beads for solid-phase oligonucleotide synthesis. *Nucleic Acids Res.* **1990**, *18* (13), 3813-3821.
(3) Fall, A.; Seck, I.; Diouf, O.; Gaye, M.; Seck, M.; Gomez, G.; Fall, Y. Synthesis of new triazolium-based ionic liquids and their use in the Morita–Baylis–Hillman reaction. *Tetrahedron letters* **2015**, *56* (36), 5128-5131.
(4) Tararov, V. I.; Kolyachkina, S. V.; Alexeev, C. S.; Mikhailov, S. N. N6-Acetyl-2′, 3′, 5′-tri-O-acetyladenosine; a convenient,'missed out'substrate for regioselective N6-alkylations. *Synthesis* **2011**, *2011* (15), 2483-2489.
(5) Harjes, S.; Jameson, G. B.; Filichev, V. V.; Edwards, P. J.; Harjes, E. NMR-based method of small changes reveals how DNA mutator APOBEC3A interacts with its single-stranded DNA substrate. *Nucleic Acids Res.* **2017**, *45* (9), 5602-5613.
(6) Kvach, M. V.; Barzak, F. M.; Harjes, S.; Schares, H. A.; Jameson, G. B.; Ayoub, A. M.; Moorthy, R.; Aihara, H.; Harris, R. S.; Filichev, V. V. Inhibiting APOBEC3 Activity with Single-Stranded DNA Containing 2′-Deoxyzebularine Analogues. *Biochemistry* **2018**, *58* (5), 391-400.
(7) Kvach, M. V.; Barzak, F. M.; Harjes, S.; Schares, H. A.; Kurup, H. M.; Jones, K. F.; Sutton, L.; Donahue, J.; D'Aquila, R. T.; Jameson, G. B. Differential inhibition of APOBEC3 DNA-mutator isozymes by fluoro-versus non-fluoro-substituted 2'-deoxyzebularine embedded in single-stranded DNA. *ChemBioChem* **2019**.
(8) Shi, K.; Carpenter, M. A.; Kurahashi, K.; Harris, R. S.; Aihara, H. Crystal structure of the DNA deaminase APOBEC3B catalytic domain. *Journal of Biological Chemistry* **2015**, *290* (47), 28120-28130.
(9) Studier, F. W. Stable expression clones and auto-induction for protein production in E. coli. *Methods Mol. Biol.* **2014**, *1091*, 17-32. DOI: 10.1007/978-1-62703-691-7_2 From NLM.

13. Experimental data for compounds synthesized

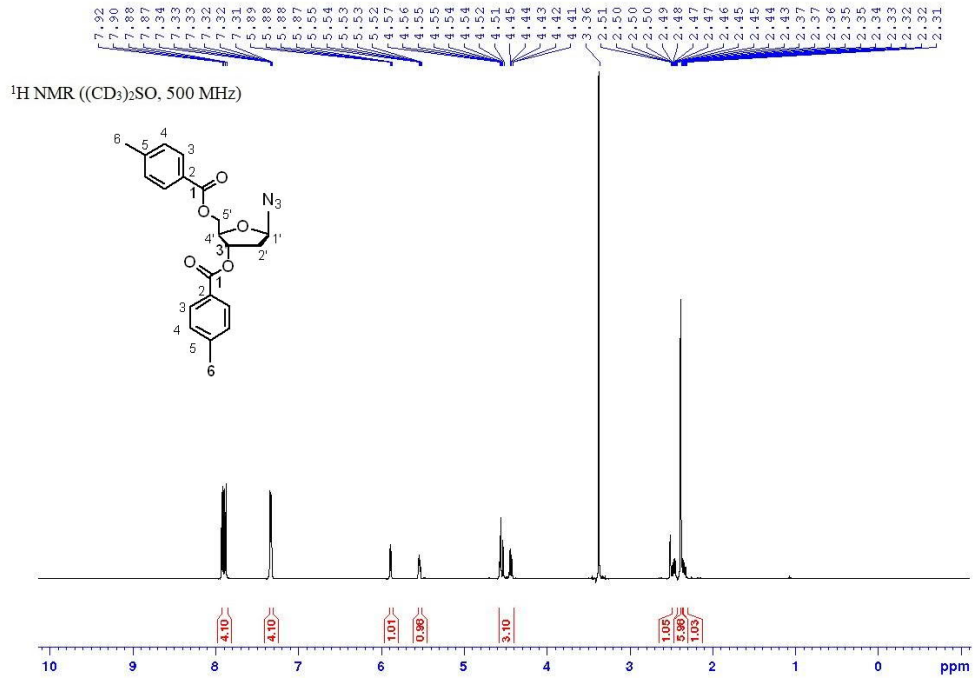

Figure S33. ^{1}H NMR spectrum of compound **2**.

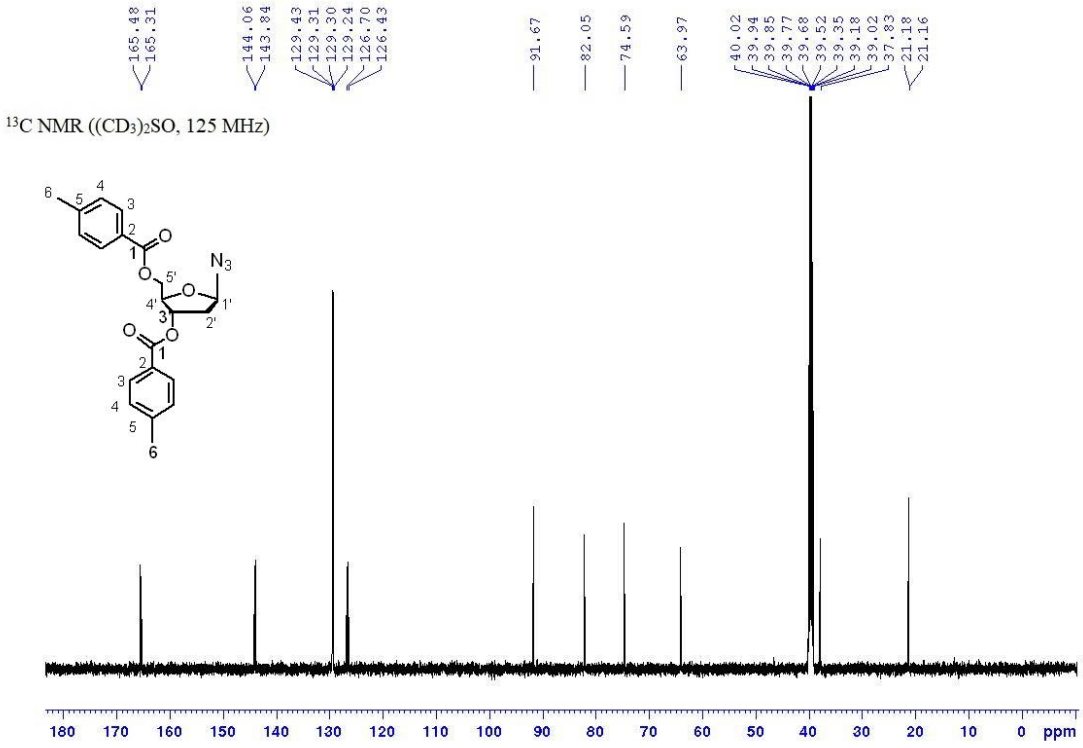

Figure S34. ^{13}C NMR spectrum of compound **2**.

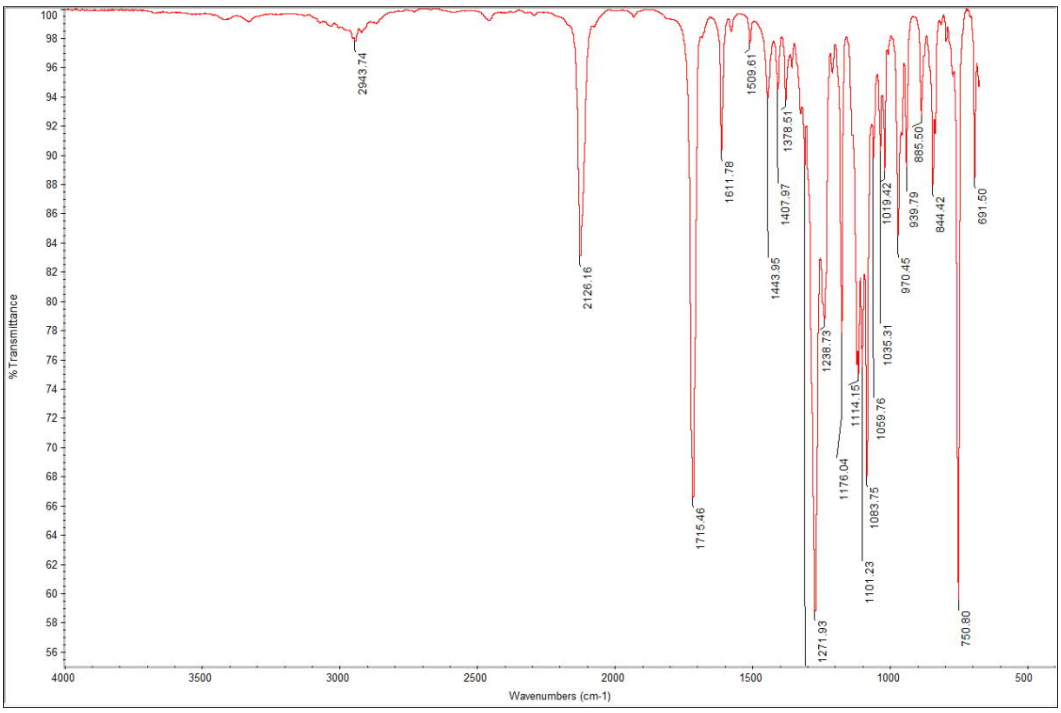

Figure S35. IR spectrum of compound **2**.

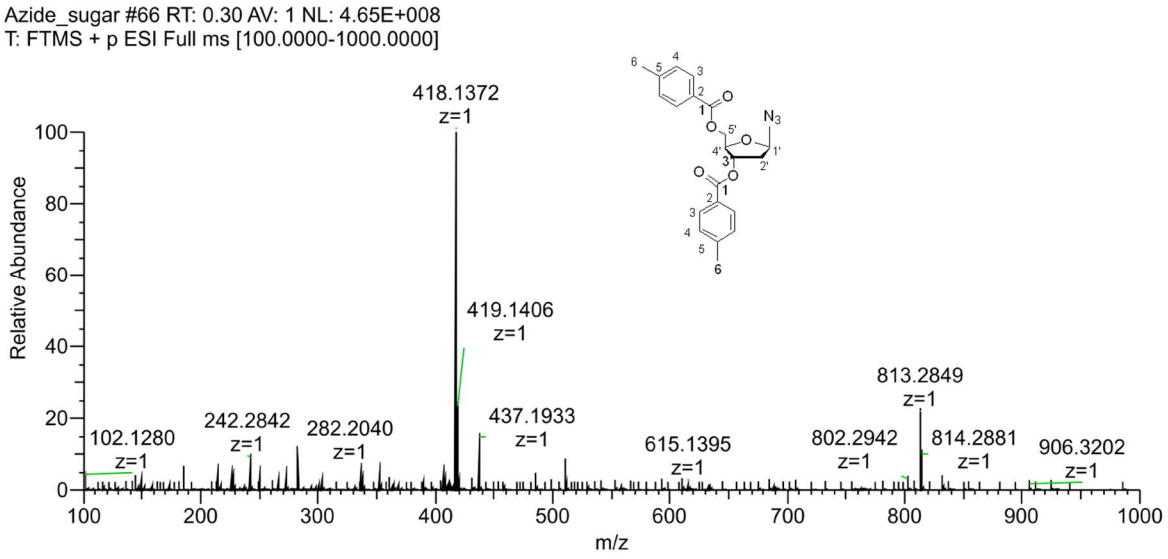

Figure S36. HRMS (ESI) of compound **2**.

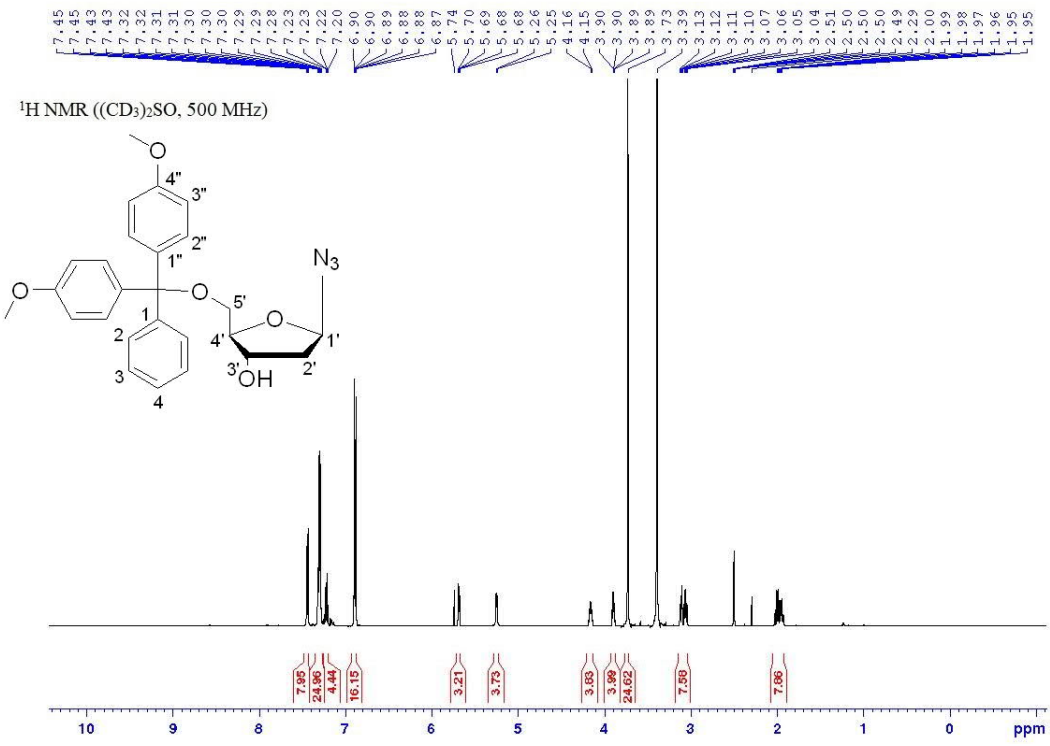

Figure S37. ^{1}H NMR of compound **3**.

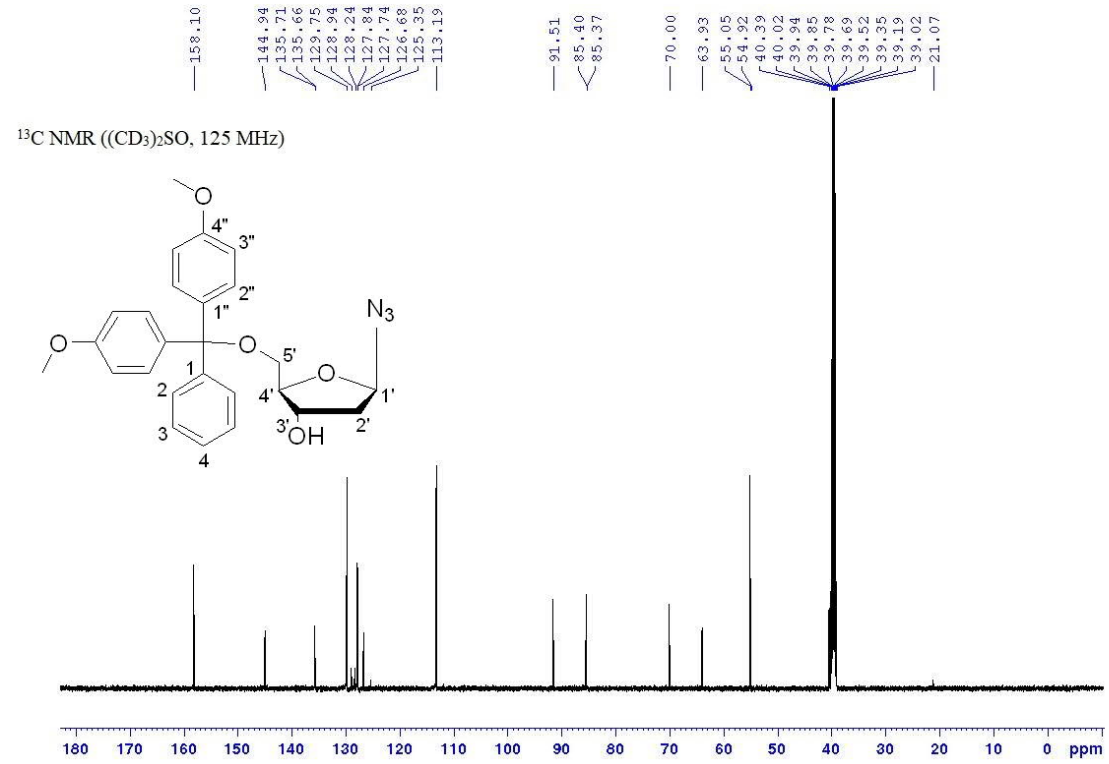

Figure S38. ^{13}C NMR of compound **3**.

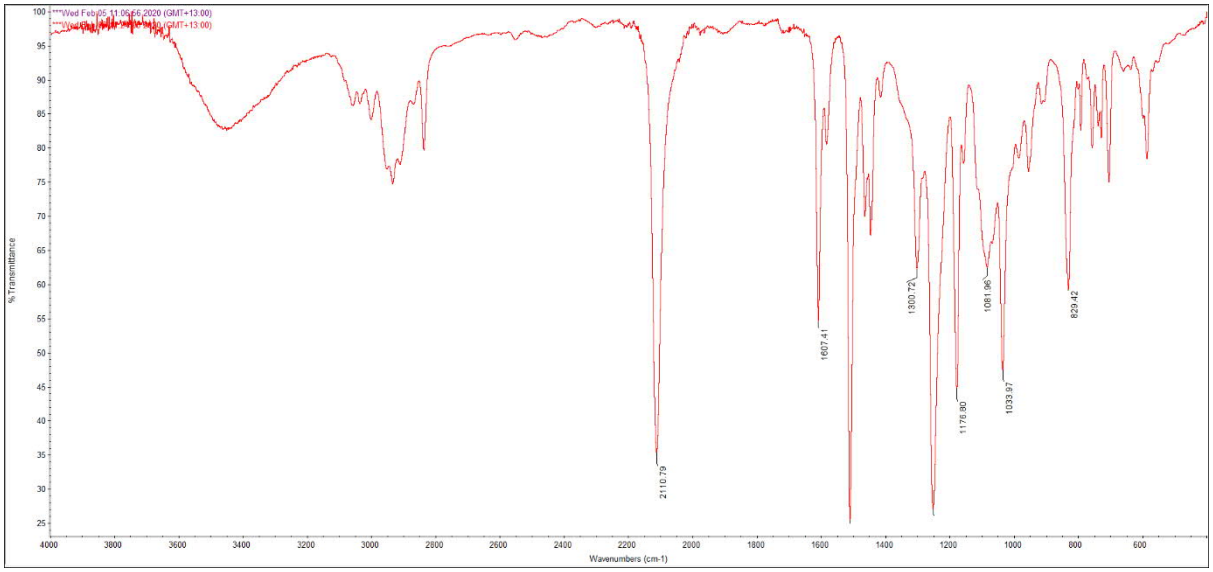

Figure S39. IR (ATR) spectrum of compound **3**.

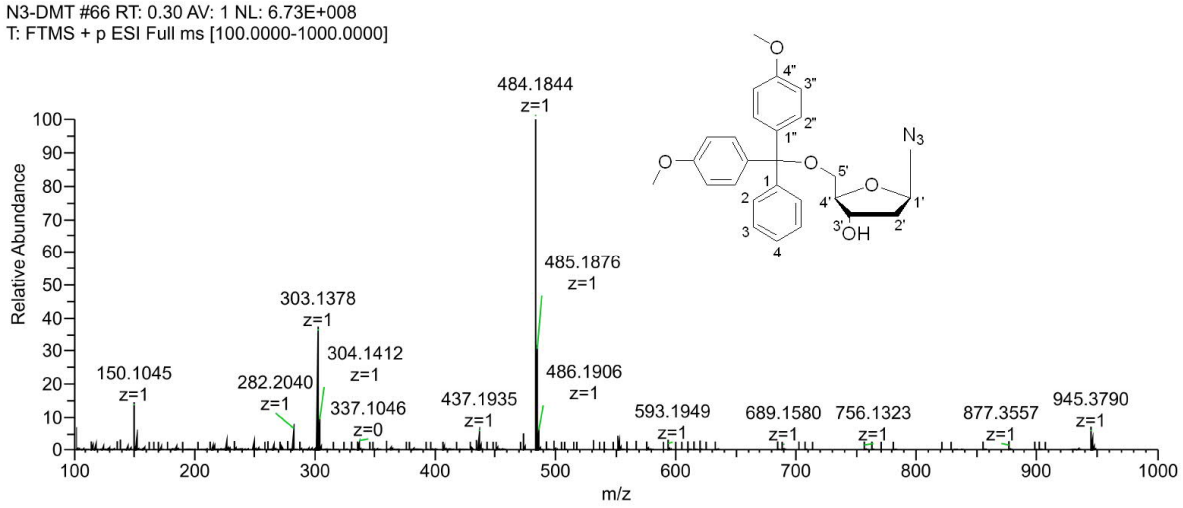

Figure S40. HRMS (ESI) of compound **3**.

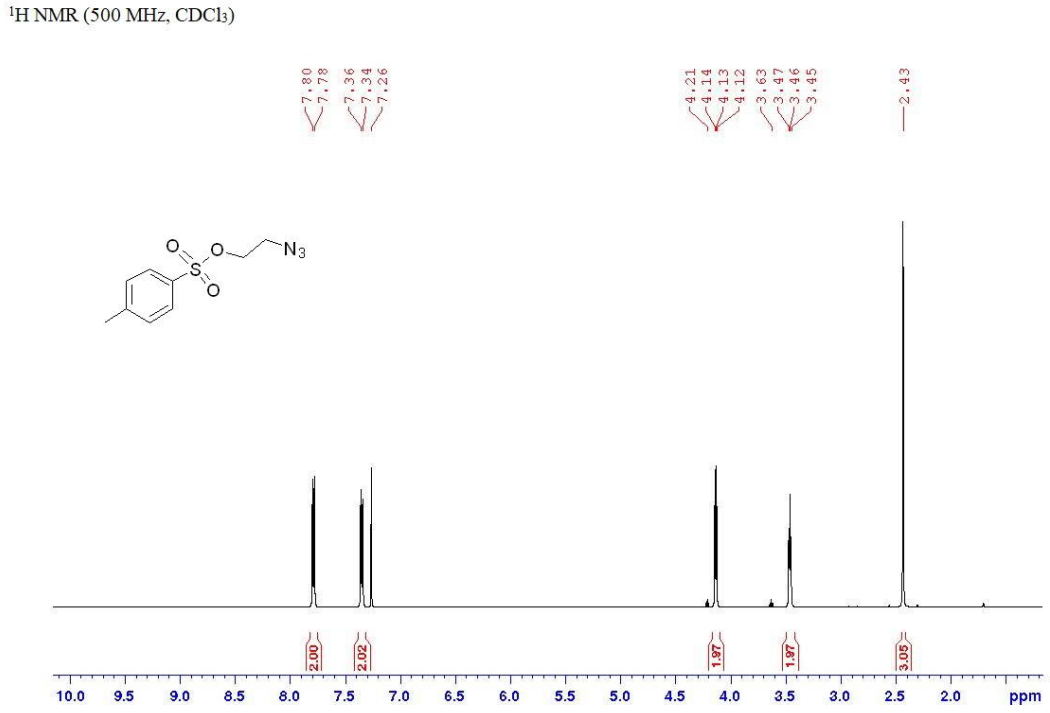

Figure S41. ^{1}H NMR spectrum of compound **5**.

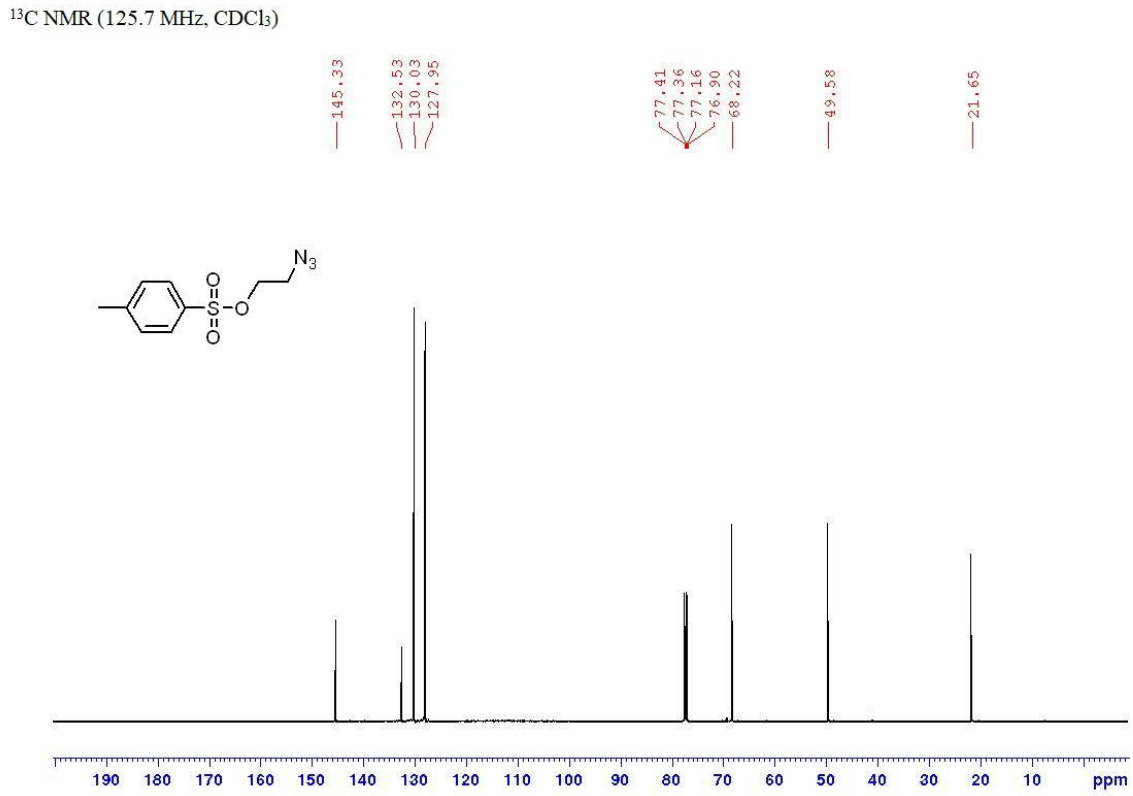

Figure S42. ^{13}C NMR spectrum of compound **5**.

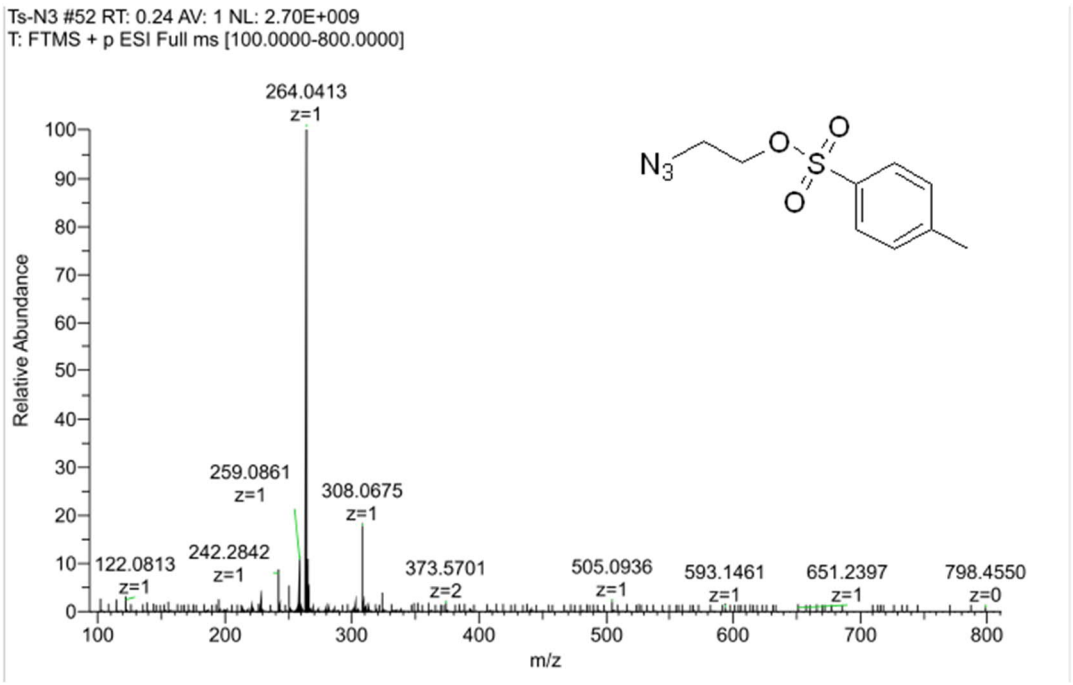

Figure S43. HRMS (ESI) of compound **5**.

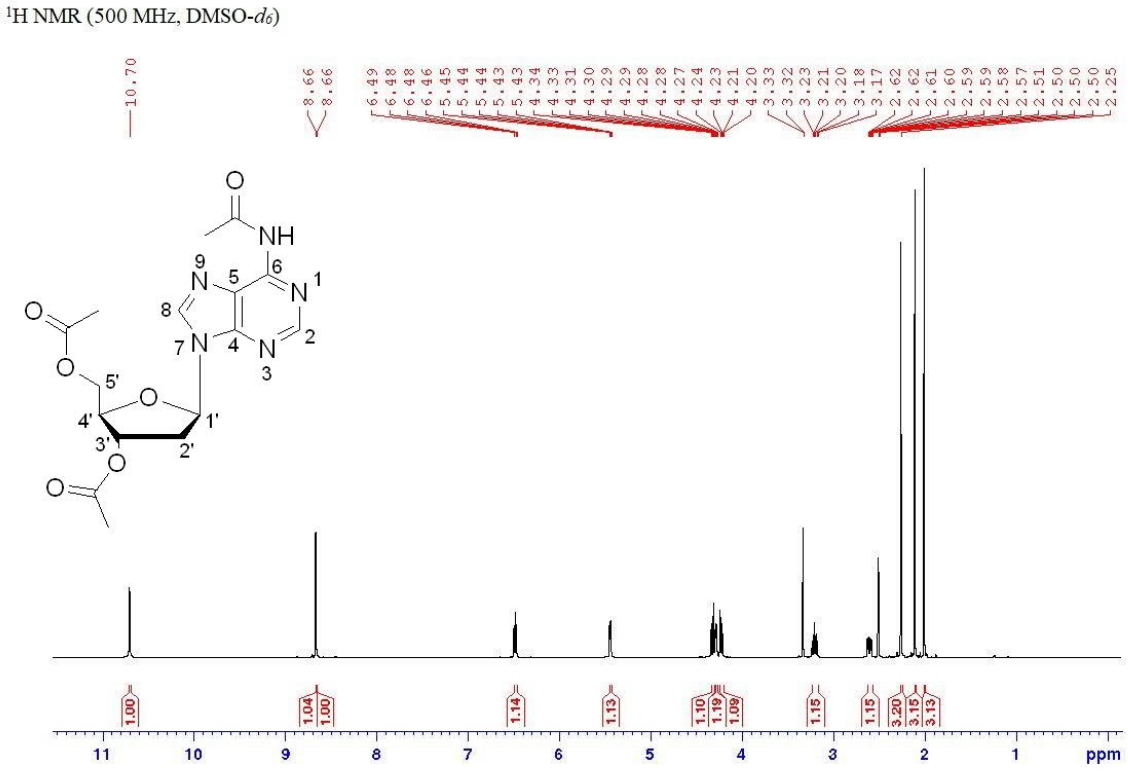

Figure S44. [1]H NMR spectrum of compound **7**.

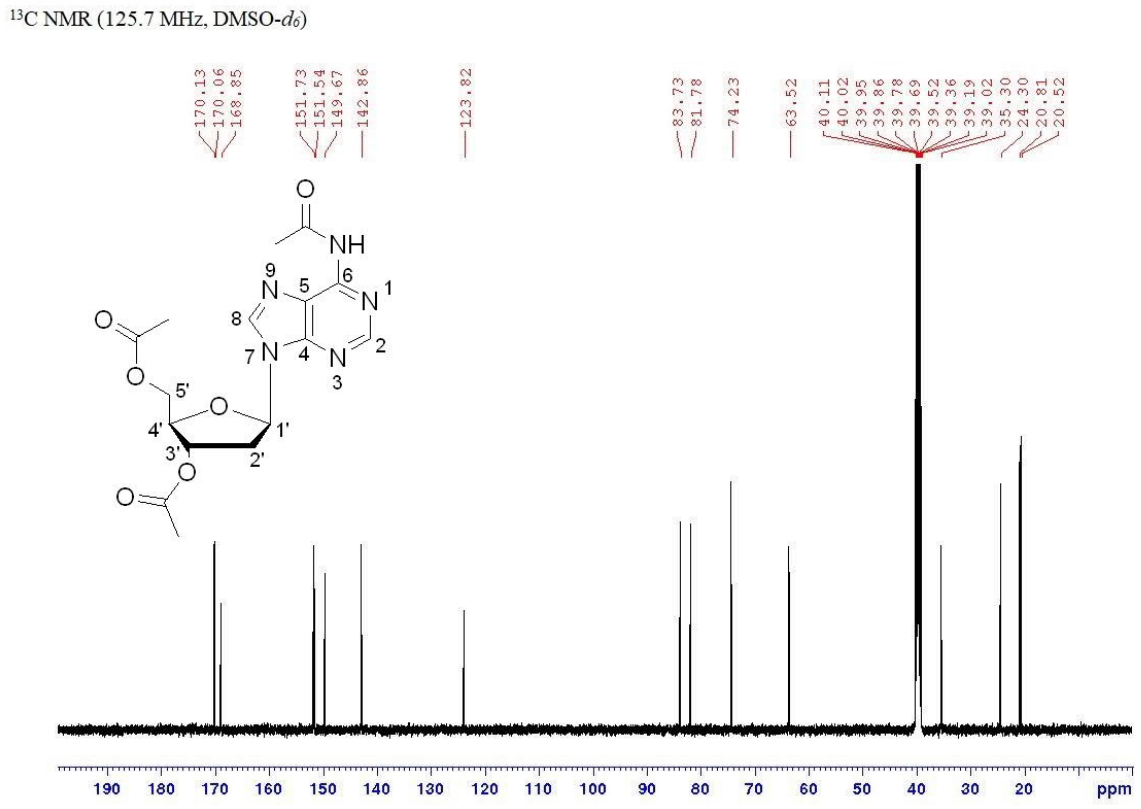

Figure S45. ^{13}C NMR spectrum of compound **7**.

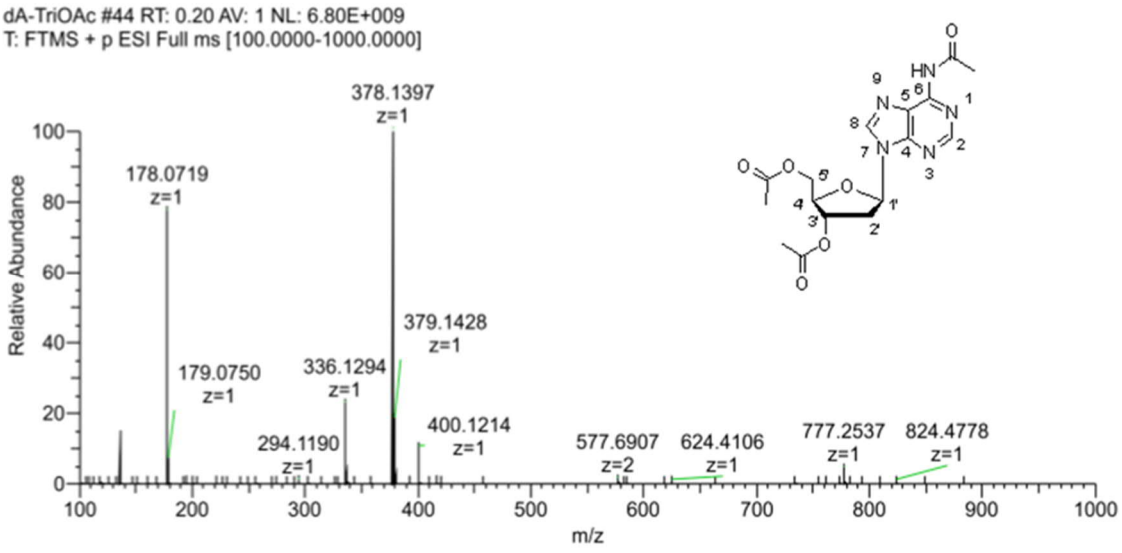

Figure S46. HRMS (ESI) of compound **7**.

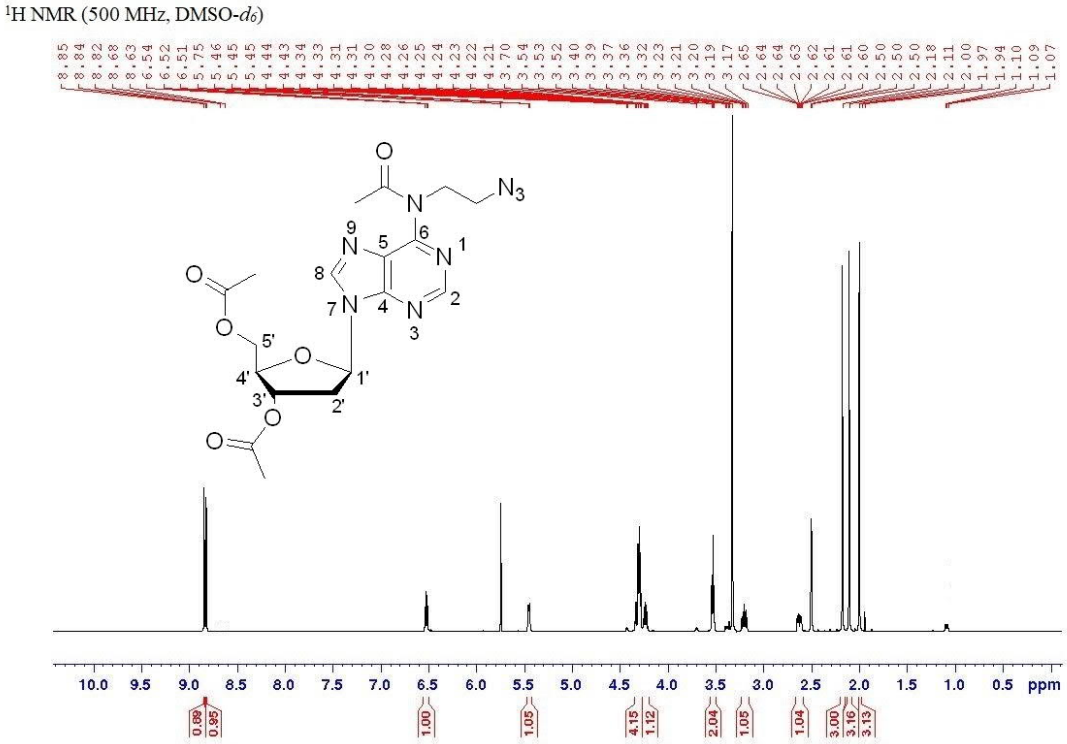

Figure S47. ^{1}H NMR spectrum of compound **8**.

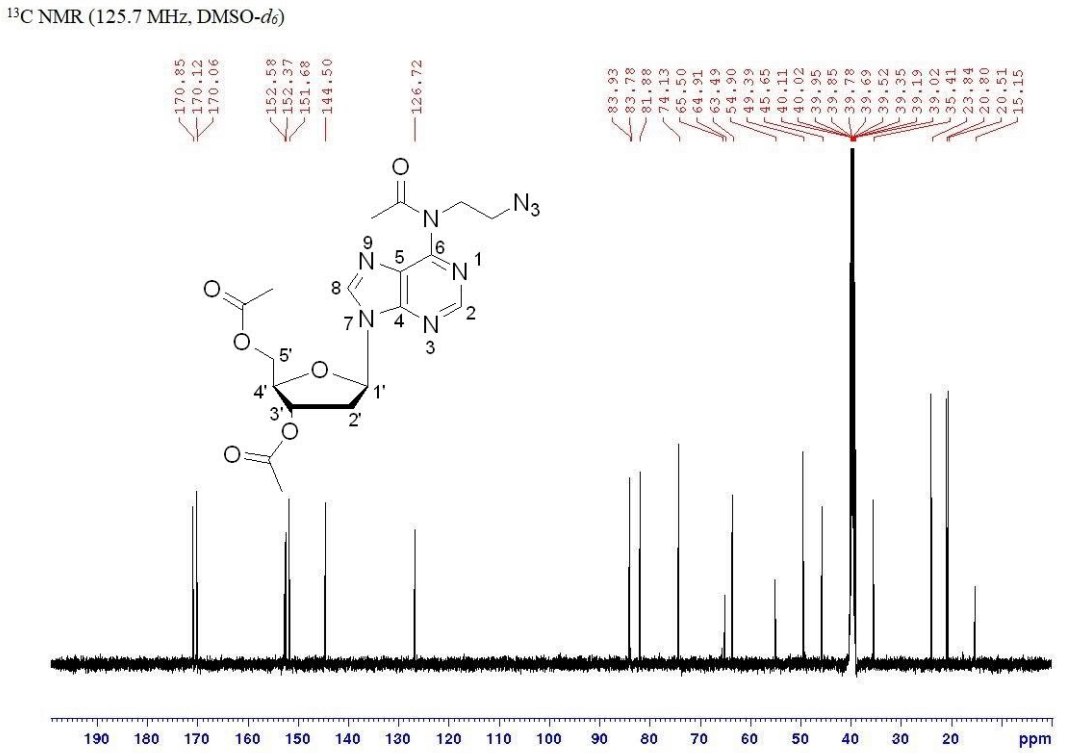

Figure S48. ^{13}C NMR spectrum of compound **8**.

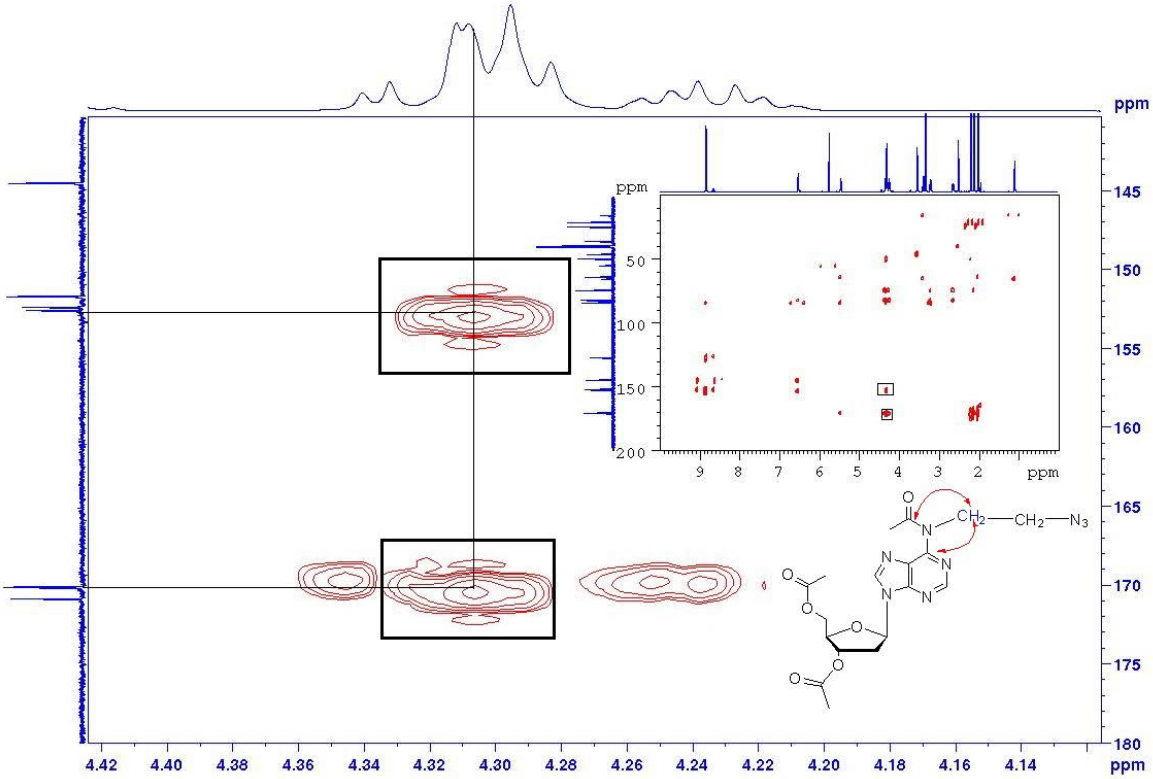

Figure S49. HMBC NMR spectrum of compound **8**.

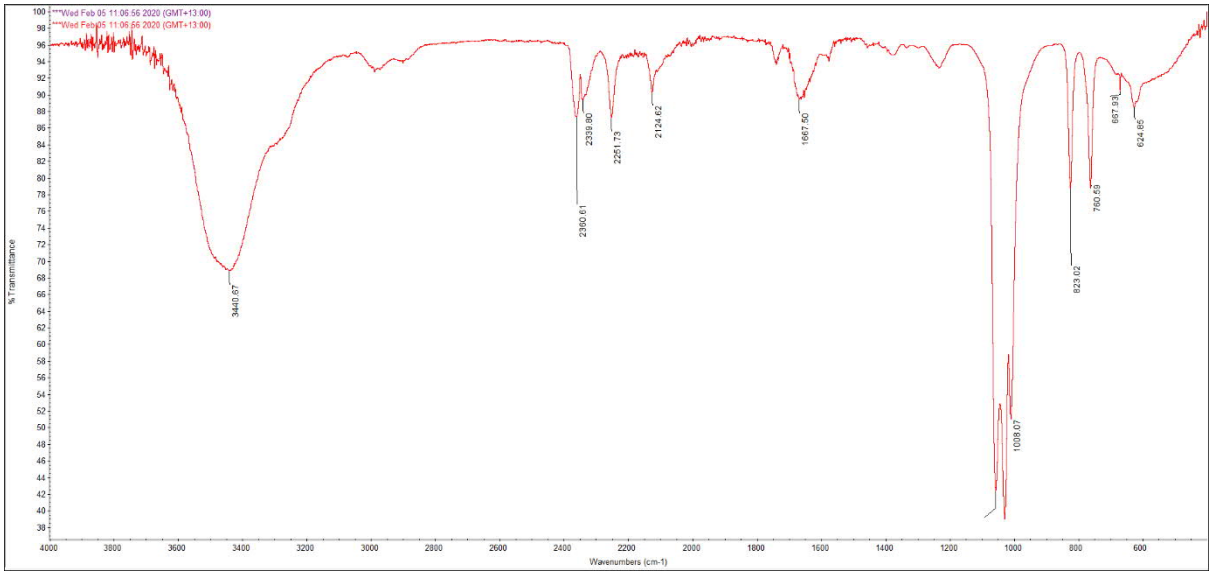

Figure S50. IR (ATR) spectrum of compound **8**.

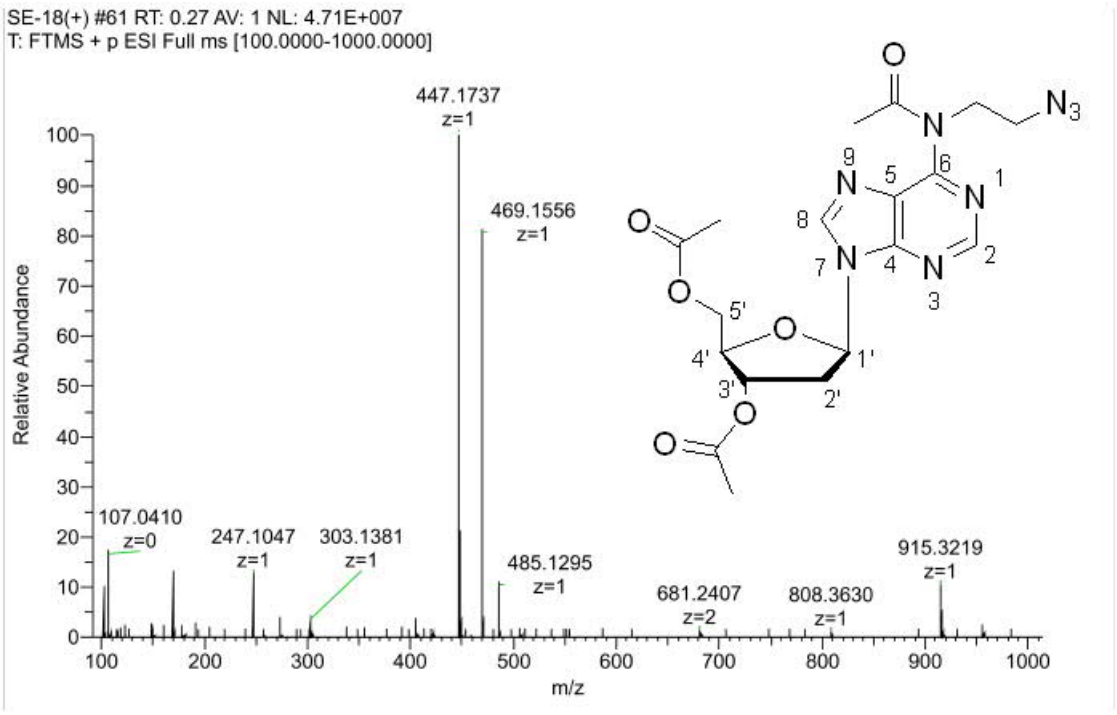

Figure S51. HRMS (ESI) of compound **8**.

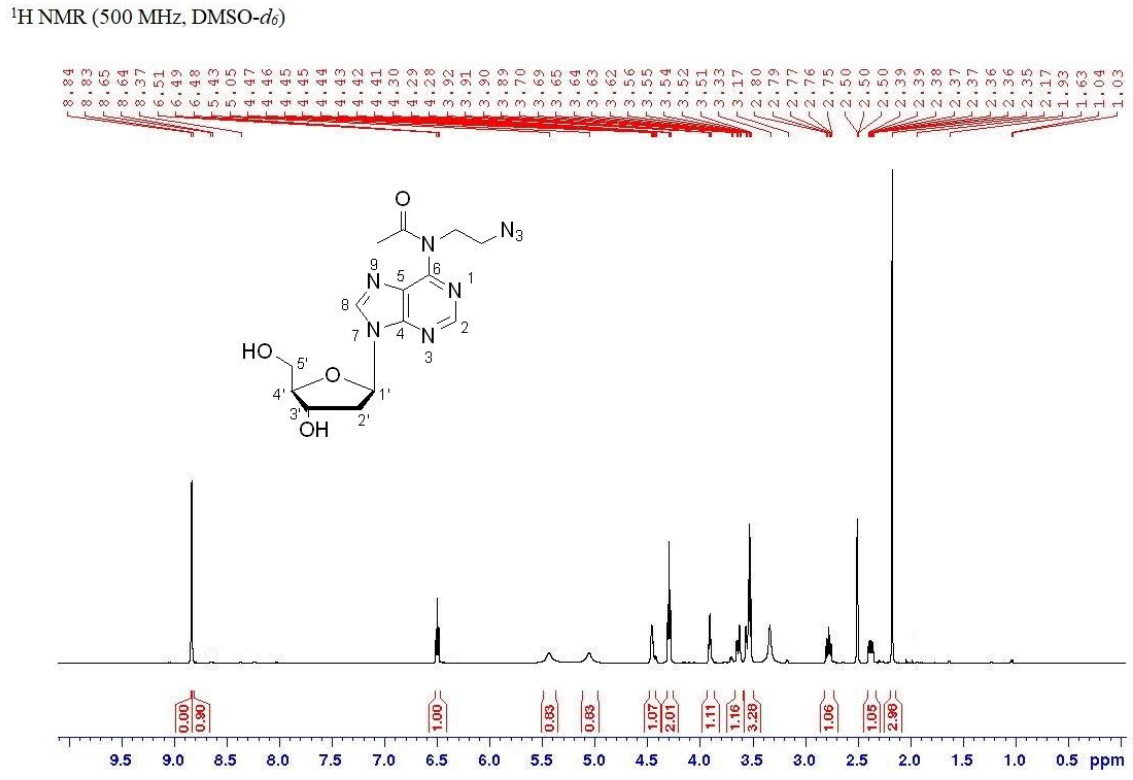

Figure S52. ^{1}H NMR spectrum of compound **9**.

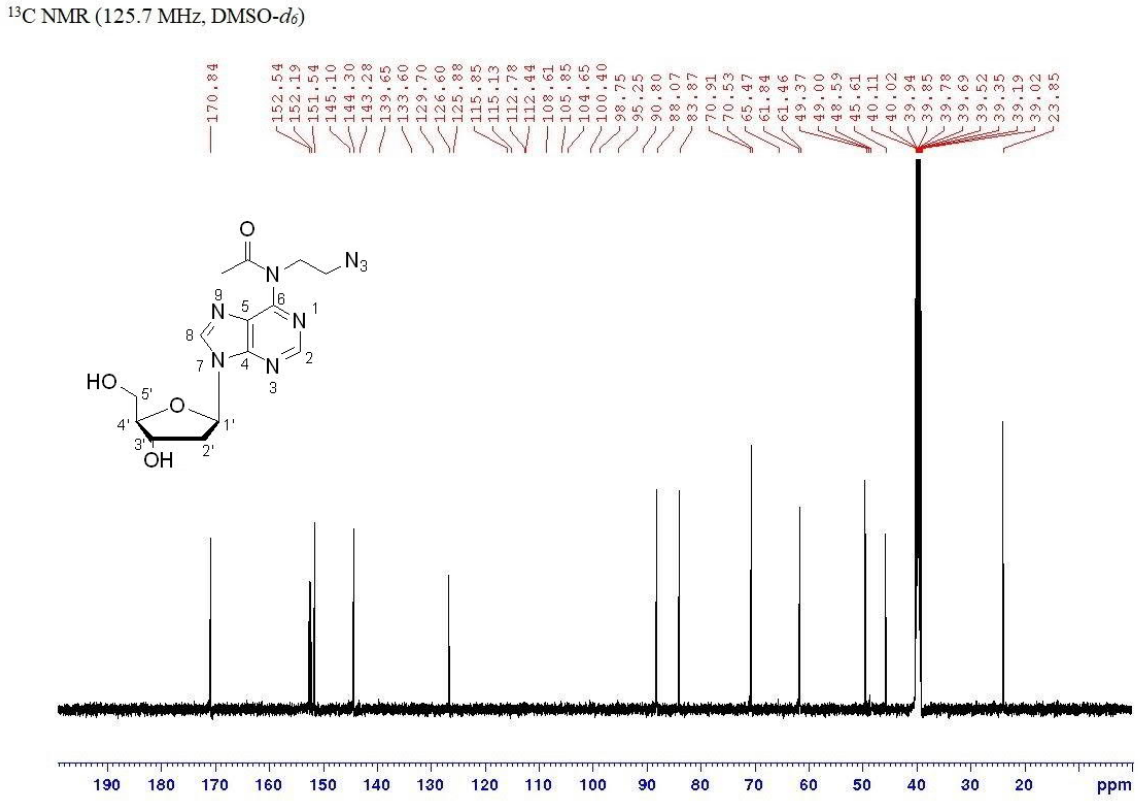

Figure S53. ^{13}C NMR spectrum of compound **9**.

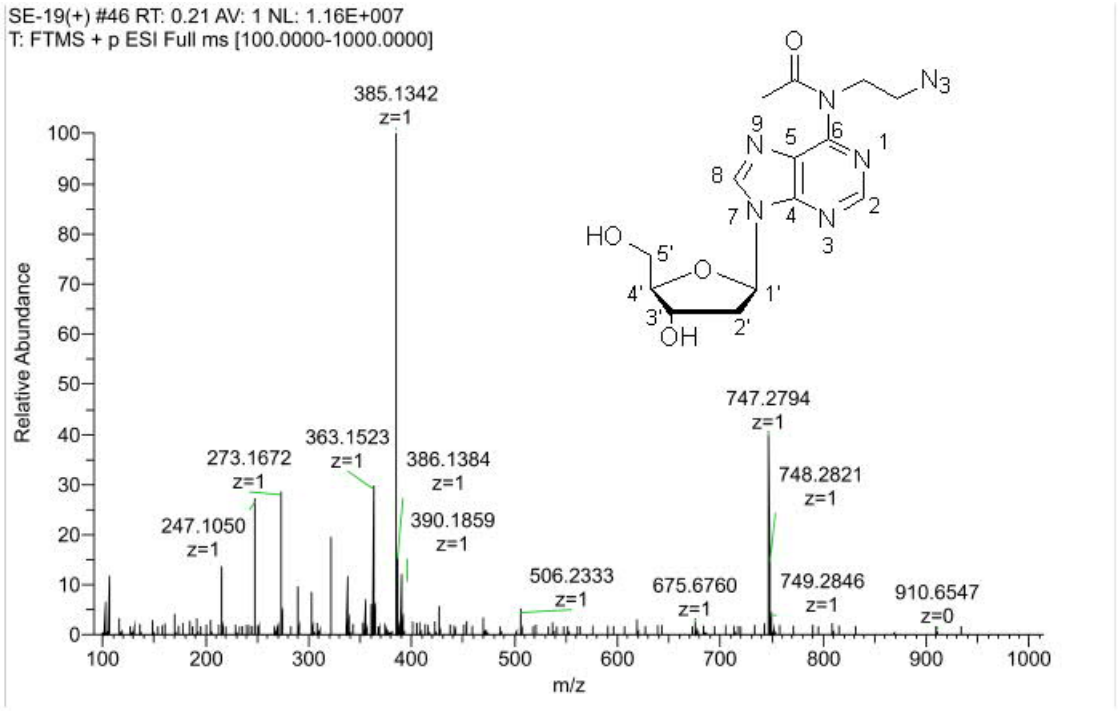

Figure S54. HRMS (ESI) of compound **9**.

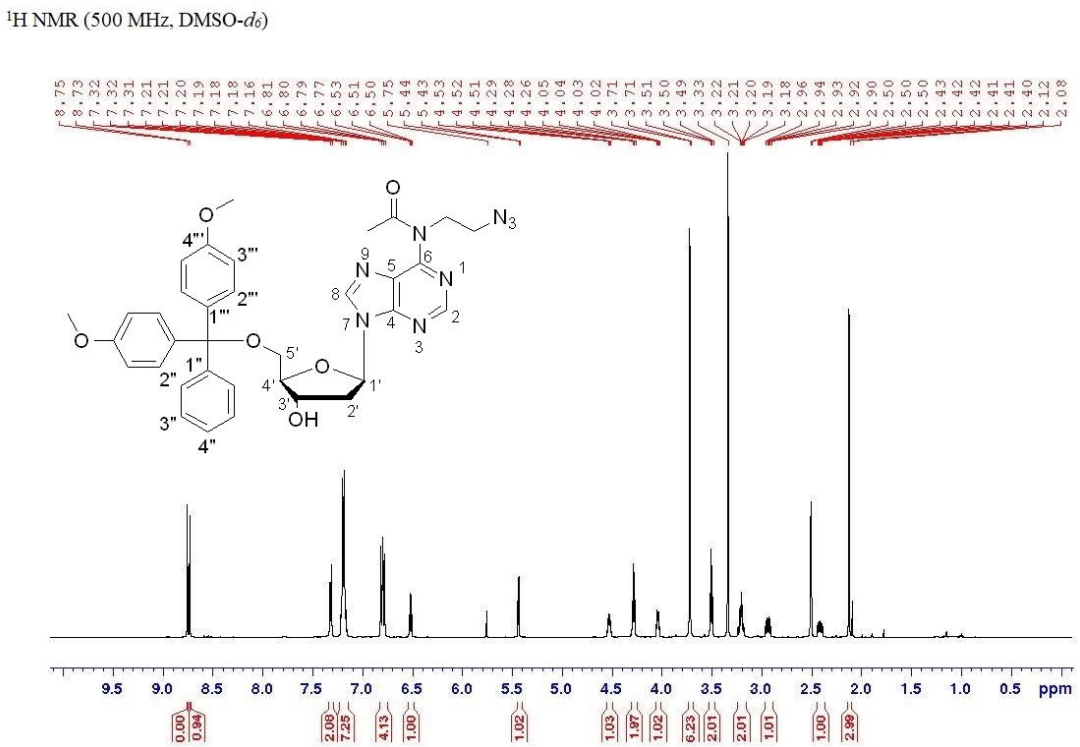

Figure S55. ^{1}H NMR spectrum of compound **10**.

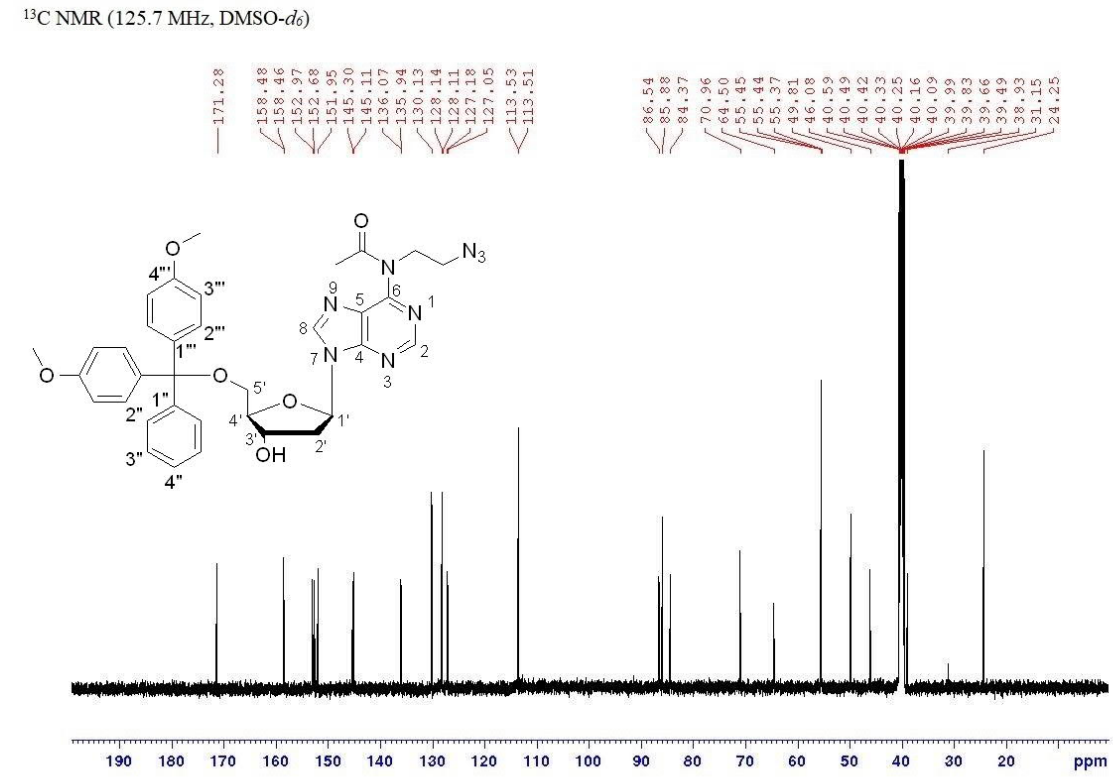

Figure S56. ^{13}C NMR spectrum of compound **10**.

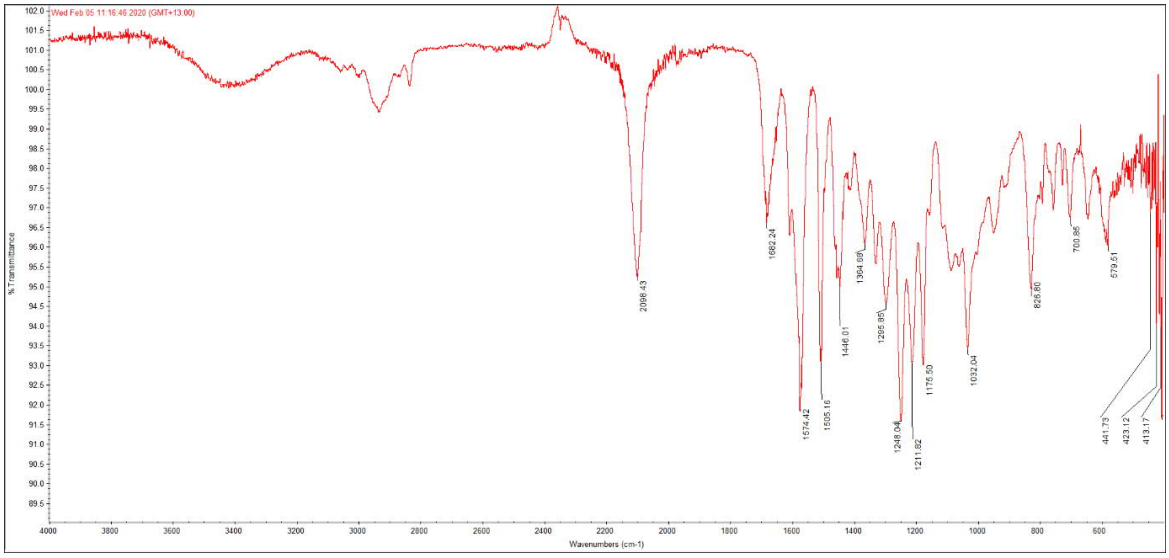

Figure S57. IR (ATR) spectrum of compound **10**.

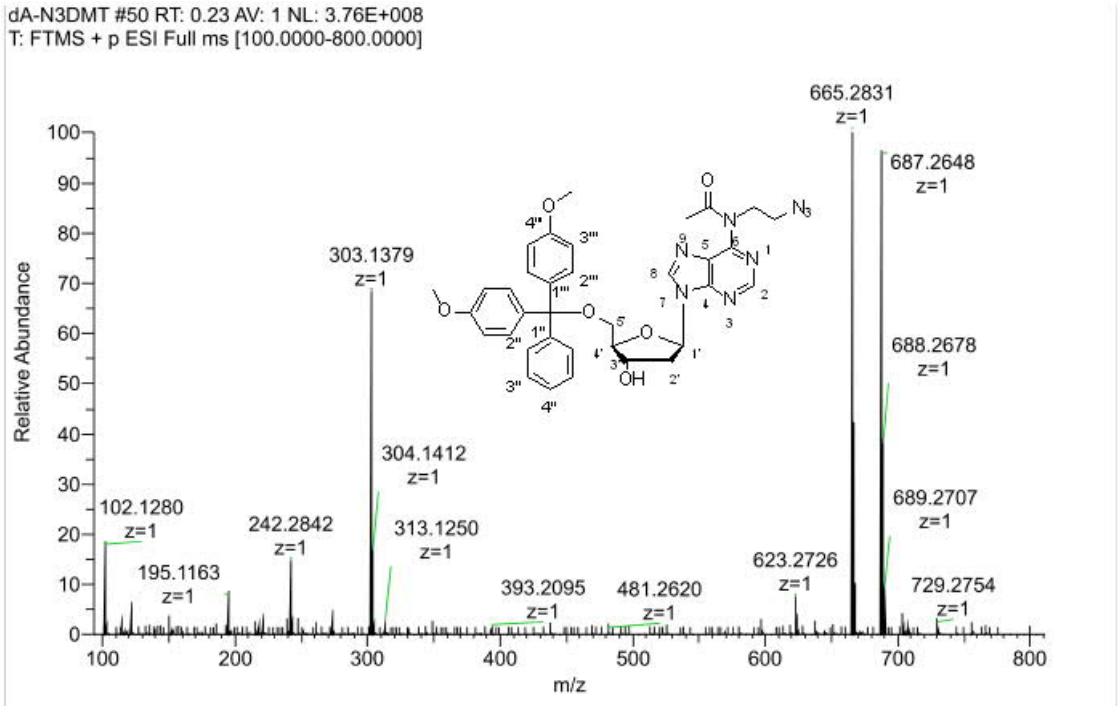

Figure S58. HRMS (ESI) of compound **10**.

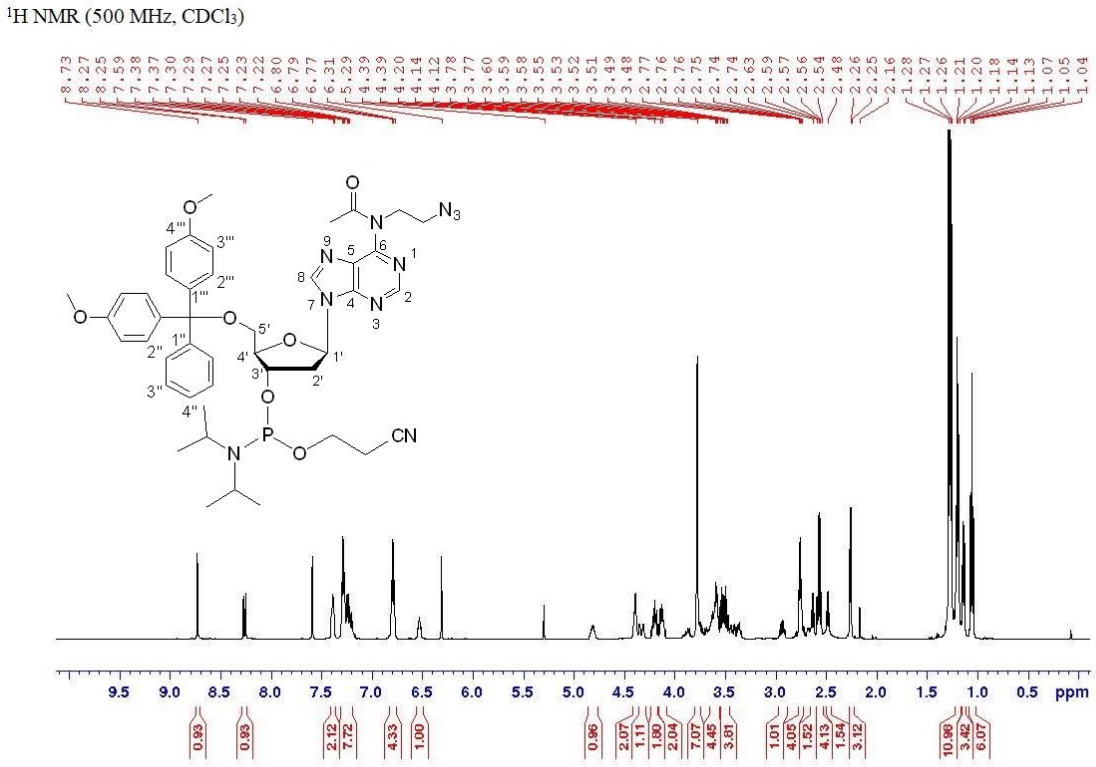

Figure S59. ^{1}H NMR spectrum of compound **11**.

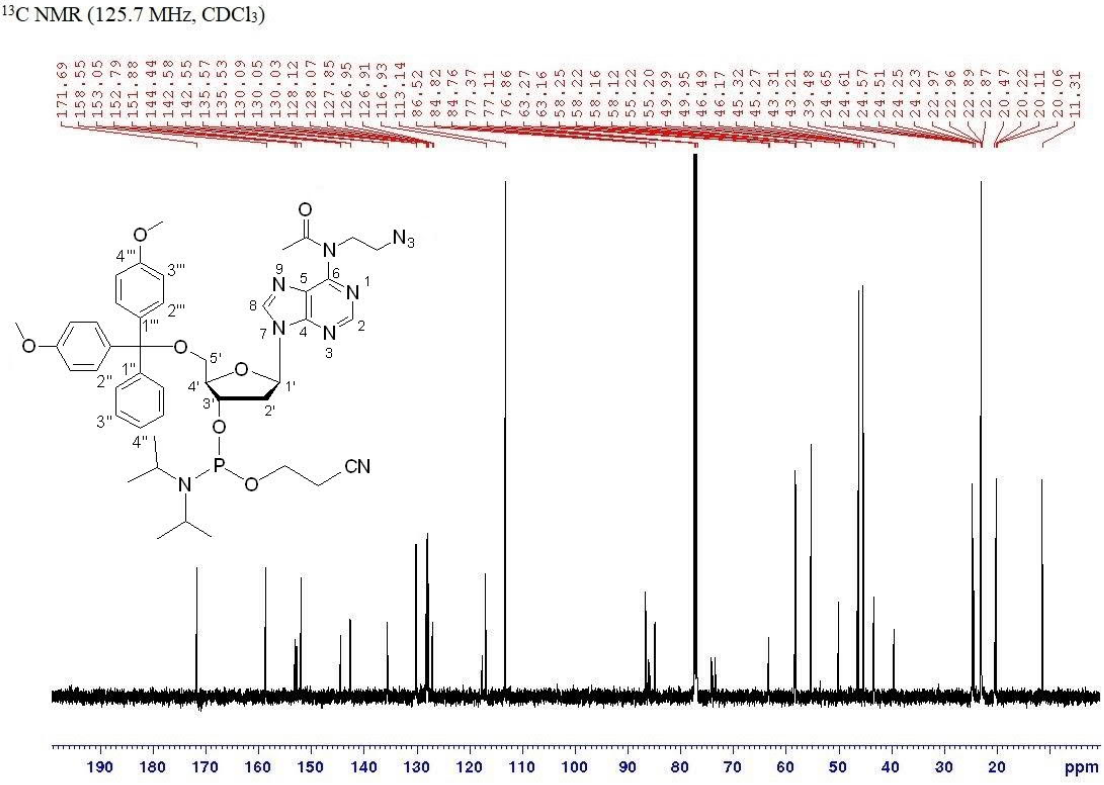

Figure S60. ^{13}C NMR spectrum of compound **11**.

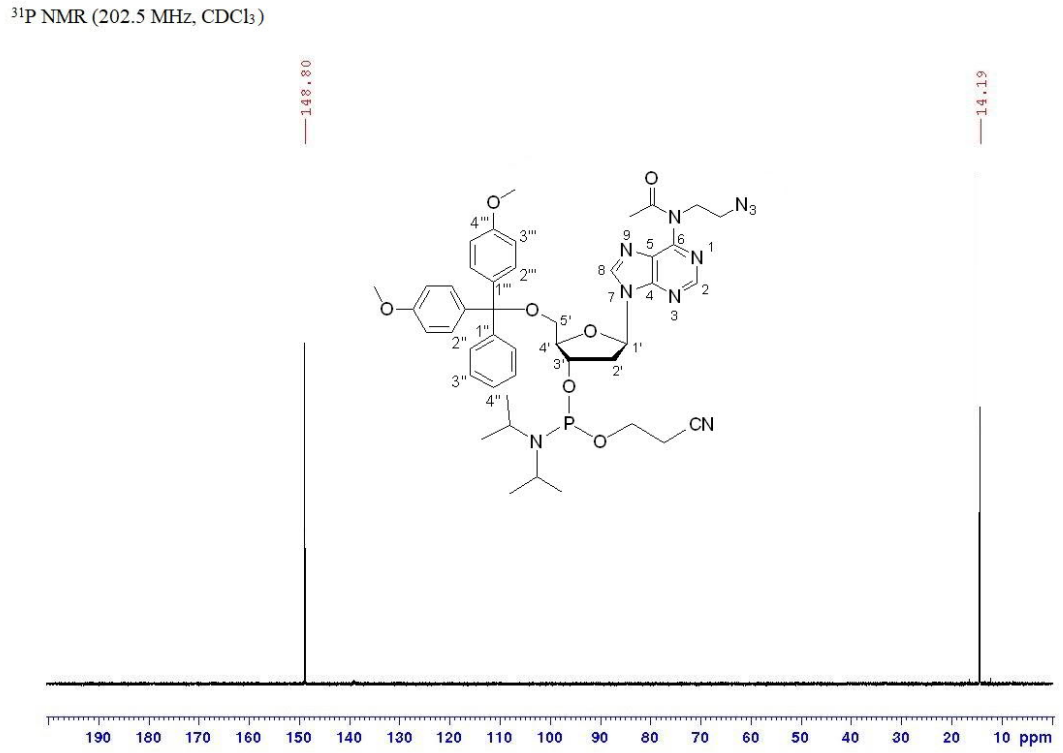

Figure S61. ^{31}P NMR spectrum of compound **11**.

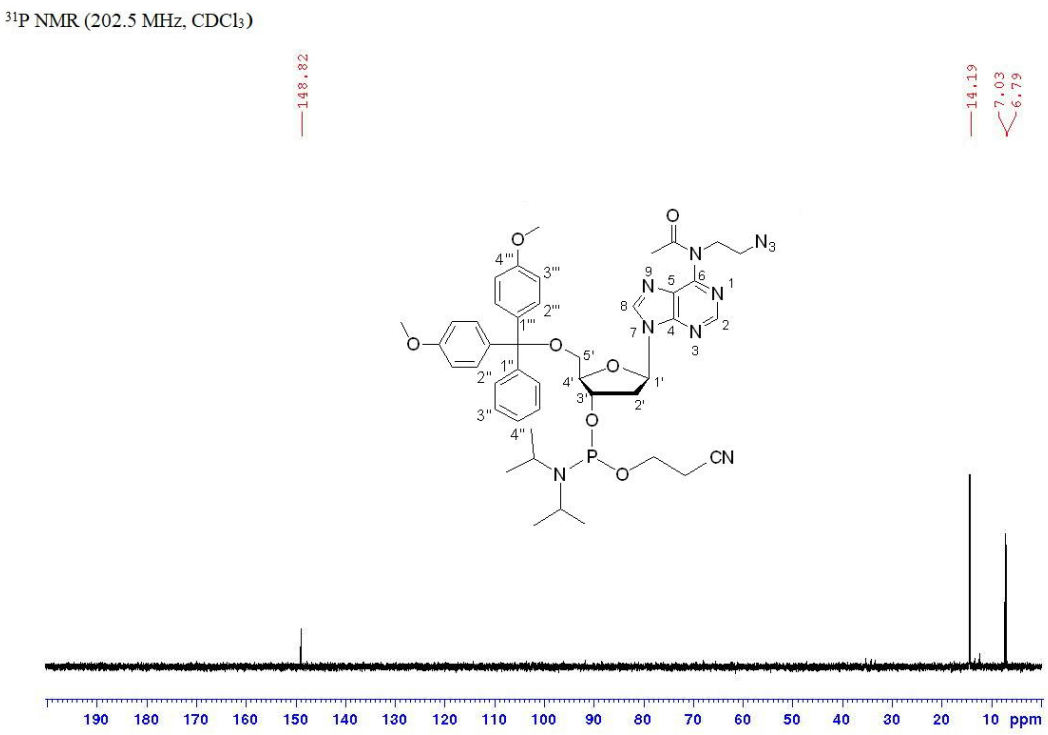

Figure S62. ^{31}P NMR spectrum of compound **11** after 24 hours at rt showing significant degradation of phosphoramidite **11**.

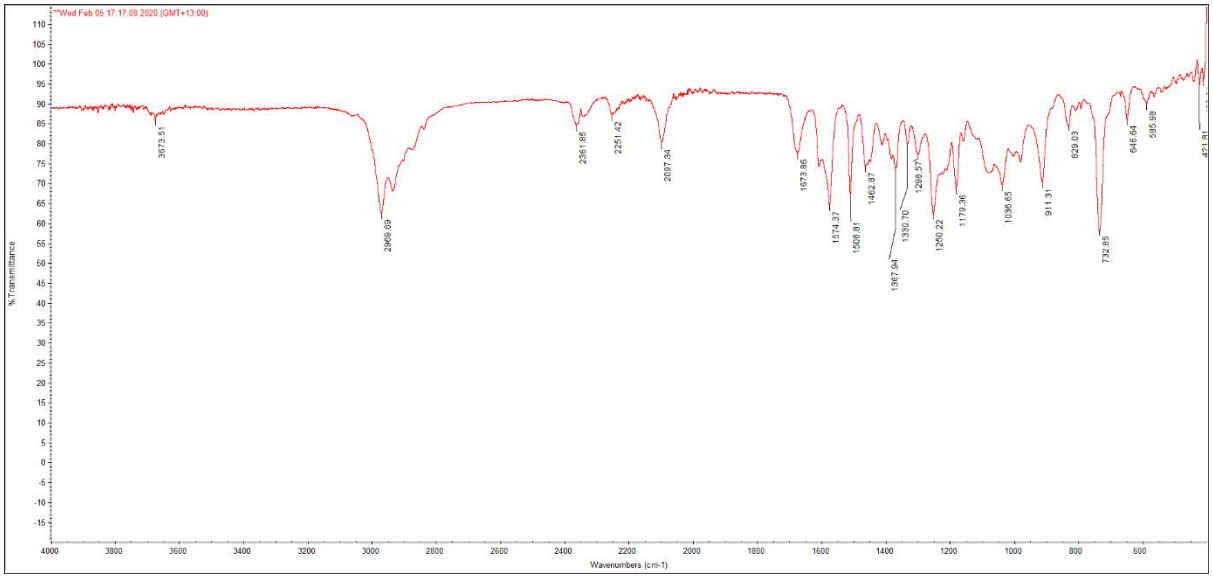

Figure S63. IR(ATR) spectrum of compound **11**.

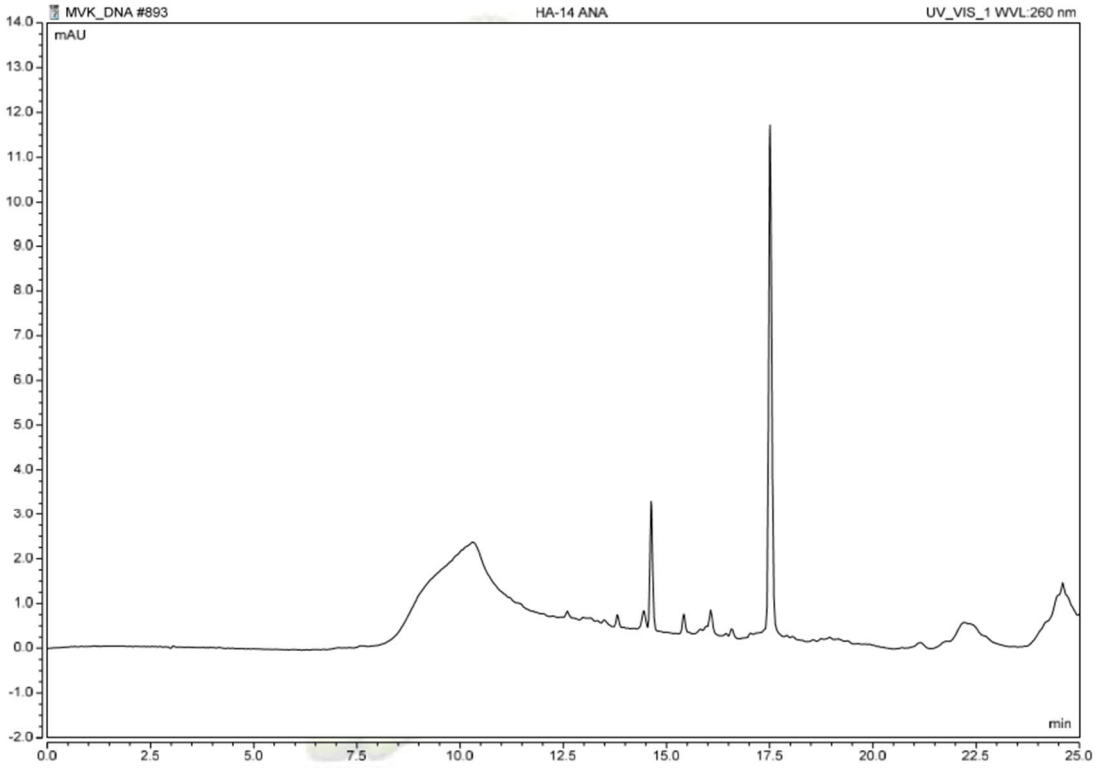

Figure S64. Reverse phase HPLC profile of dC-9-mer. Note that the broad peak at 10 min is an artefact of the column.

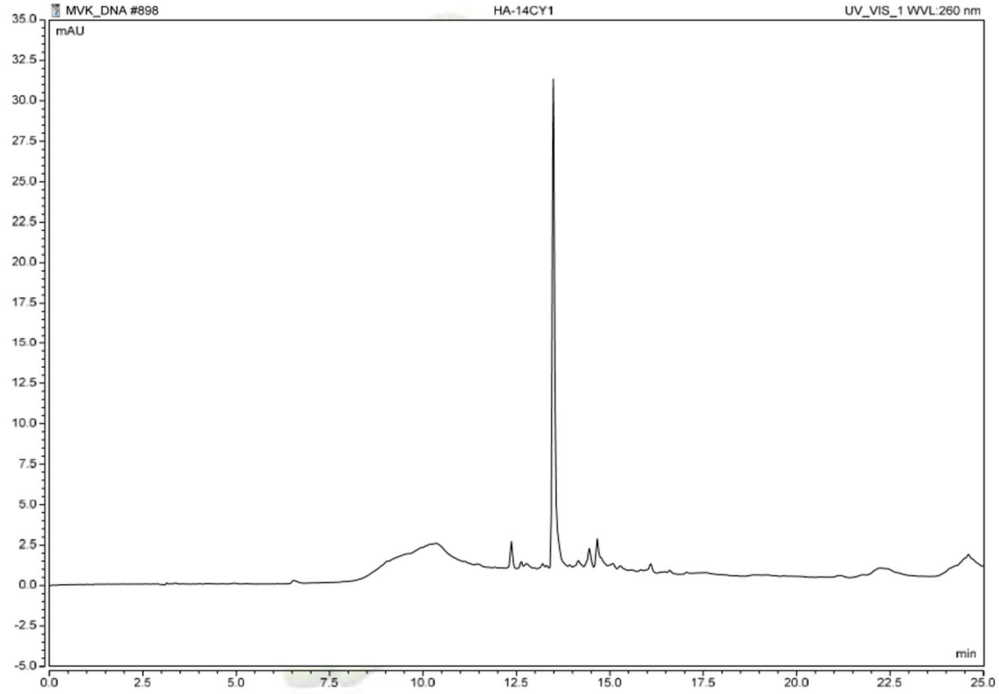

Figure S65. Reverse phase HPLC profile of dC-9-mer-X**.** Note that the broad peak at 10 min is an artefact of the column.

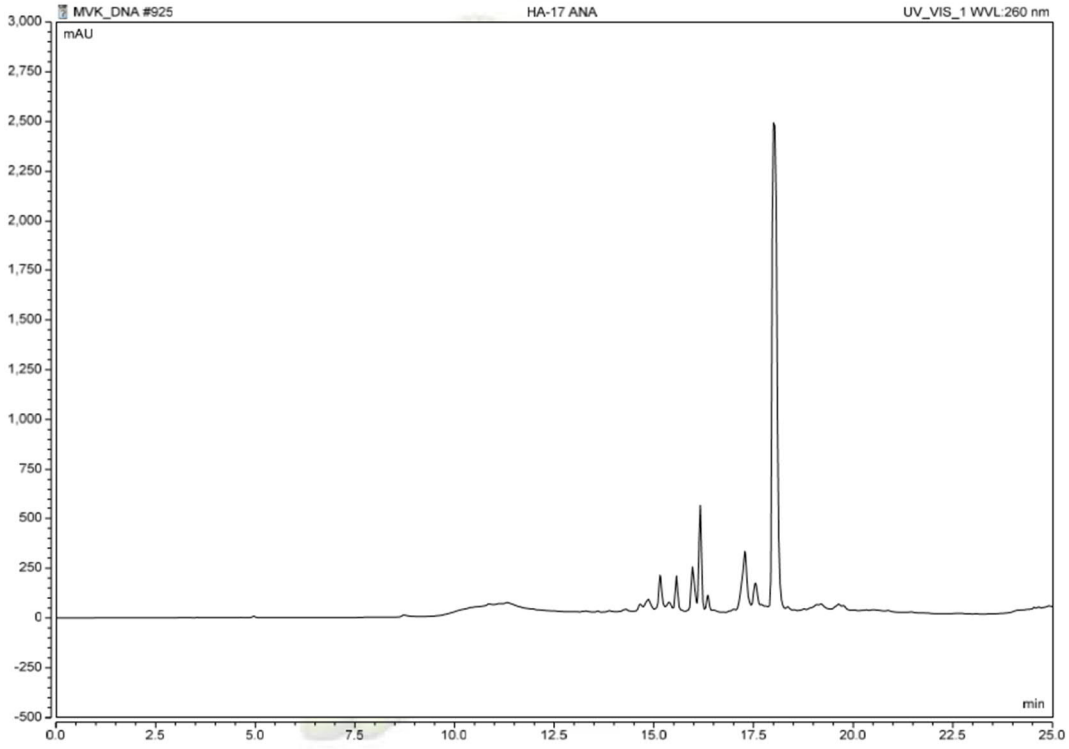

Figure S66. Reverse phase HPLC profile of dC-7-mer. Note that the broad peak at 10 min is an artefact of the column.

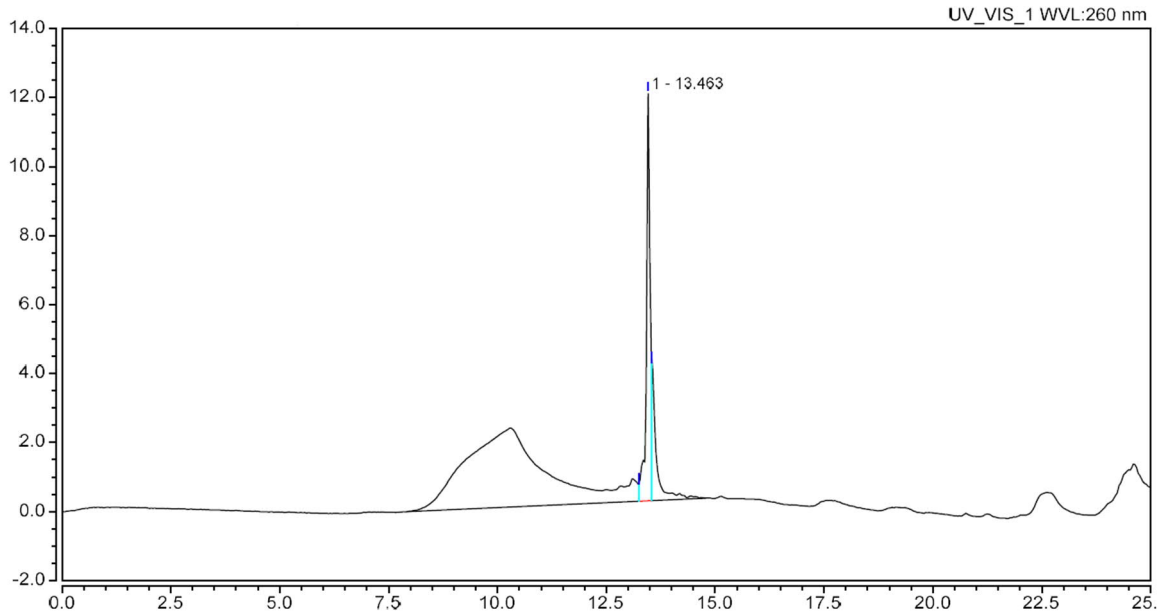

Figure S67. Reverse phase HPLC profile of dC-7-mer-X. Note that the broad peak at 10 min is an artefact of the column.

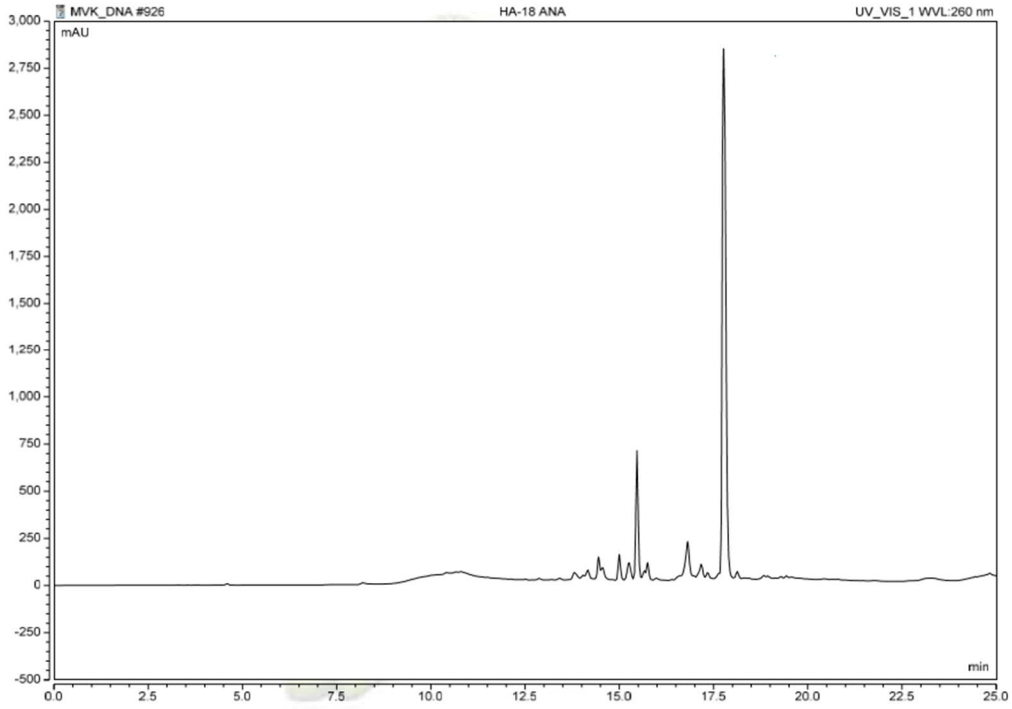

Figure S68. Reverse phase HPLC profile of dC-5-mer. Note that the broad peak at 10 min is an artefact of the column.

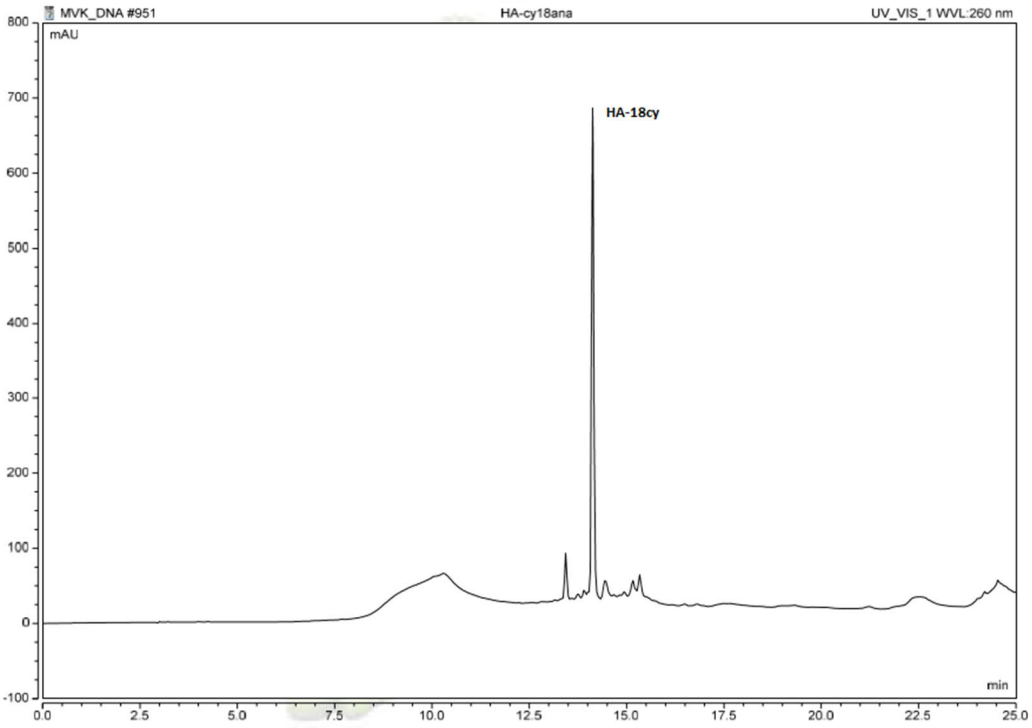

Figure S69. Reverse phase HPLC profile of dC-5-mer-X. Note that the broad peak at 10 min is an artefact of the column.

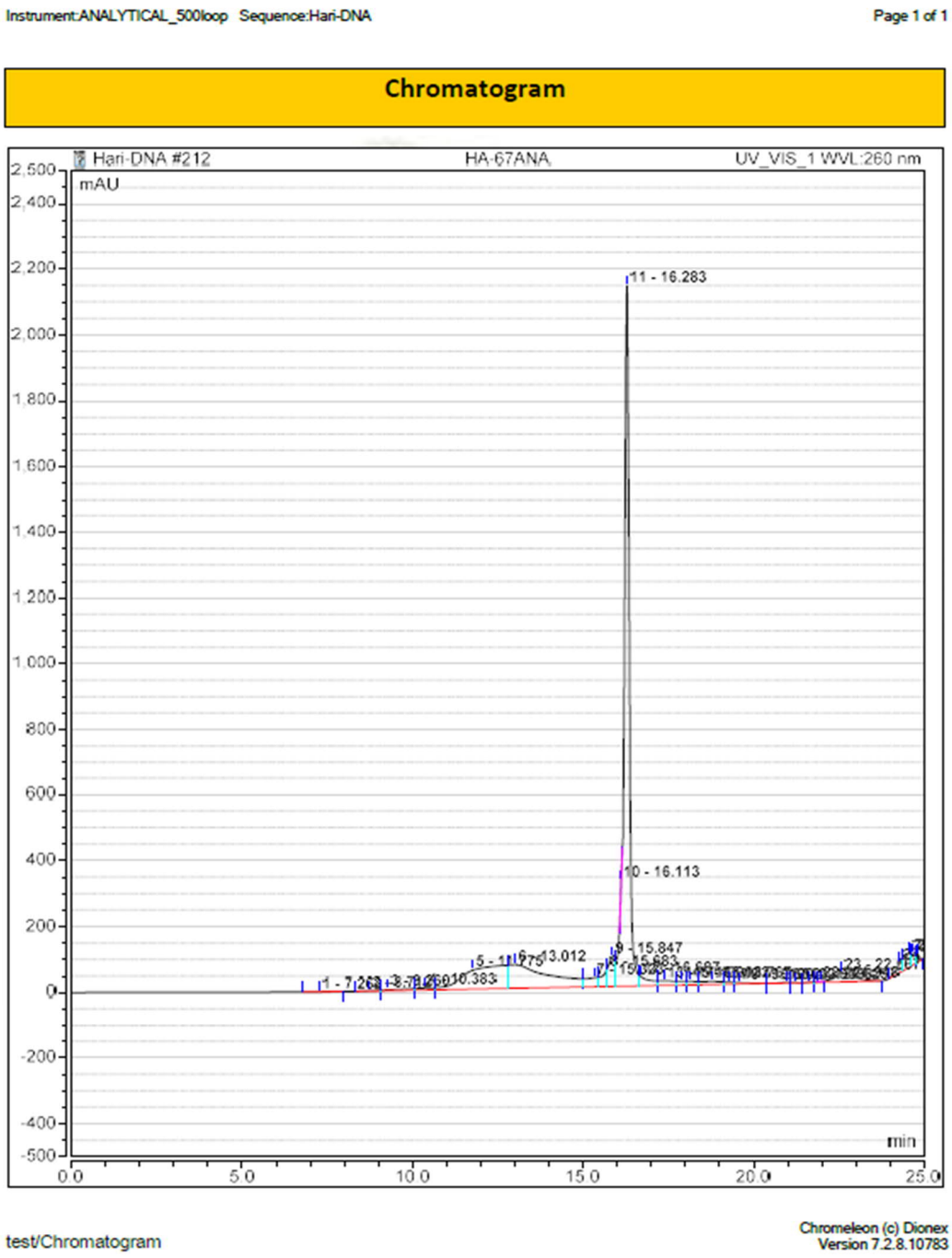

Figure S70. Reverse phase HPLC profile of dC[U^{E}(–2), A^{N3}(+1)]. Note that the broad peak at 12 min is an artefact of the column.

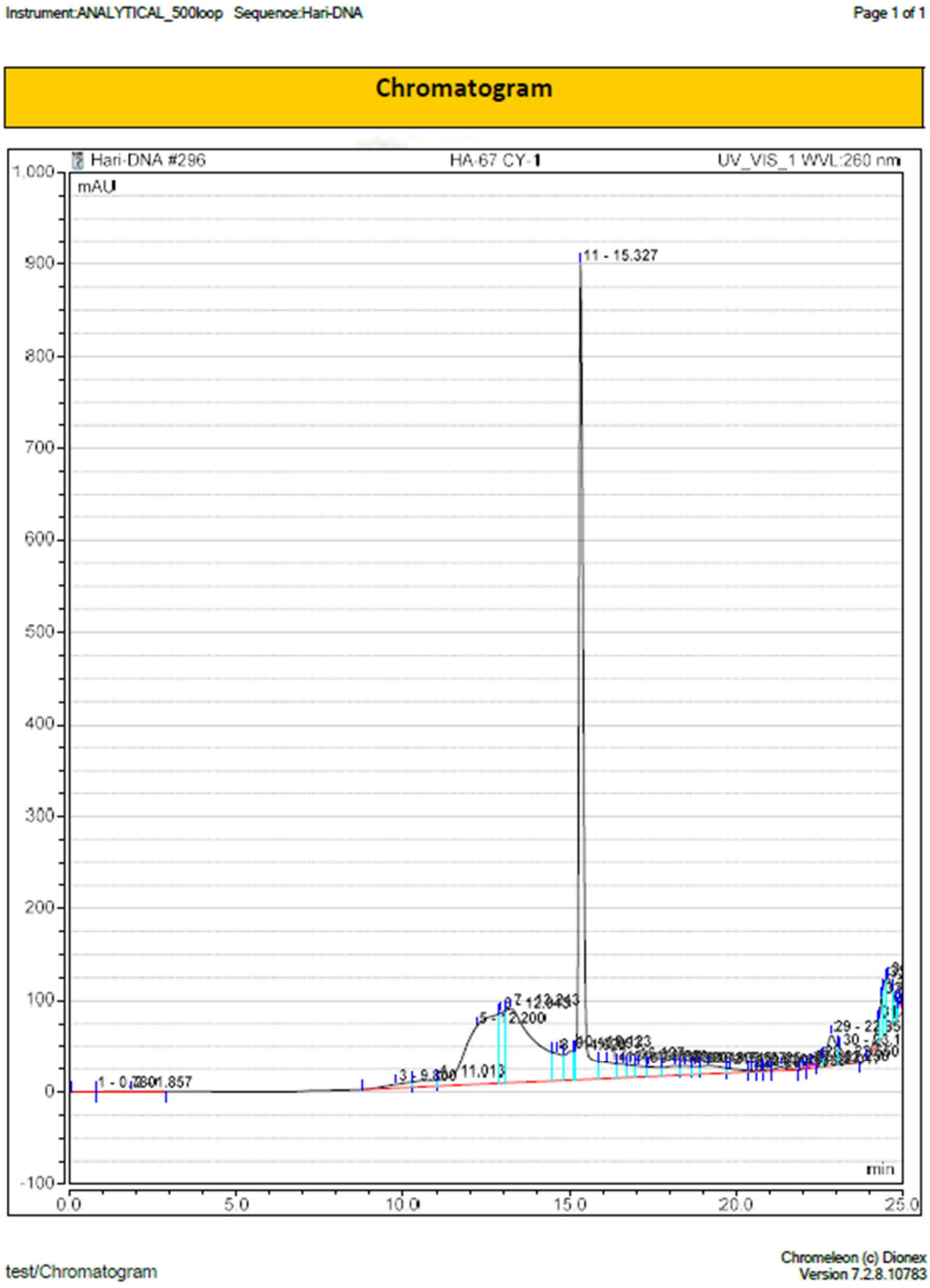

Figure S71. Reverse phase HPLC profile of dC[U^{E}(−2), A^{N3}(+1)]X. Note that the broad peak at 12 min is an artefact of the column.

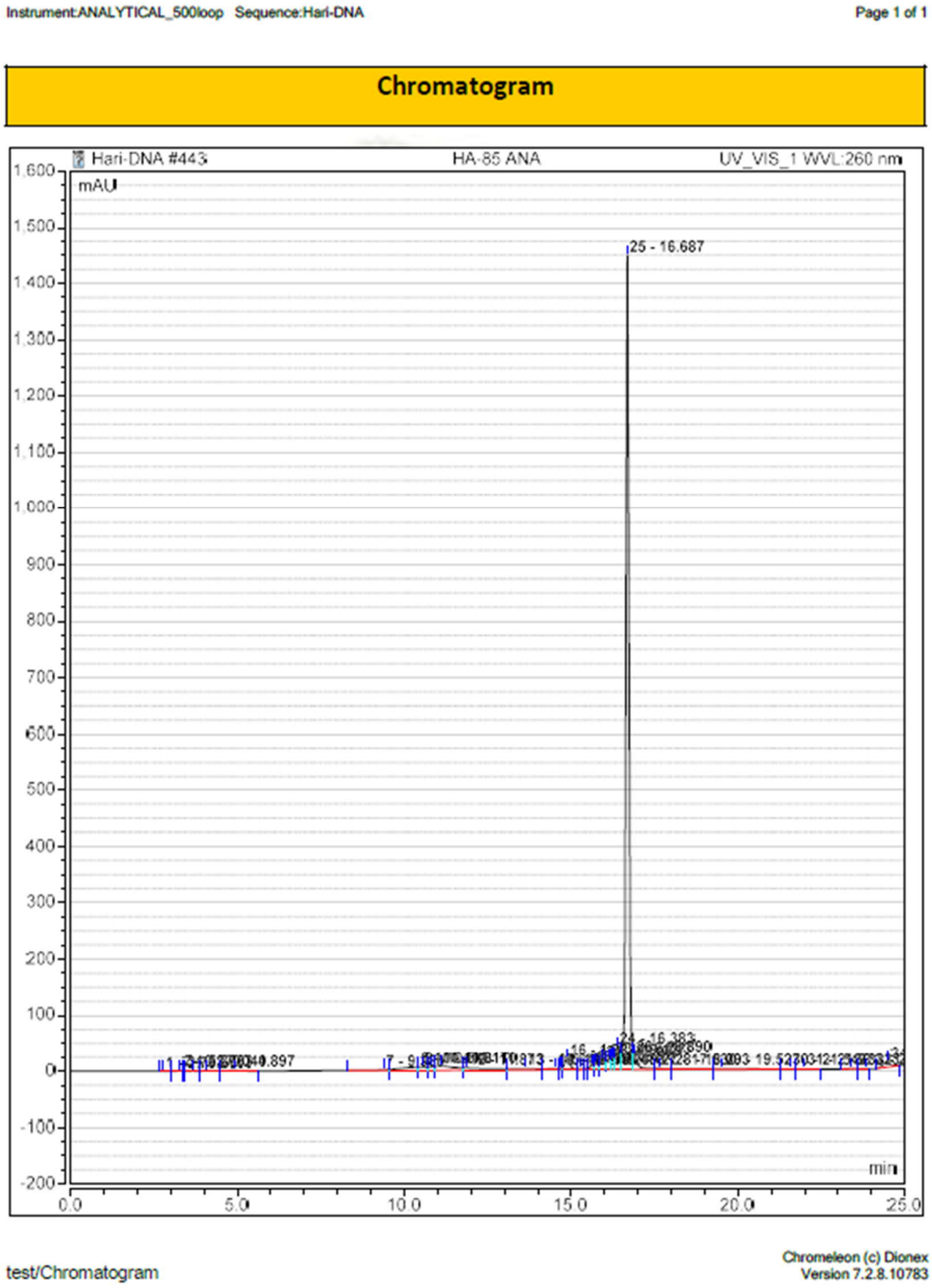

Figure S72. Reverse phase HPLC profile of dC[U^{E}(−3), A^{N3}(+1)]. Note that the broad peak at 12 min is an artefact of the column.

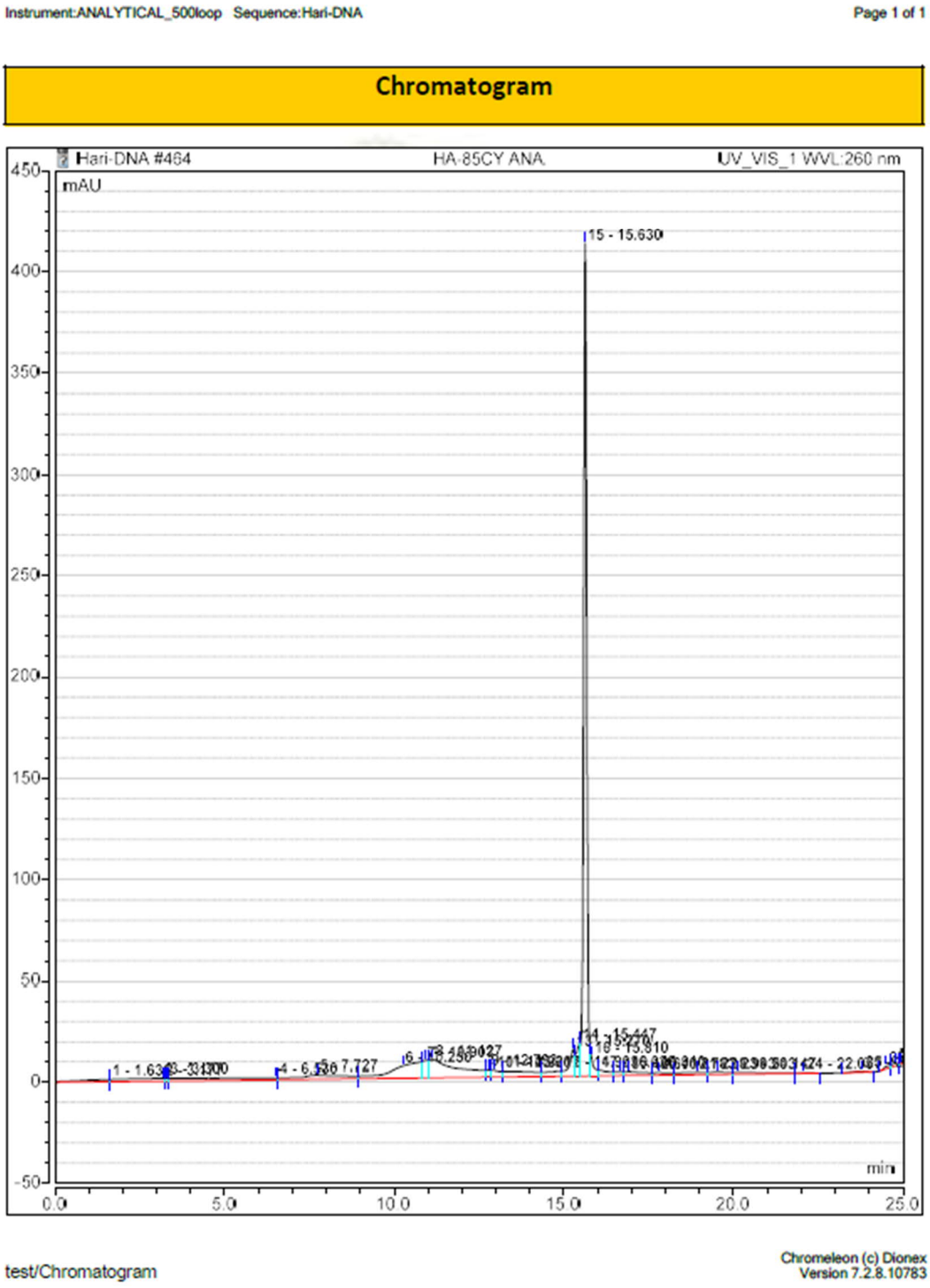

Figure S73. Reverse phase HPLC profile of dC[U^{E}(–3), A^{N3}(+1)]X. Note that the broad peak at 12 min is an artefact of the column.

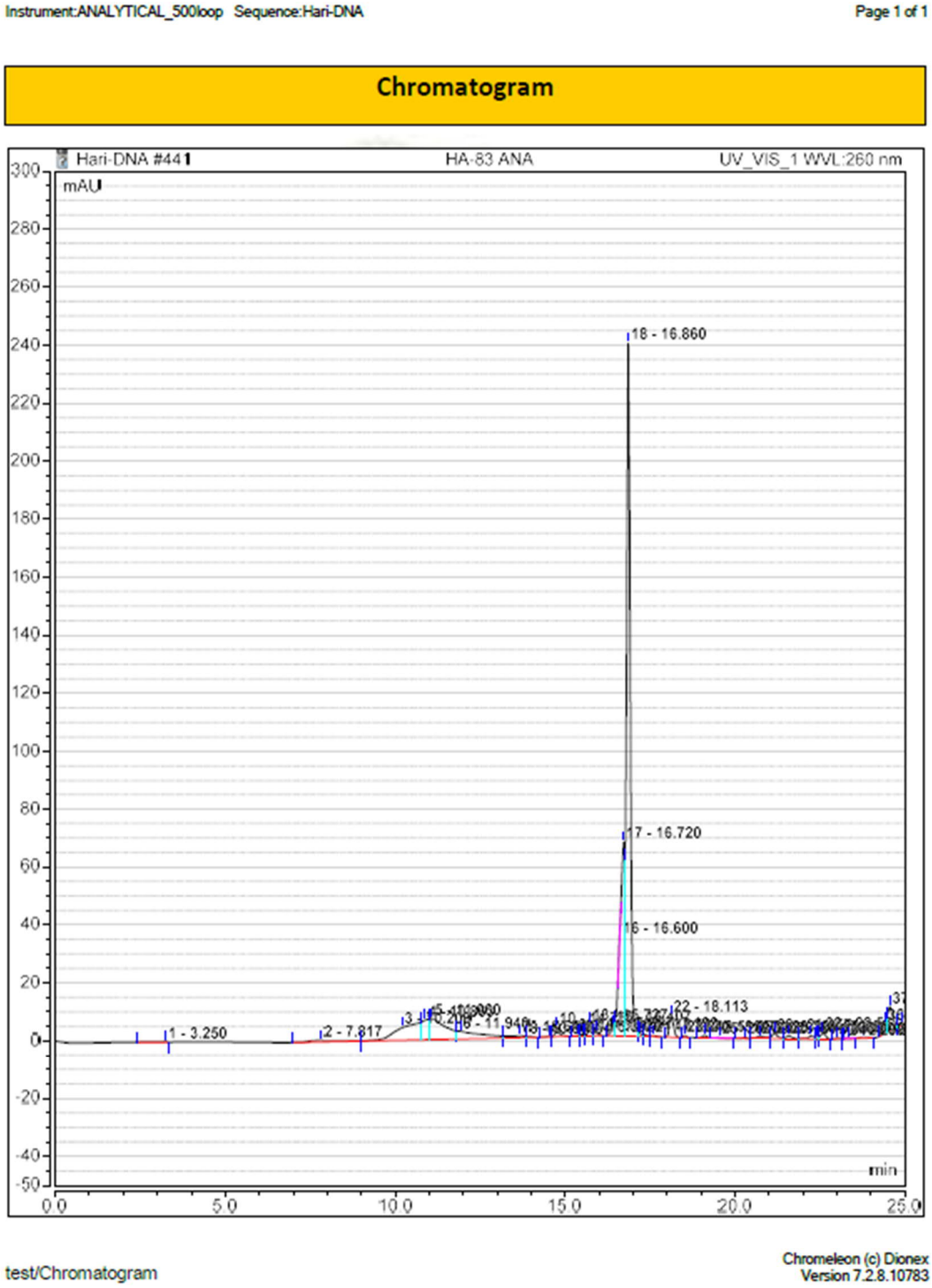

Figure S74. Reverse phase HPLC profile of dZ[U^{E}(–3), A^{N3}(+1)]. Note that the broad peak at 11 min is an artefact of the column.

Figure S75. Reverse phase HPLC profile of dZ[U^{E}(–3), A^{N3}(+1)]X. Note that the broad peak at 11 min is an artefact of the column.

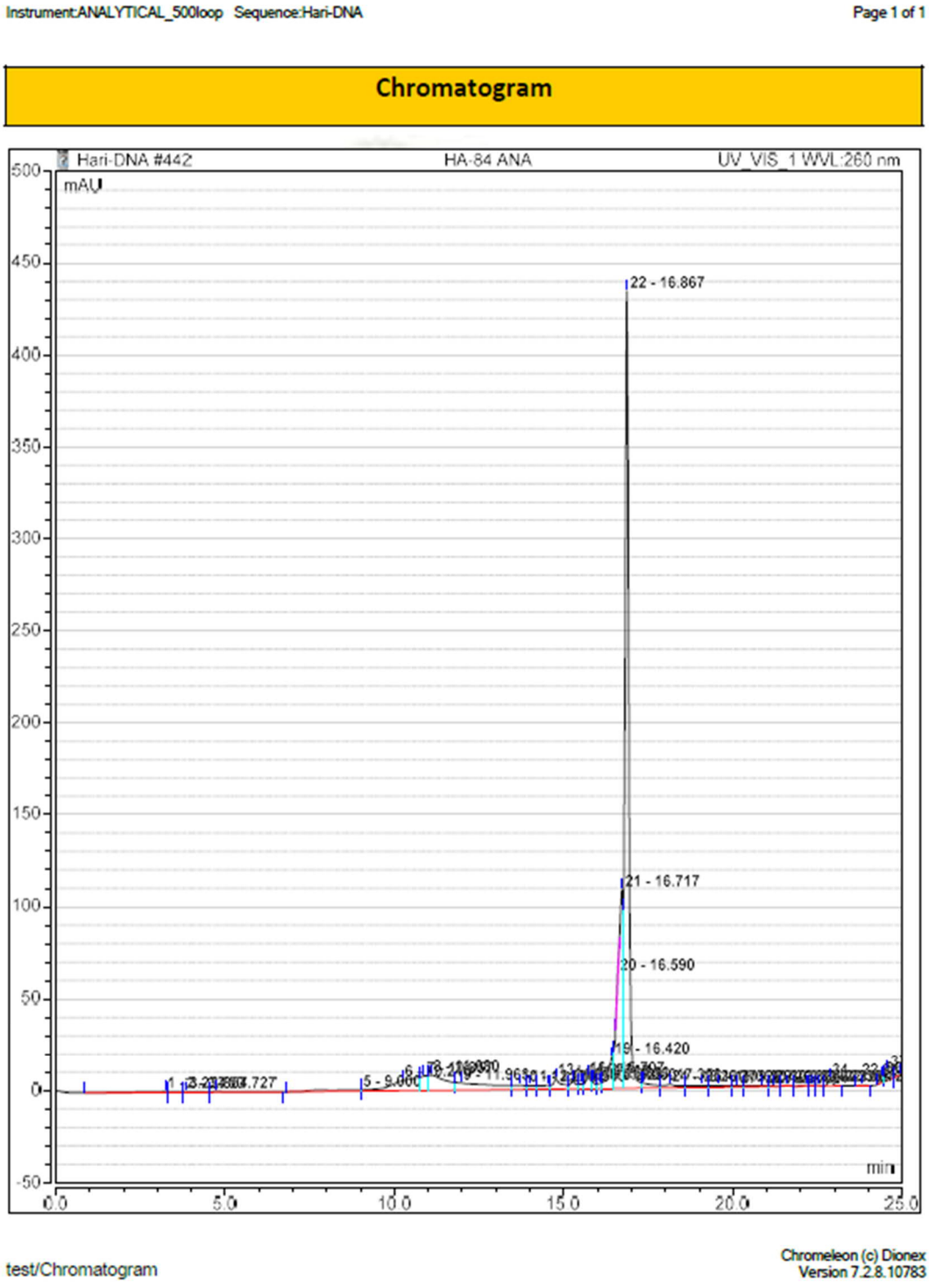

Figure S76. Reverse phase HPLC profile of dZ[U^{E}(–2), A^{N3}(+1)]. Note that the broad peak at 11 min is an artefact of the column.

Figure S77. Reverse phase HPLC profile of dZ[U^{E}(–2), A^{N3}(+1)]X. Note that the broad peak at 11 min is an artefact of the column.

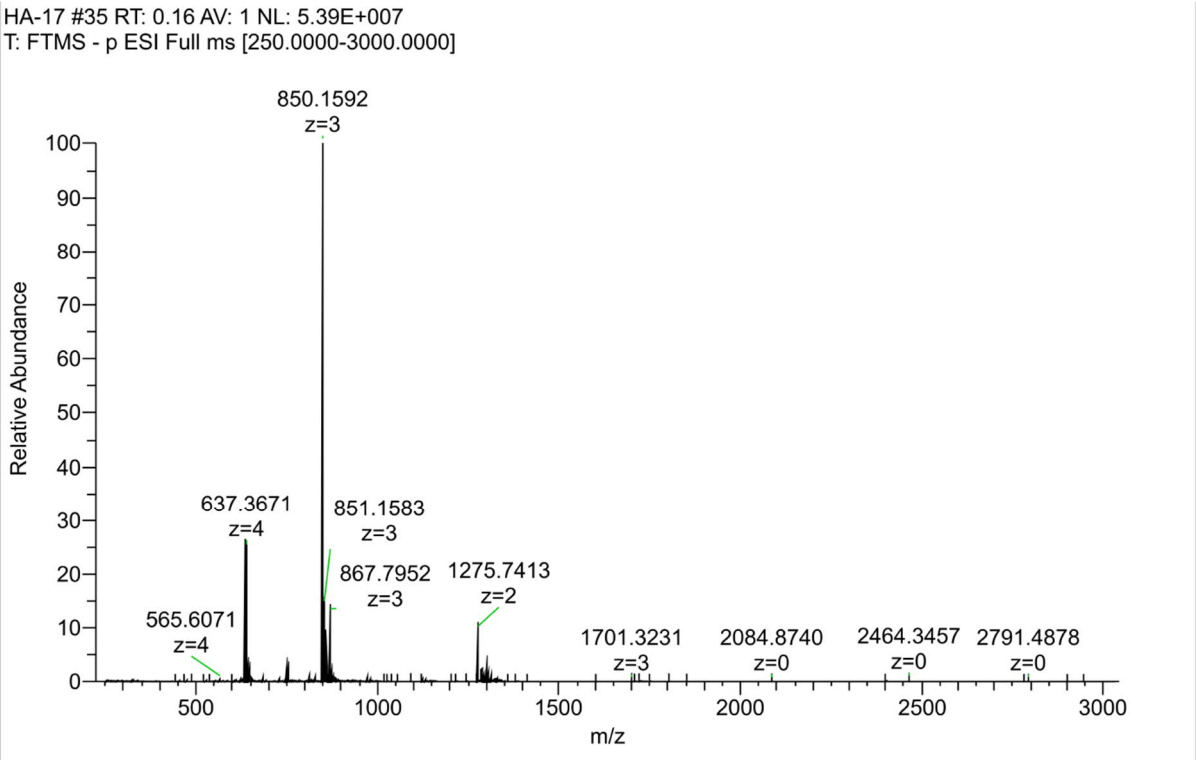

Figure S78. HRMS (ESI) of dC-9-mer.

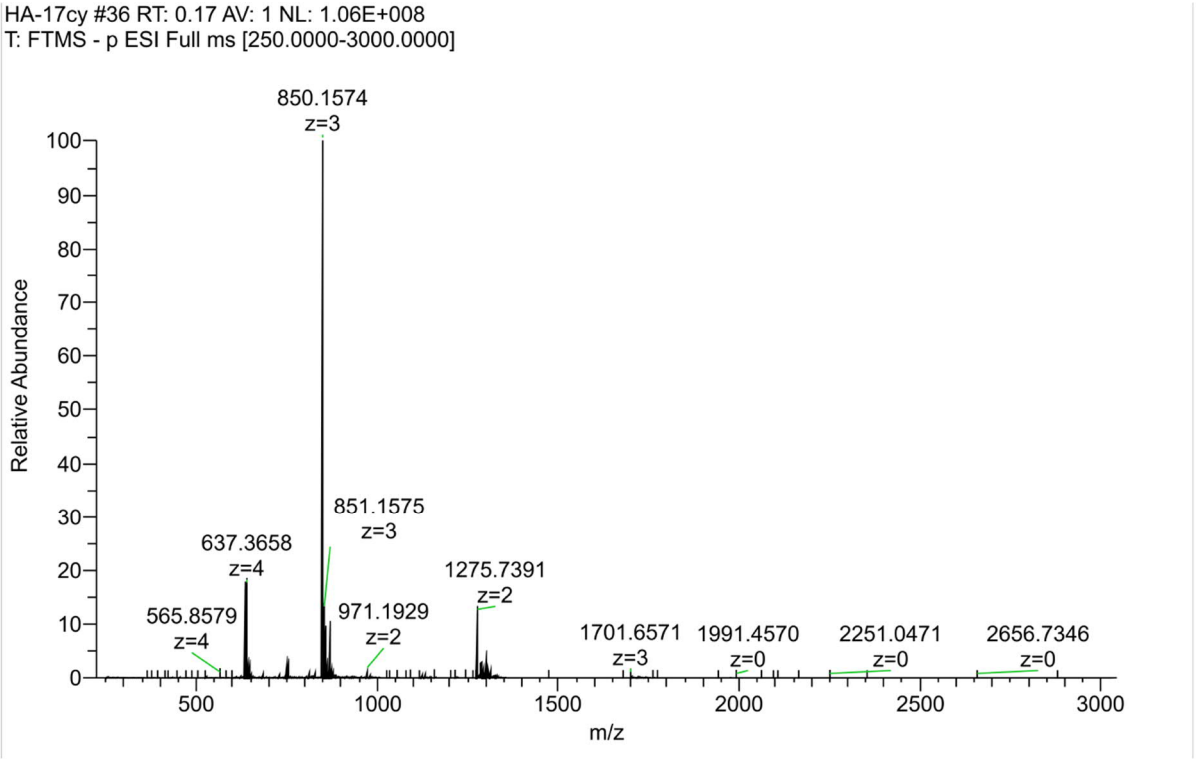

Figure S79. HRMS (ESI) of dC-9-mer-X.

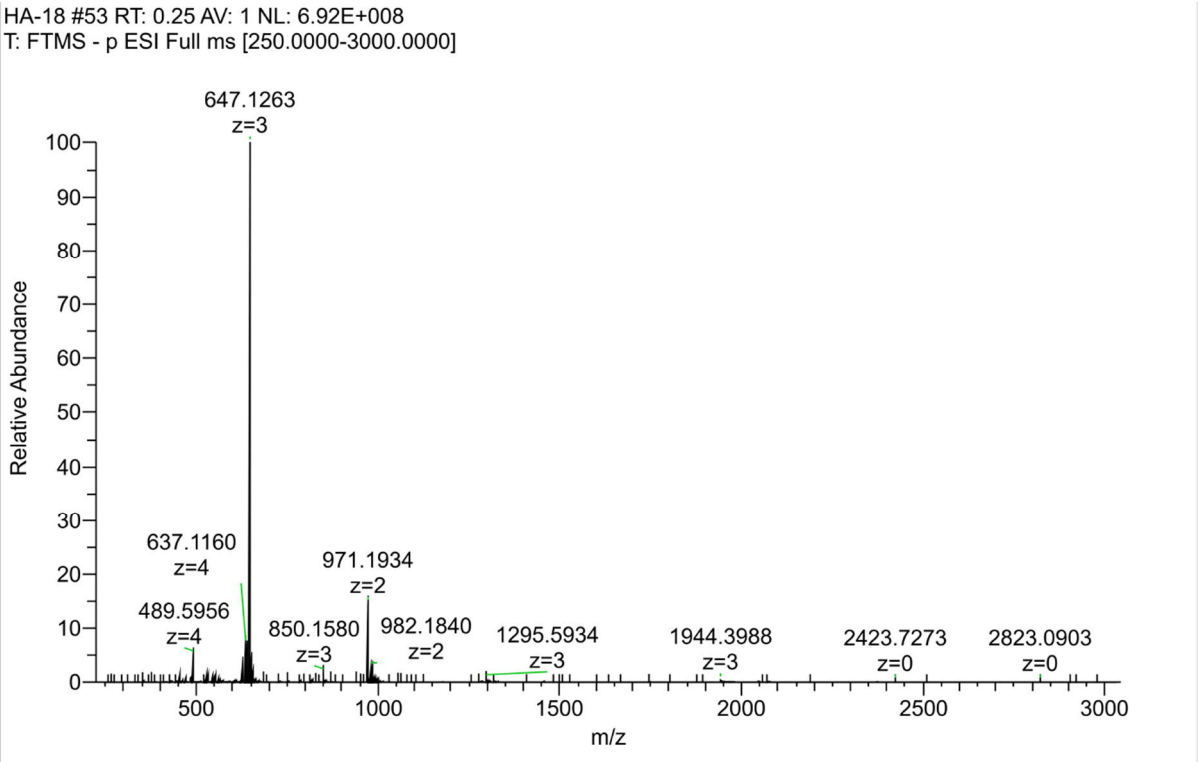

Figure S80. HRMS (ESI) of dC-7-mer.

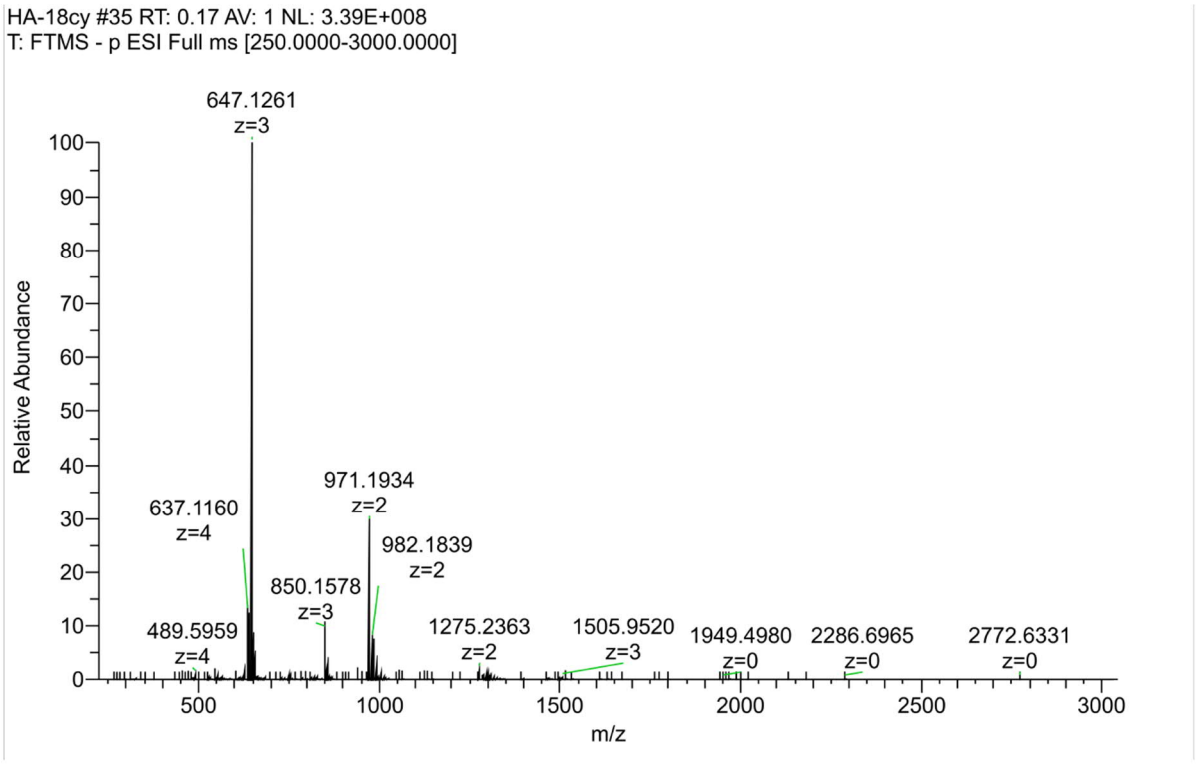

Figure S81. HRMS (ESI) of dC-7-mer-X.

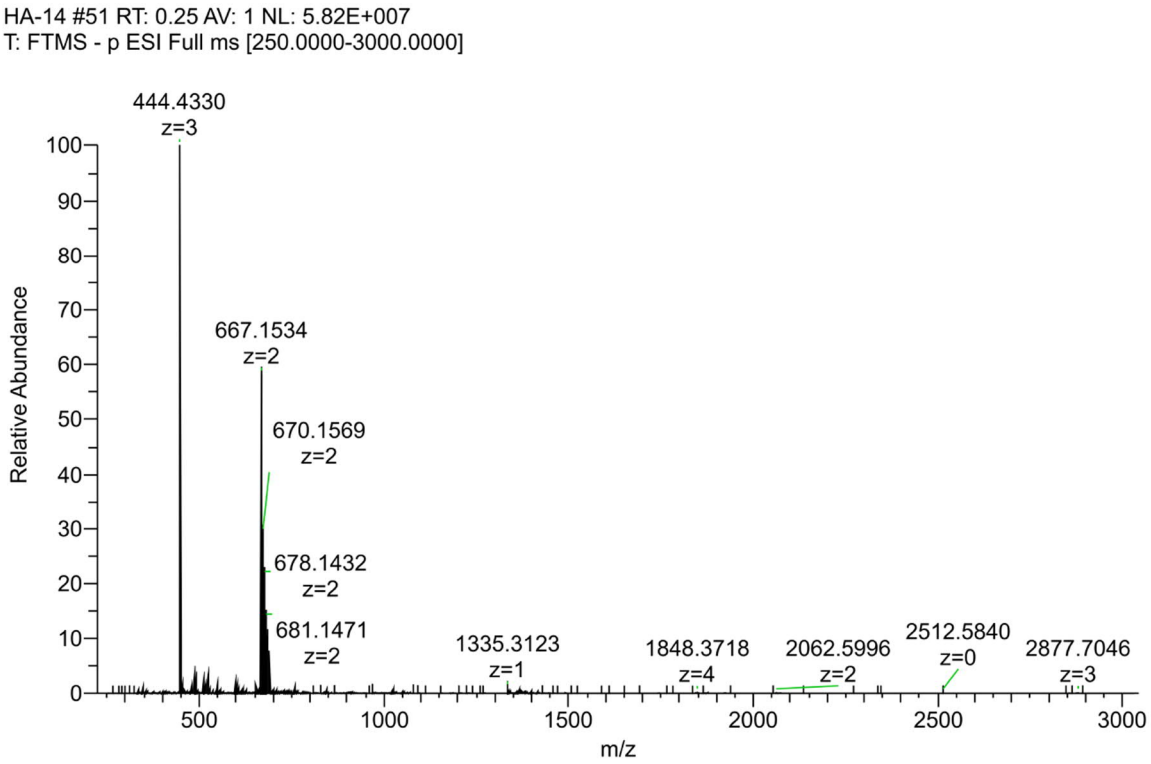

Figure S82. HRMS (ESI) of dC-5-mer.

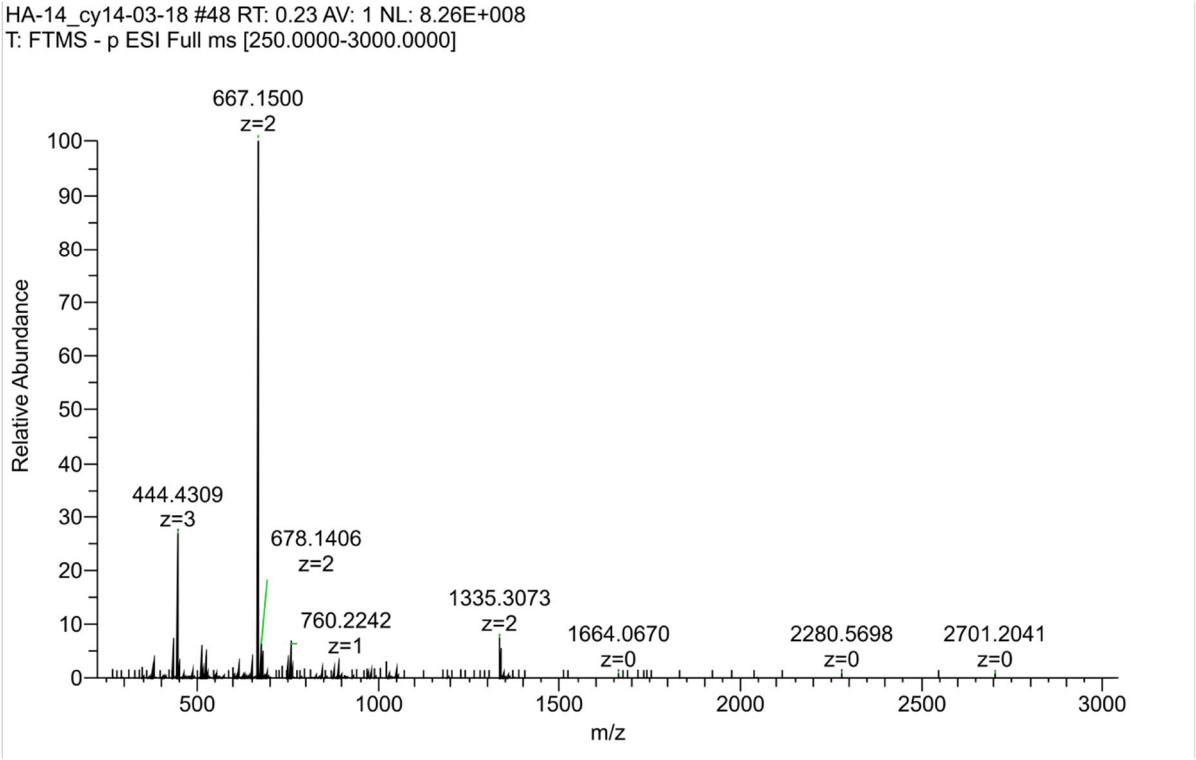

Figure S83. HRMS (ESI) of dC-5-mer-X.

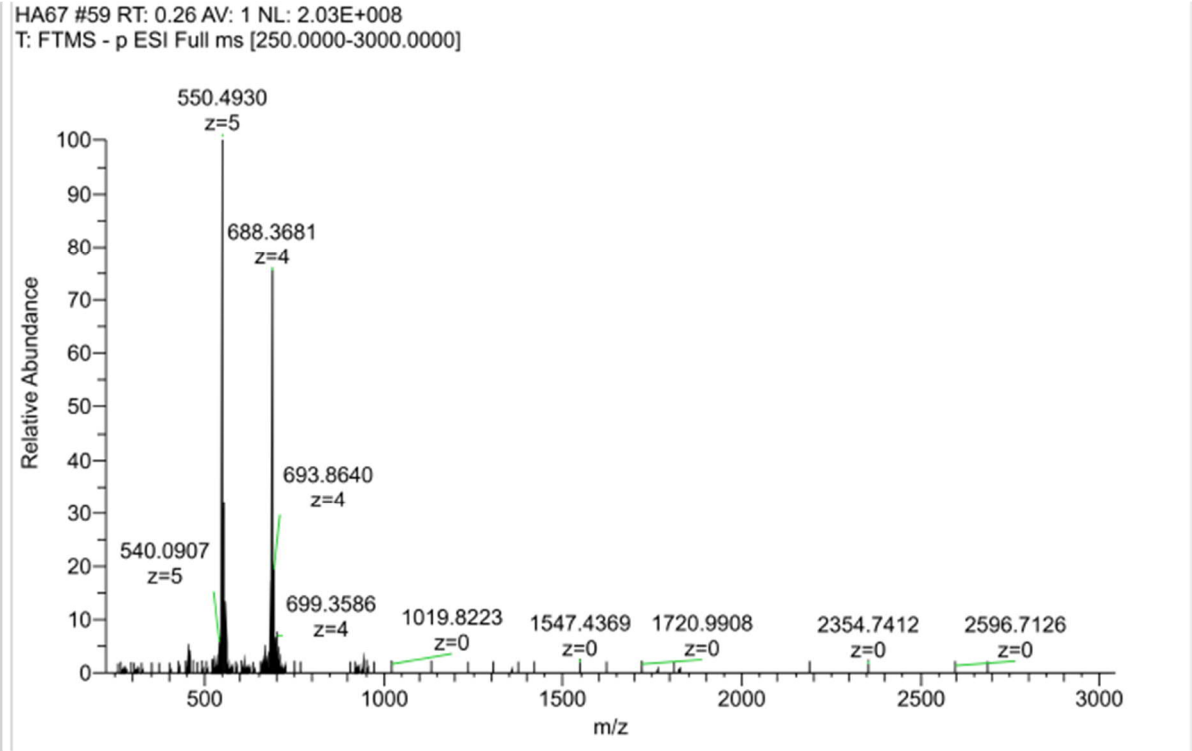

Figure S84. HRMS (ESI) of dC[U^{E}(–2), A^{N3}(+1)].

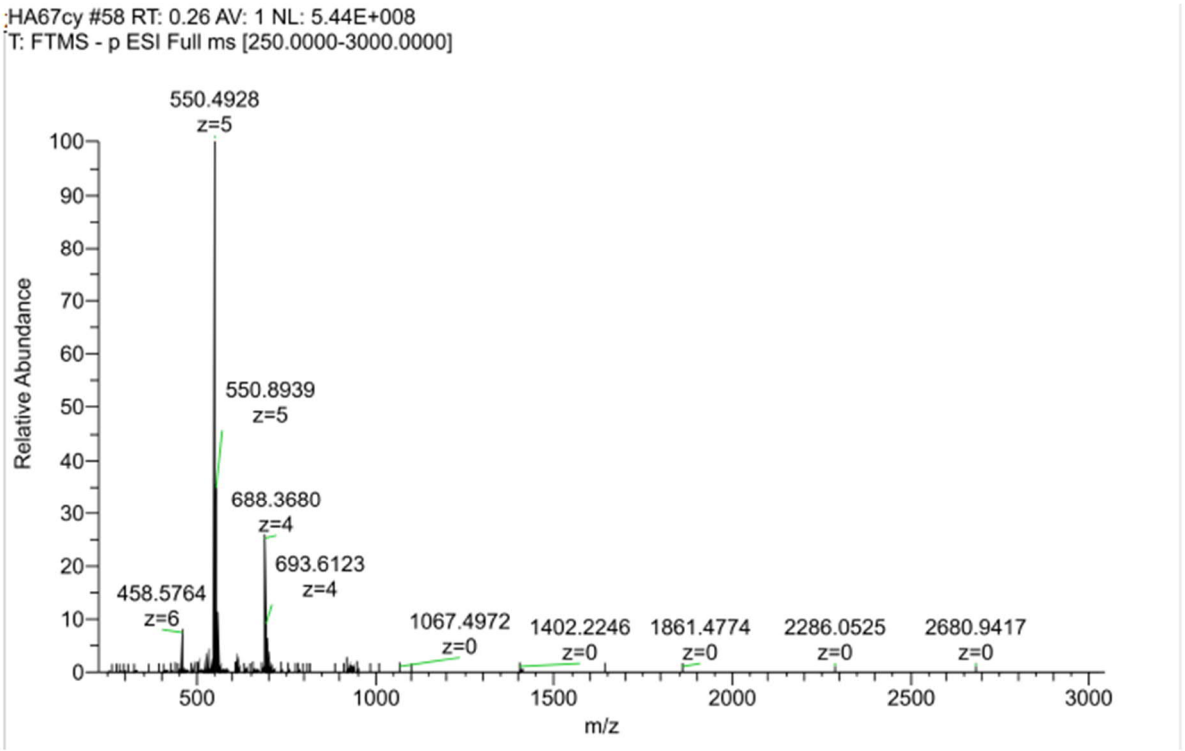

Figure S85. HRMS (ESI) of dC[U^{E}(–2), A^{N3}(+1)]X.

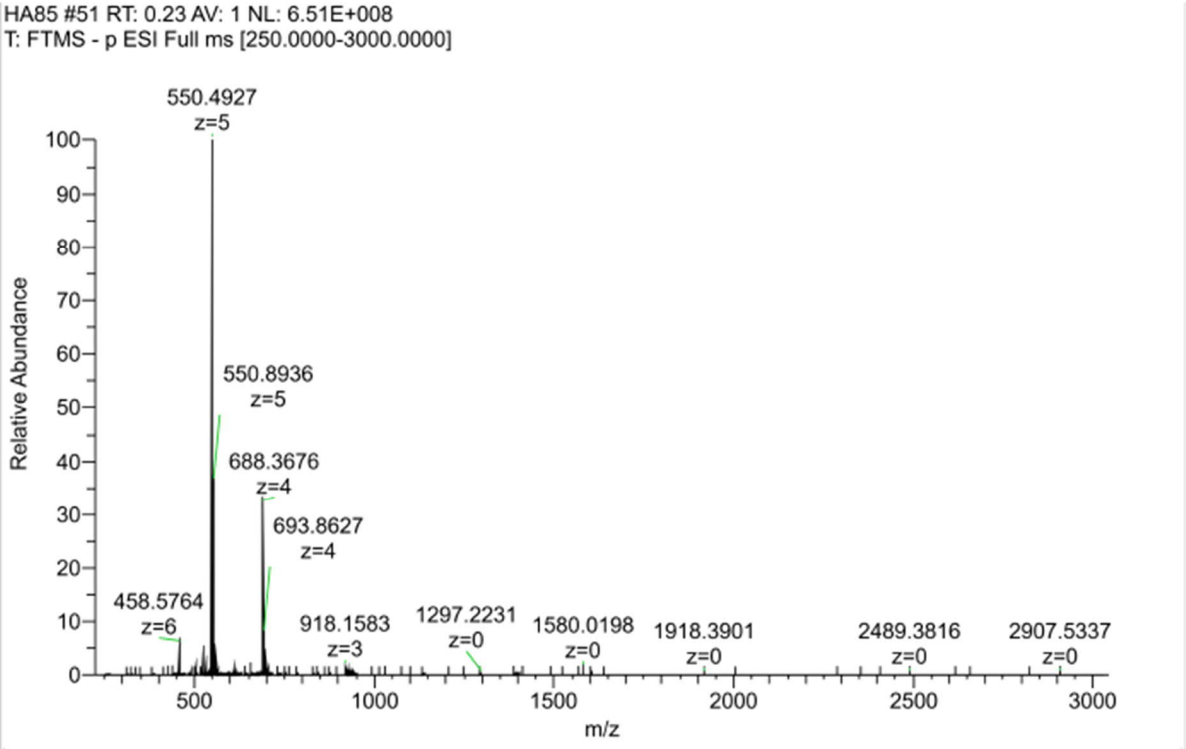

Figure S86. HRMS (ESI) of dC[U^{E}(–3), A^{N3}(+1)].

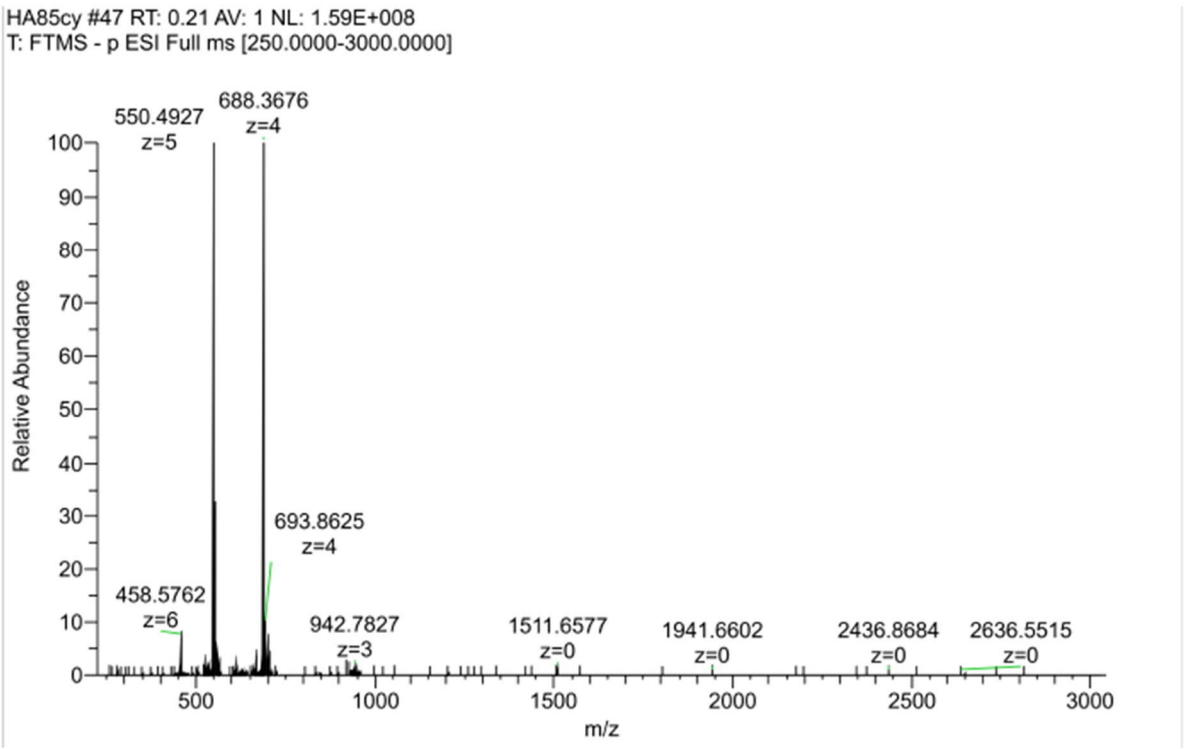

Figure S87. HRMS (ESI) of dC[U^{E}(–3), A^{N3}(+1)]X.

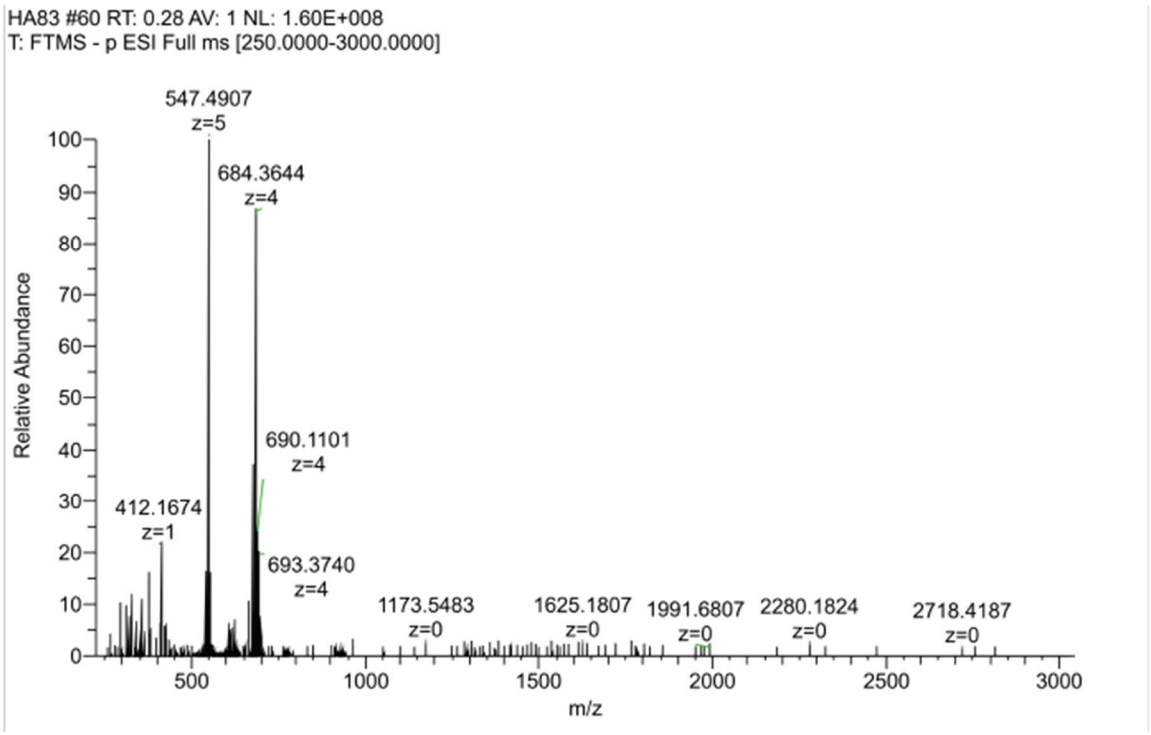

Figure S88. HRMS (ESI) of dZ[U^{E}(–3), A^{N3}(+1)].

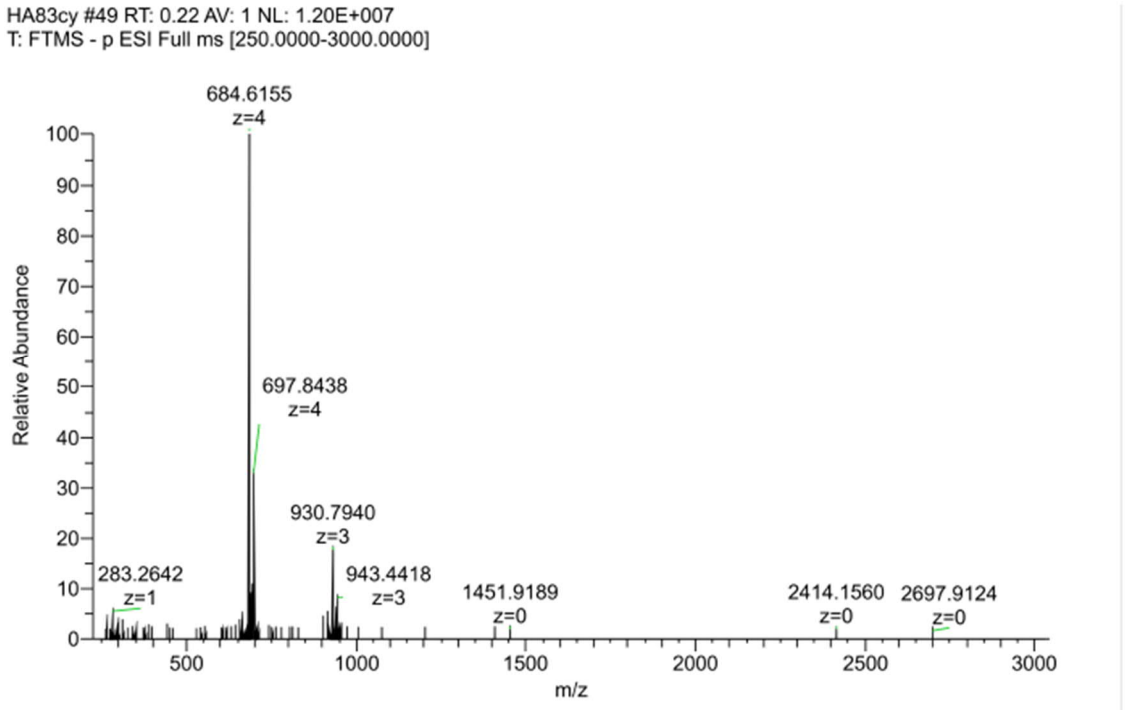

Figure S89. HRMS (ESI) of dZ[U^{E}(–3), A^{N3}(+1)]X.

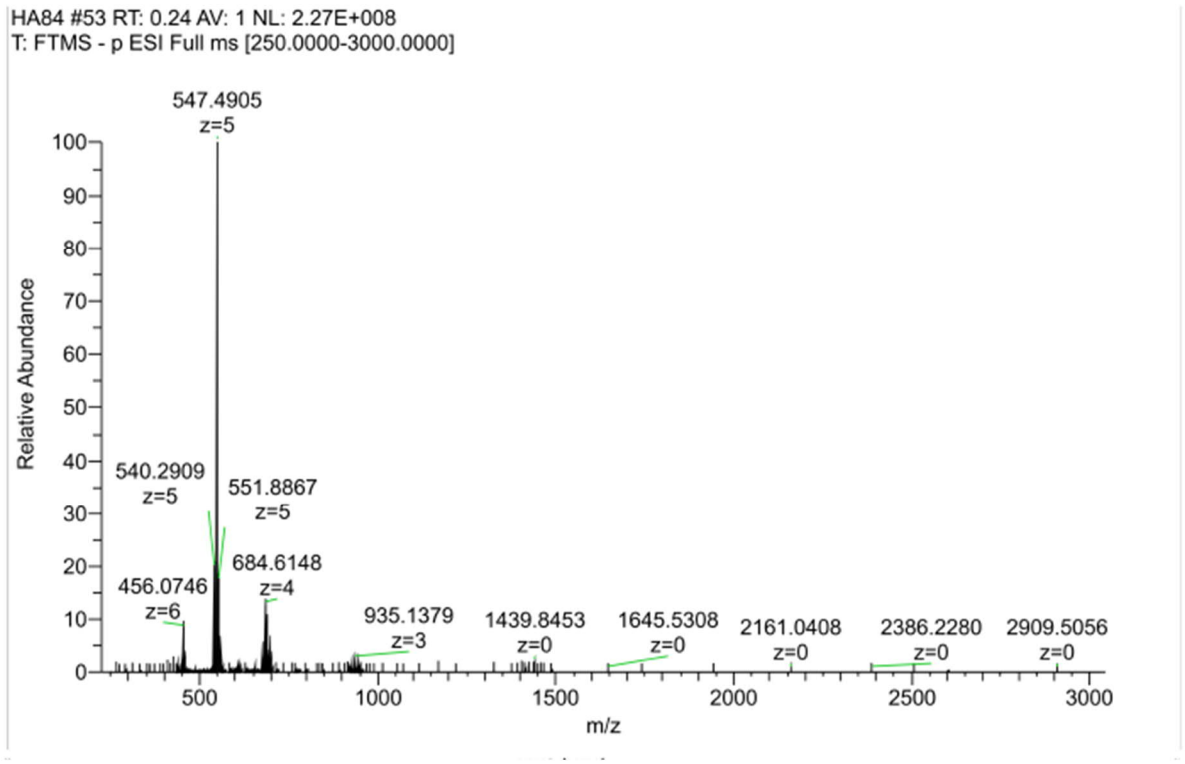

Figure S90. HRMS (ESI) of dZ[U^{E}(–2), A^{N3}(+1)].

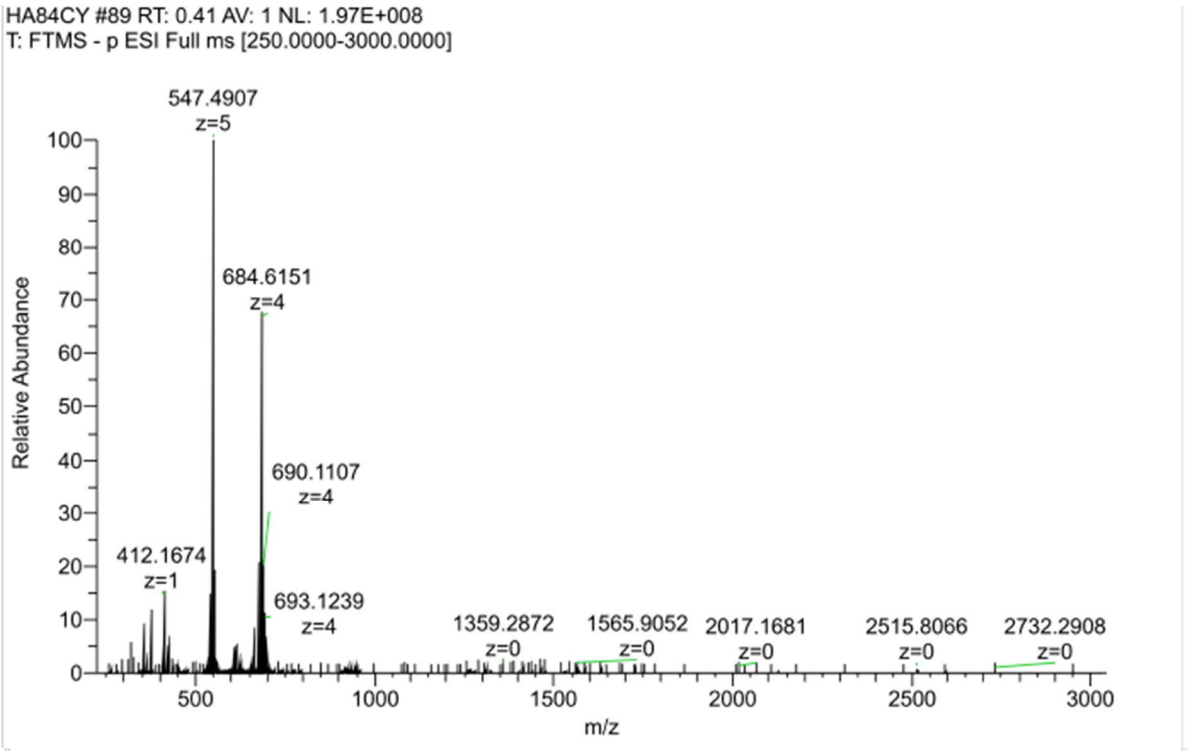

Figure S91. HRMS (ESI) of dZ[U^{E}(–2), A^{N3}(+1)]X.